A study of the electrospinning of lignin-PVA solutions

Materials Technology- 4th semester

AALBORG UNIVERSITET

Shantanu Shashikant Rassay

Contents

1 Introduction

Over the years, fibres have emerged as key components in both technological and life science areas. These long structures with relatively negligible diameter have found themselves useful in a multitude of ways. Natural and synthetic polymeric fibres of Silk, Polyester, Nylon are the basis of the textile industry. Composite materials, a class of materials that have widespread applications due to their high strength to weight ratio, constitute of fibres as the reinforcing component. Glass fibres are arguably the most commonly used fibres for reinforcement in composites. Along with high strength they also exhibit excellent impact resistance. These properties coupled with lightweight, have been found useful in the construction of more fuel-efficient aircrafts. Similarly, Aramid fibres and Boron fibres when used as reinforcement, result in composites having high impact resistance and compressive strength, respectively. Another commonly used material as fibres for reinforcement in composites is Carbon. Like glass fibre reinforced composites, carbon fibre reinforced composites also make up a large proportion of the materials used in building aircrafts. The structural application of carbon fibre-reinforced composites is being employed by several industries where strength, stiffness, low weight, and outstanding fatigue characteristics are critical material requirements. Automobile companies in order to meet consumer demands have sought to carbon fibre-reinforced composites in the construction of body, interiors, chassis, hoods, and electrical components. Similarly, the marine industry is using CRFCs to construct ship and boat components. Carbon fibre-reinforced composites have enabled the construction of longer and lightweight wind turbine blades while also ensuring a long service life due to excellent fatigue characteristics. Moreover, the use of carbon fibres does not limit to reinforcement in composites. It has been found that activated carbon fibres are useful as absorbents for energy storage and air purification. Activation of carbon fibres using agents like KOH and NaOH has been carried out to give them a porous structure. Micropores on the carbon fibres enable them to have a high sorption capacity. The lightweight and high electrical conductivity of carbon fibres have also made them potential candidates for electrode materials in fuel cells and supercapacitors. The performance of a supercapacitor is defined by the surface area available on the electrode to store ions. Carbon fibres have high specific surface area as well as high conductivity, which makes them a perfect electrode material for high performance supercapacitors.

It is evident that the applications of the exceptional mechanical and electrical properties of carbon fibres are extensive. The manufacturing process and raw material (or precursor) used in producing carbon fibres play a vital role in attaining these properties. The manufacturing process is a two-step process which involves; a fibre spinning process and a heat treatment step. While the structural and functional properties of carbon fibres are heavily dependent on the heat treatment step, the physical aspects of the fibres depend on the fibre spinning process. Some applications require specific structures of non-woven mats or specific morphologies. Several fibre-spinning techniques have been employed but none exhibit the versatility and ease of electrospinning. Furthermore, electrospinning has enabled the production of fibres having diameter in the nanometer range. Electrospinning involves using electrostatic forces to stretch a polymer solution which undergoes evaporation as it is being stretched, eventually depositing solid polymer fibres on a collector. A set of process and solution parameters govern the electrospinning process. Altering these parameters allows the production of various fibre architectures and morphologies. The most commonly used precursor for production of carbon fibres is polyacyrlonitrile (PAN). Electrospinning of PAN solutions in dimethylformamide (DMF) produce PAN fibres which on suitable heat treatment yield high quality carbon fibres. However, since PAN is derived from petroleum products and the costs associated with manufacturing PAN are high, researchers have looked for low-cost and sustainable precursors. Lignin, a natural polymer found in plants has emerged as a potential precursor for carbon fibres. Lignin is a polymer characterised by its complex aromatic molecular structure, which differs depending on its source. Researchers have produced carbon fibres from electrospun lignin fibres. However, due to its complex structure, the electrospinning of lignin for production of carbon fibres has been under scrutiny in recent times

This project studies the electrospinning of softwood lignin and polyvinyl alcohol (PVA) blend solutions in aqueous NaOH in order to learn about their potential for carbon fibres. This is done by characterizing the kraft lignin used in this study, and then carrying out electrospinning of various solutions consisting of mixtures of kraft lignin and PVA in different concentrations in aqueous NaOH, followed by characterizing the resultant fibres. The effects of changing process parameters like applied voltage, flow rate and tip-collector distance on the lignin-PVA fibre morphology have been attempted to study. Solution parameters like viscosity, surface tension, conductivity, solvent volatility also play a vital role in the electrospinning process and how the materials used in this study affect these properties is investigated. The need of using another polymer along with lignin, PVA in this case, has been discussed. On doing the above mentioned tasks, a correlation between the fibres morphologies, the electrospinning parameters and lignin used in this study can be made, which is the aim of this project.

2 | Lignin - Structure

The strong contention of lignin becoming a precursor for carbon fibres comes from its abundance in nature and its aromatic structure. Lignin is the second most abundant lignocellulosic natural polymer after cellulose [Akpan and Adeosun, 2019]. It is mainly found in the cell wall of plant and woody species. Moreover, lignin is a byproduct in the pulp and paper industry, making it easily accessible. Currently 50–70 million tonnes of lignin is produced annually at pulp and paper facilities world-wide and about 98% of the lignin obtained at the paper industries is being burned as low value fuel to generate electricity and heat [D.S. Bajwa, 2019]. Lignin has a complex and non-uniform structure, which has contributed to its hindered valorization. It is a three-dimensional amorphous polymer formed by the disordered polymerization of phenylpropane monomers with hydroxyl or methoxy substituents. The three basic types of monomers that make lignin are; coniferyl alcohol, sinapyl alcohol, and p-coumaryl alcohol, also known as monolignols (shown in Figure 2.1). Regardless of the source, lignin is biologically synthesized from these three monolignols but depending on the source, the amount of each unit in the polymer differs [Akpan and Adeosun, 2019].

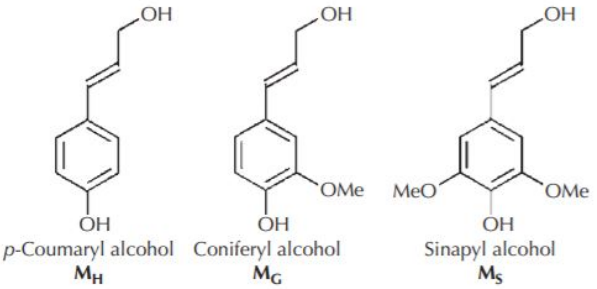

Figure 2.1: The three basic monomers of lignin; p-Coumaryl alcohol M_H, Coniferyl alcohol M_G, and Sinapyl alcohol M_S [Sun, 2010]

Once synthesized in the cytoplasm, monolignols are transported to the cell wall where they are oxidized and polymerized to form lignin comprised of two major unit types - guaiacyl P_G, derived from coniferyl alcohol M_G and syringyl P_S, derived from sinapyl alcohol M_S . p-Hydroxyphenyl units P_H, derived from p-coumaryl alcohol M_H, occur only as a minor component of lignin [Sun, 2010].

These monolignols form lignin macromolecules via free radical coupling mechanisms in a polymerization process called lignification. The polymerization is initiated by enzymatic (laccase and/or perioxidase) dehydrogenation of a monolignol. Lignification starts with dehydrogenative dimerization or cross-dimerization of two monolignol molecules and continues with further cross-coupling of the preformed dimers or oligomers and incoming monolignols so that lignin macromolecules are produced [Sun, 2010]. Cross-coupling between two growing lignin macromolecules may also occur when a free phenolic guaiacyl unit is available for free radical coupling with another free phenolic guaiacyl or syringyl unit [Sun, 2010]. The coupling between molecules takes place in a chemical combinatorial manner, so that the ratio of possible outcomes depends largely on the chemical nature of each of the monomers and the circumstances in the cell wall [Akpan and Adeosun, 2019]. Thus, the lignin structure depends largely on the availability of the monolignol radicals. Lignin polymerization is extremely flexible such that it allows the incorporation of any phenolic that by chance is within the vicinity of the lignification site subject to its tendency of chemical cross-coupling [Akpan and Adeosun, 2019]. The complexity in lignin's structure is evident from the nature of its polymerization process. Representative structures of lignin are shown in Figure 2.2.

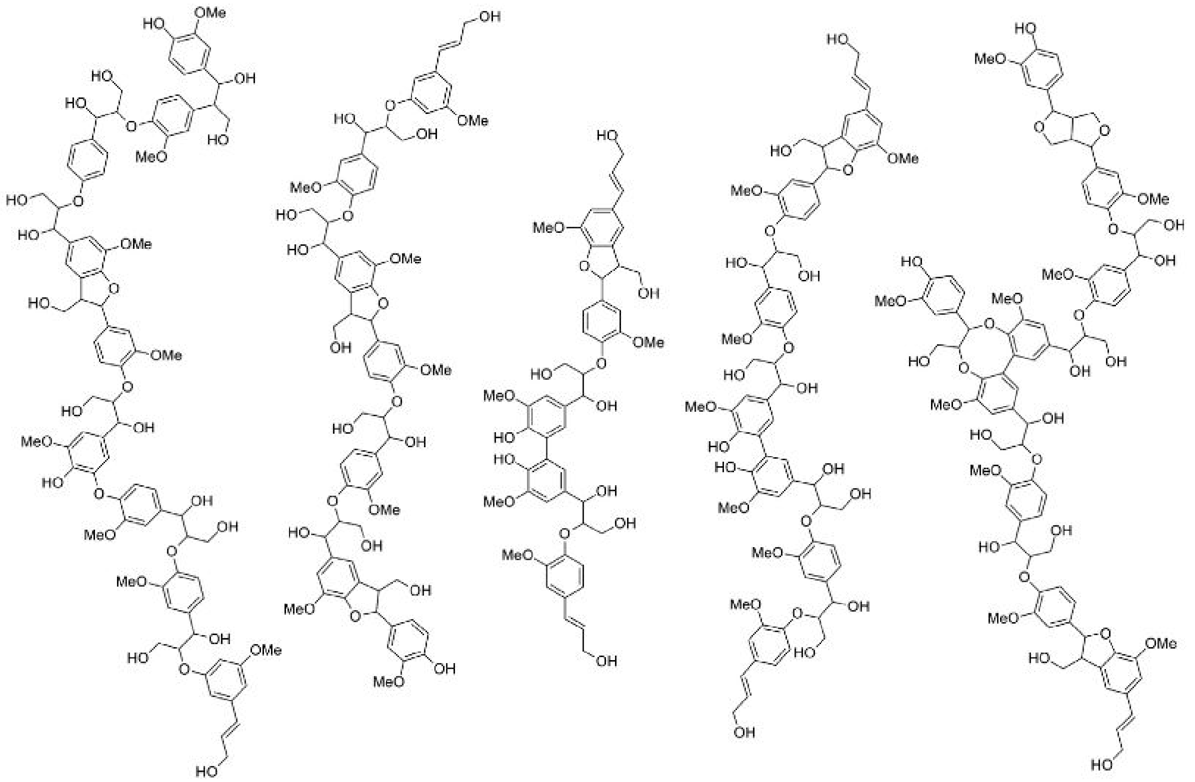

1a **1b** **1c** **1d** **1e**

Figure 2.2: Representative structures of lignin polymer [Heiko Lange, 2013]

Lignin is present in plants as a part of a biopolymer called ligonocellulose which is also composed of cellulose and hemicellulose. Thus, in order to isolate the lignin from this copolymer, it has to undergo an extraction process. Industries and researchers use several extraction techniques to achieve this and the structure and properties of the native lignin alter, depending on the extraction technique used. Thus, lignin is also classified on the basis of the extraction process. Out of several types of techniques the most common ones are Kraft lignin, Lignosulphonates and Organosolv lignin.

2.1 Kraft lignin

Kraft lignin is obtained industrially by applying an aqueous solution containing sodium sulphide and sodium hydroxide to dissolve lignin from lignocellulose forming a black solution called 'black liquor'. The Kraft process proceeds by cleaving the 1,4 links in cellulose, thereby allowing the lignin component of the copolymer to be extracted. In the process, lignin with aliphatic thiol groups is produced with extensive hydrophobic character and thus Kraft lignin shows low solubility in water [Akpan and Adeosun, 2019]. Evaporation and precipitation methods are then used to recover the lignin from the liquor. Kraft lignin undergoes substantial structural changes during extraction including cleavage of aryl ether bonds arising from depolymerisation during the cooking process [Akpan and Adeosun, 2019]. The molecular weights of kraft lignin have been reported within the range of 200 to 200,000 Da, with polydispersity within the range of 2-8 [Allison Tolbert, 2014]. However, the molecular weight of kraft lignin can be variable depending on the type of wood, analysis method, and isolation procedure. Figure 2.3 shows the structure of Kraft lignin.

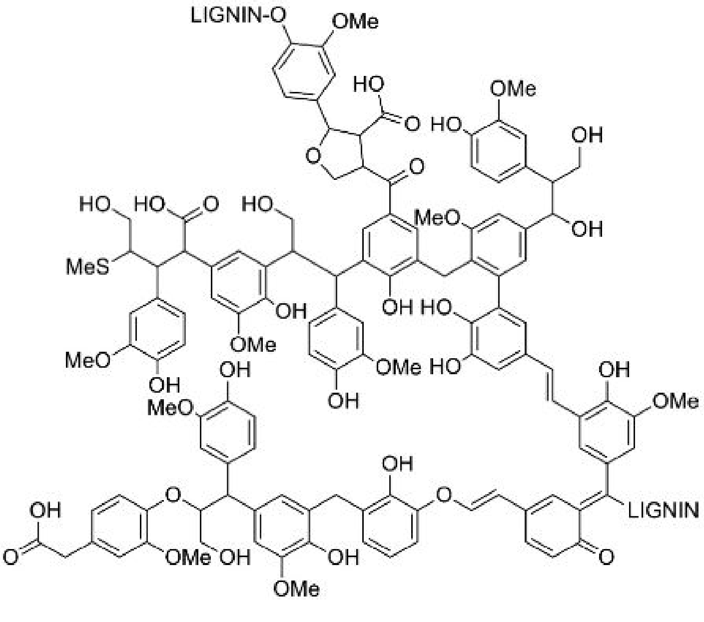

Figure 2.3: Structure of Kraft lignin [Heiko Lange, 2013]

2.2 Lignosulphonates

Lignosulphonate is the sulphonated lignin that is removed from wood by sulphite pulping process. This process uses sulphurous acid and/or a sulphite salt containing magnesium, calcium, sodium, or ammonium at varying pH levels to produce lignin denoted as lignosulphonates. Compared to Kraft lignin (1.2% sulphur), lignosulphonates contain a relatively high sulphur content (5%). Unlike Kraft lignin, the presence of hydrophilic sulphite groups together with hydrophobic aromatic structures makes lignosulphonate to be amphiphilic in nature [Akpan and Adeosun, 2019]. Figure 2.4 shows the structure of lignosulphonate lignin. The physicochemical properties of lignosulphonates are affected by the metal cation (Mg, Ca, Na or NH_4) of the sulphite salt used during the pulping process. They possess relatively high weight-average molecular weight, with low amount of OH groups and a broad distribution of molecular weights.

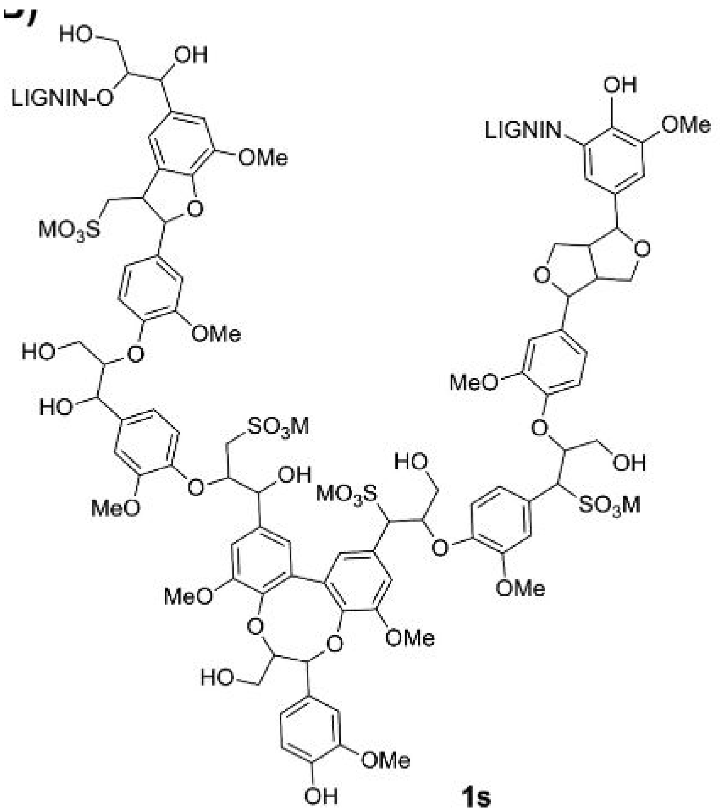

1s

Figure 2.4: Structure of Lignosulphonate lignin [Heiko Lange, 2013]

2.3 Organosolv lignin

Organosolv lignin is obtained via a pulping process in which a mixture of organic solvent/solvents and water is used as a cooking medium. The most commonly used solvents are: acetic acid, formic acid, ethanol, and peroxiorganic acids. The best known variant is the Allcel process which uses ethanol or an ethanol–water mixture [Heiko Lange, 2013]. Organosolv lignin can be easily separated from the pulping solvents either by solvent removal and recovery, or by precipitation with water accompanied by distillation to recover solvent. The homogeneity of organosolv lignin is higher than that of lignosulphonates or Kraft lignins and they have a relatively lower average molecular weight [Akpan and Adeosun, 2019]. They also possess higher amount of phenolic hydroxyl groups and thus are known to exhibit hydrophobicity [William O.S. Doherty, 2011].

It is clear that the structure of lignin is highly heterogeneous before as well as after its extraction. As a result of this complex and non-uniform structure the usability of lignin in high value applications is limited and inadequate. To overcome this, fractionation of lignin to obtain lignin fractions with a more uniform structure and narrow molecular weight distribution has been employed. Several fractionation techniques have been utilized such as ultrafiltration, pH dependent successive precipitation and solvent extraction. In solvent extraction, lignin fractions are isolated by treating the lignin with solvents of varying polarities. Insoluble and soluble fractions with different average molecular weights are obtained with each solvent but this time with a narrower weight distribution and homogeneity in the structure. In pH dependent precipitation, the lignin fractions are obtained by treating the parent lignin with different concentrations of an acidic solvent like concentrated sulphuric acid. The difference in pH leads to precipitation of different lignin fractions. Fractionation leads to the attainment of lignin with well defined structure and molecular weight.

From the monomers involved in the polymerization of lignin it is clear that lignin is rich in carbon. In that sense, lignin has high potential to be a precursor for carbon fibres The conversion of a precursor to a carbonaceous material is a thermochemical one. The material undergoes heat treatment at temperatures lying in the range of 1000 °C to 2000 °C in an inert atmosphere, which leads to removal of non-carbon elements and eventually resulting in a solid carbonaceous material. It has been a challenge to transform the complex and amorphous structure of lignin to a crystalline structure of carbon fibres. However, apart from the material characteristics the fibre spinning process also plays an important role in achieving high grade carbon fibres.

3 Electrospinning

3.1 Electrospinning process

Electrospinning is a fibre fabrication technique capable of producing continuous fibres having diameter in the nanometer range. It has been extensively used in the fabrication of polymeric fibres but has been found useful in preparing metal and ceramic fibres as well [Sungyeoul Kim and Yoon, 2015; Panda, 2007]. Electrospinning draws nanofibers from the material solution or melt using electrostatic forces. A basic electrospinning setup consists of three primary components; a needle which acts as an electrode, a collector which is the counter-electrode and a voltage supply. Figure 3.1 shows a vertical electrospinning setup. A polymer solution is filled into the needle, to which an electric field is applied using a high voltage power supply. On application of sufficient voltage, an electrified jet of polymer solution erupts from the polymer droplet on top of the needle and moves towards the direction of the collector. On its way to the collector, the solvent from the solution evaporates and solid polymeric fibres are deposited on the collector. Fibres are highly valuable and highly functional objects in technical and life science areas. For an application, in addition to choosing the right material with the desired properties, it is important to have knowledge of how to achieve particular fibre -characteristic intrinsic structures via the fibre processing technique. Electrospinning, which on first impression appears to be a simple process to produce nanofibres has several complex processes behind it, which in turn are governed by a number of process and solution parameters.

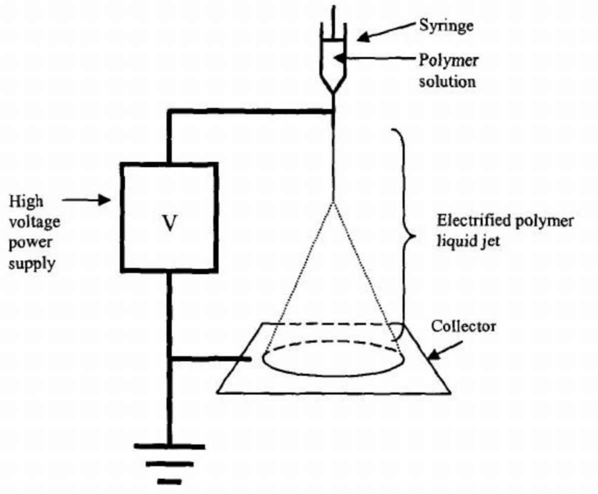

Figure 3.1: Schematic representation of an electrospinning setup [Seeram Ramakrishna and Fujihara, 2005]

The electrospinning process is initiated when charges induced in the solution and an external electric field work to stretch the solution at the tip of the needle such that the electrostatic forces overcome the surface tension of the solution and an electrified jet is produced [Li and

Xia, 2004]. On application of a high voltage, the solution droplet at the tip of the needle gets electrified and experiences two types of electrostatic forces; a repulsive force between the surface charges and the Coulombic force exerted by the external electrical field [Li and Xia, 2004]. At a critical value of voltage, these forces stretch the solution droplet such that it attains a conical shape, commonly known as Taylor cone, which further stretches to form a linear fluid jet. The jet initiates from the tip of the Taylor cone due to the electric field enhancement at the protrusion [Joachim H. Wendorff and Greiner, 2012]. Figure 3.2 shows the Taylor cone and the jet leaving from its tip. At the protrusion, there is higher local charge density which results in electric field concentration and thus the stronger electrostatic forces initiate the jet from this region [David Lukas and Pokorny, 2008]. The linear path of the electrified fluid jet is usually short-lived. At some distance away from the needle tip the jet is no longer able to follow a straight path in the direction of the collector. It bends, turns sideways and undergoes a sequence of spiraling motions. Due to this continuous bending motion, the path of the jet increases and the jet becomes thinner before settling on the collector. This deviation of the fluid jet from a straight part via a bending motion is commonly known as bending instability. Figure 3.3 shows the path of a polymer jet experiencing bending instability. The bending instability is caused by the repulsive electrostatic interactions between adjacent charges in the polymer jet, resulting in deviations from the perfect lateral orientation of the fibre jet. This initiates the spiraling motion of the jet. The jet takes a linear path as long as the longitudinal stress in it is high enough to counteract these instabilities. After a certain time, this stress decays and the jet takes a bending motion due to the electrostatic forces [Darrell H. Reneker and Koombhongse, 2000]. Another instability acting on the polymer solution jet is the Rayleigh instability which is controlled by the surface energy contributions of the solution. The surface tension of the solution tends to minimize the surface area of the solution jet by breaking the long cylindrical element into individual isolated droplets [Joachim H. Wendorff and Greiner, 2012]. This results in deposition of polymer beads on the collector. The instability becomes weaker with increasing electric fields and surface charges, respectively, and it becomes totally suppressed above a critical field for which the electric force coming from the surface charges exceeds the surface-tension [Joachim H. Wendorff and Greiner, 2012]. Another axisymmetric instability observed in fluid jets is completely due to charge contributions. A change in the jet's radius causes a modulation of the surface charge density. This in turn generates tangential electrical forces that couple to the radius modulation and amplify it. The formation of beads along a fibre is the final result of such an instability [Carroll and Joo, 2009]. It is the presence of these instabilities and their superpositions that leads to the formation of a range of fibre architectures and thus functions. Electrospinning is a unique process which allows the production of uniform nanofibers, beaded fibres, porous fibres, fibers with flat ribbon-like cross-section, among various other morphological features. All these characteristics can be achieved by proper control of the process and solution parameters. Each parameter has a science of its own which influences the electrospinning process. The solution parameters which influence the process include surface tension, viscosity, conductivity and solvent volatility. Viscosity is majorly a property of the material used to obtain fibres of, whereas, surface tension, conductivity and solvent volatility are solvent properties. The process parameters that affect the fibre morphology are applied voltage, solution feed rate, tip - collector distance, needle diameter and type of collector. Additionally, the ambient parameter relative humidity has also found to influence the electrospinning process and fibre morphology.

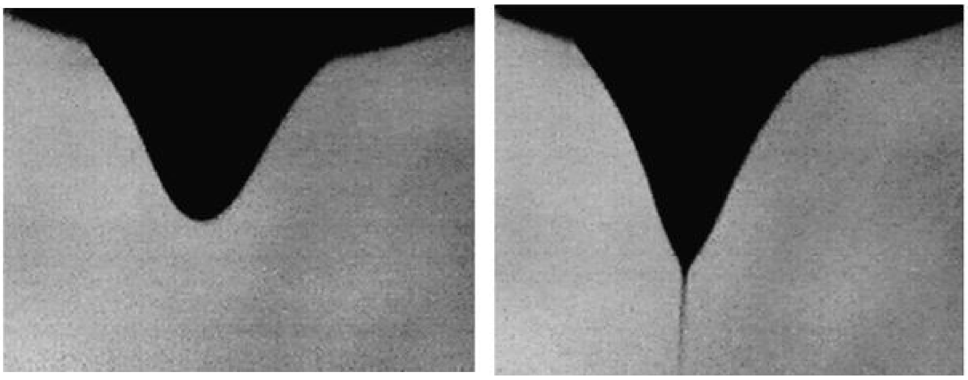

(a) (b)

Figure 3.2: Taylor cone (a) without jet initiation and (b) with jet initiation [Reneker and Yarin, 2008]

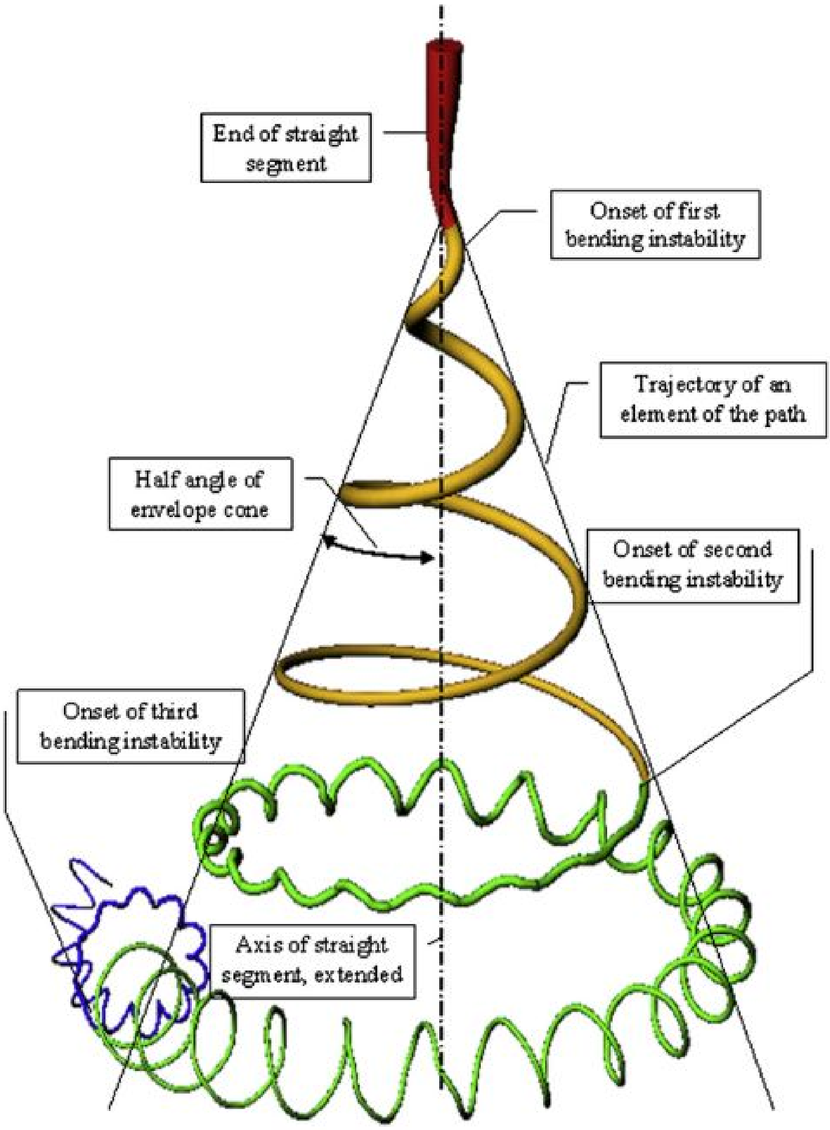

Figure 3.3: Schematic representation of the path of the jet as a result of the bending instability setting in [Reneker and Yarin, 2008]

3.2 Electrospinning of lignin fibres

The complex and amorphous structure of lignin is a hindrance in the production of highly ordered carbon fibres. Lignin-based carbon fibres produced by conventional fibre spinning processes have yielded in carbon fibres with mechanical properties that would classify them as general-purpose carbon fibres and not high grade carbon fibres [Meng Zhang, 2014; Shimizu, 1992]. High-modulus, high-strength carbon fibres from lignin require that the molecules are more organized. This molecular orientation, or the lack thereof, appears to be the primary limitation for the formation of high-modulus carbon fibres from lignin [Vipul Dav and Glasser, 1993]. The production of lignin fibres with small diameters could facilitate a more organized arrangement of atoms and electrospinning offers a simple way to produce such fibres. In addition to this, it has also been found that not all types of lignin are suitable for conventional fibre spinning techniques like melt-spinning [Ylva Nordström, 2007]. Thus, electrospinning of lignin fibres has been performed and studied extensively. As mentioned in section 3.1, solution properties play an important role in the formation of desired fibres morphology. One of these properties is viscosity. If the solution viscosity is not high enough, circular uniform fibres are not produced and instead electrospraying or formation of beaded fibres could take place. A major issue with lignin is that it is unable to form sufficiently high viscosity solutions. To overcome this, synthetic polymers like PVA and PEO are added to lignin solutions. Ian Dallmeyer [2010] carried out the electrospinning of seven different technical lignin types using DMF as the solvent. They found that pure lignin solutions did not produce uniform fibres due to their low viscosities and thus added Polyethylene oxide (PEO) to the solutions. On addition of PEO, they achieved uniform fibres with diameters in the range of 700 nm to 1300 nm, from various polymer concentrations. Mariko Ago and Rojas [2012] produced uniform fibres from aqueous solutions composed of Softwood kraft lignin, Polyvinyl alcohol (PVA) and Cellulose nanocrystals (CNCs). They first electrospun fibers from the aqueous solutions of PVA and Lignin at different concentrations. The fibres obtained from these solutions, on average, had radii lying in the range 60 nm to 500 nm. On adding CNCs, they observed that there was significant increase in viscosity of the solutions which lead to fibres of larger radii. On contrast to electrospinning of lignin solutions in the presence of a binder polymer, Manuel Lallave and Loscertales [2007] electrospun pure Alcell lignin fibres in solutions of ethanol-water mixture. They produced uniform lignin fibres with diameters ranging from 400 nm to 2 µm. It is clear from literature survey that electrospinning of lignin leads to the formation of fibres in the nanometer range. The electrospinning results depend on the type of lignin used and the parameters involved in the process. A thorough description of the parameters is given in the following section.

3.3 Solution Parameters

3.3.1 Conductivity

As mentioned earlier, the electrospinning process is initiated when the solution contains sufficient charges to overcome the surface tension of the solution. This calls into picture the ability of the solution to carry charges, that is, its conductivity. Furthermore, the stretching of the fluid jet and the path it takes also depends on the conductivity. Since the stretching of the solution is due to mutual repulsive forces between surface charges, an increase in number of charges by increasing the conductivity increases the amount of stretching and in turn has found to result in fibres with smaller diameter. Angammana and Jayaram [2011] studied the effects of solution conductivity on the electrospinning of aqueous polyethylene oxide (PEO) solutions. Sodium chloride was added to prepare solutions with varying conductivity. They reported a decrease in fibre diameter with increase in conductivity of the solution used. The PEO/water solution with no NaCl added to it had the lowest conductivity and produced fibres having highest average diameter. The linear path of the fluid jet and its bending instability region has a major influence on the fibre diameter. Surface charge density, which increases with conductivity, is a main factor that decides the stretching and path of the fluid jet. The increase in conductivity of a solution means a greater number of ions in the solution. This leads to a higher amount of charges on the surface of the polymer under the external electric field. The higher surface charge density leads to stronger electrostatic forces which encourage elongation of the jet, resulting in smaller fibre diameter. This enhanced stretching also leads to formation of beadless fibres as compared to beaded fibres produced from solution with a lower conductivity [Xinhua Zong and Chua, 2002]. Angammana and Jayaram [2011] reported a decrease in tangential electric field on the surface of the jet due to increase in conductivity of the solution. At high conductivities, the decrease in tangential electric field fails to keep the jet in a straight part for a long time and enhances the bending instability. This results in a longer jet path and eventually shorter fibre diameters. However, this decreased tangential force has a negative effect on the formation of the Taylor cone during jet initiation. Another observation related to conductivity is the formation of multiple jets from a single polymer droplet [Angammana and Jayaram, 2011; Sureeporn Koombhongse, 2001]. An increase in conductivity increases the probability of ejection of multiple number of jets. This behaviour has been attributed to enhanced local electrical field at the droplet surface as a result of the increased amount of charges. Addition of salts to the electrospinning solution is a common way of increasing its conductivity. Xinhua Zong and Chua [2002] studied the effect of addition of ionic salts on the fibre morphology. Three different salts, namely NaCl, KH_2PO_4 and NaH_2PO_4, were used to perform a comparison study. They found that the average fibre diameter reduced with size of the salt used. Fibres electrospun from the solution containing NaCl produced fibres with lowest average diameter [Xinhua Zong and Chua, 2002]. The reasoning reported behind this was that the ions of NaCl have a smaller radius, which gives them a higher charge density and thus higher mobility under an external electric field. The higher mobility causes the stretching forces acting on the fluid jet to be stronger, resulting in thinner fibres. Delaram Fallahi [2009] found that an increase in solution conductivity lead to increase of the fibre diameter. Addition of LiCl to solutions of polyacrylonitrile in DMF increased their conductivity. The high conductivity lead to stronger elongation forces which could lead to more volume of solution being drawn and thus thicker fibres [Delaram Fallahi, 2009; Chidchanok Mit-uppatham and Supaphol, 2004a]. From the studies mentioned above it is clear that conductivity increases the number of ions in the solution which leads to a higher charge density. However, this effects the electrospinning process via a number of phenomena and the fibre morphology achieved depends on the dominance of the phenomena.

3.3.2 Surface Tension

Another solution property which plays an important role in the initiation of the electrospinning process is surface tension. The surface molecules of a liquid experience an inward force due to the phenomenon of surface tension resulting in the surface to attain a minimum area. This surface tension gives the electrostatic forces in the solution something to overcome before the charges can deform the droplet at the tip of the needle and move towards the collector. For a solution with lower surface tension, the critical applied voltage required for formation of the Taylor cone and jet initiation is lower [Li Yao, 2003]. After the fluid jet has been formed and is on its path to the collector, the surface tension continues to minimize the surface area of the fluid body giving rise to the possibility of Rayleigh instability to occur. The solution properties viscosity, surface tension and net charge density majorly influence the formation of beads and beaded fibres [H. Fong, 1999]. The occurrence of Rayleigh instability results in the formation of beads [Weiwei Zuo and Zhang, 2005]. Figure 3.4 shows the electrospinning of beads as a result of the Rayleigh instability. As mentioned earlier, the Rayleigh instability is completely driven by surface tension. The surface tension tends to break the fluid jet into droplets, but the viscosity and net charge density tend to work against this and keep the solution jet stretched. Thus, whether beads will form or not is decided by effect of which property is more dominant. The dominant influence of surface tension over viscosity and net charge density leads to the formation of beads and beaded fibres [Jian-Yi Zheng and Sun, 2014; H. Fong, 1999]. When the viscosity of the solution is low, more free solvent molecules are together and due to the surface tension, these molecules tend to contract the surface of the liquid jet. This aggregation of solvent molecules and the force due to surface tension leads to the spherical beads along the fibre. Weiwei Zuo and Zhang [2005] studied the effect of surface tension on bead formation by keeping the solution conductivity of the various solutions constant. The solutions with higher surface tension produced beaded fibres with larger beads. A solution with higher surface tension would require a high voltage for jet initiation and at the same time produce beaded fibres. Thus, selecting a solvent for electrospinning requires consideration of the surface tension of the solvent.

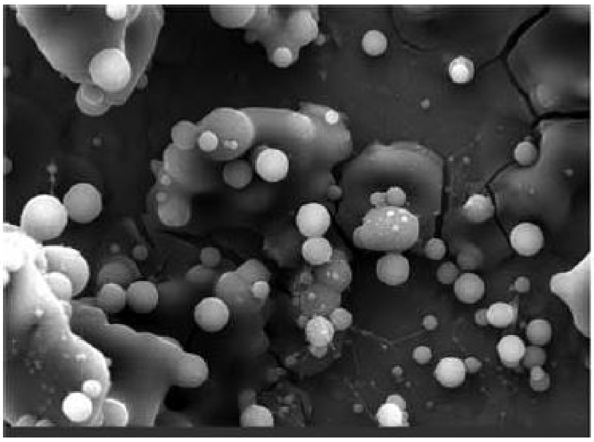

Figure 3.4: Deposition of beads as a result of the Rayleigh instability due to dominant influence of surface tension [Vida Poursorkhabi and Misra, 2015]

3.3.3 Viscosity

Viscosity has been regarded by researchers as one of the highly influential parameters in electrospinning. Viscosity of polymer solutions is due to the internal friction between entangled, swollen macromolecules and the surrounding solvent molecules [Brazel and Rosen, 2012]. It plays an important role in maintaining an elongated polymer solution jet once it has left the tip of the needle. The breaking of the fluid jet due to Rayleigh instability is avoided when the solution has high enough viscosity. For such a solution, the polymer chains interact with the solvent molecules to a higher extent, causing the solvent molecules to be distributed along the entangled chains [Seeram Ramakrishna and Fujihara, 2005]. This prevents the surface solvent molecules from contracting the surface enough to break the jet. Thus, one of the conditions for electrospinning of fibres to take place is that the solution should have sufficient viscosity. When a polymer is unable to create sufficient viscosity with the desired solvent, binder polymers are added in order to achieve that viscosity. polyethylene oxide and polyvinyl alcohol are commonly used binder polymers. H. Fong [1999] observed the effect of viscosity on fibre formation by electrospinning aqueous solutions with different concentrations of Polyethylene oxide (PEO) and found that the occurrence of beads reduced as the solution used got more viscous. As viscosity gets higher, the bead shape goes from spherical to spindle-like and the distance between adjacent beads on a fibre gets larger. An increase in viscosity has found to result in uniform fibres with larger diameter [Vida Poursorkhabi and Misra, 2015; K. Nasouri and Kaflou, 2012]. The increase in viscosity imparts stronger viscoelastic forces against the stretching forces due to the charges. This stronger viscoelastic force prevents the electrostatic forces from stretching the solution as much as they would a solution with lower viscosity [Teeradech Jarusuwannapoom, 2005]. The lesser stretching results in fibres with larger diameter. Furthermore, the stronger viscoelastic forces due to increase in viscosity reduce the jet path by reducing the bending instability region causing thicker fibres to be formed [Seeram Ramakrishna and Fujihara, 2005]. Since viscosity of the electrospinning solution is function of the polymer-solvent system, there is a critical concentration at which the sufficient viscosity is attained. This brings into picture the role of polymer concentration and molecular weight of the polymer used. These factors affect the viscosity of the solution and in turn the electrospinning process. Various researchers through experimental and theoretical analyses have found that there is a power law relation between diameter of the fibre and viscosity of the solution as well as between the diameter and polymer concentration. These power law relations are:

$d \propto \eta^{\alpha}$

$d \propto C^{\beta}$

where d is the diameter of the electrospun nanofibres, η the solution viscosity, C the solution concentration and α and β are the scaling exponents.

A combination of the two relations gives rise to the following relation between viscosity and concentration [K. Nasouri and Kaflou, 2012] :

$\eta \propto C^{\delta}$

where δ is the scaling exponent and depends on the polymer. Ji-Huan He and Yu [2008] experimentally verified this relation and found the scaling exponent to have a value of 6 for polyacrylonitrile with a molecular weight of 70,000 Da.

The increase in viscosity of a solution with concentration of the polymer is due to increase in number of chain entanglements. The molecular weight of the polymer used has the same effect and the viscosity of a solution will be higher using a polymer with higher molecular weight at the same concentration [Seeram Ramakrishna and Fujihara, 2005]. Vida Poursorkhabi and Misra

[2015] studied the effect of molecular weight on the electrospinning process by using two molecular weights of PEO in their solutions, one 200,000 Da and the other 5,000,000 Da. The viscosity of the solutions prepared using PEO of molecular weight 5M Da were higher than their 200k Da counterparts. For the same concentration, solution with 200,000 Da PEO gave beads while the one with 5,000,000 Da gave uniform fibres. It has been made clear that high viscosity facilitates electrospinning of uniform fibres. However, highly viscous solutions become difficult to electrospin and in some case do not spin at all. Extremely high viscosities are achieved at high concentrations of polymer. In such cases, the droplet formed at the tip of the needle dries out which makes jet initiation hard [Xinhua Zong and Chua, 2002]. Teeradech Jarusuwannapoom [2005] carried out electrospinning of polystyrene solution in t-butylacetate at various concentrations. At a concentration of 20% (w/v) the solution viscosity was 290 cP and the electrospinning lead to formation of uniform fibres. Whereas, at 30% (w/v), a viscosity of 1936 cP was attained, and the highly viscous solution clogged the tip of the needle and no electrospinning could be performed [Teeradech Jarusuwannapoom, 2005]. Solutions with insufficient viscosity lead to electrospinning of beads and solutions with extremely high viscosity hinder the entire electrospinning process. Thus, for a particular polymer-solvent system there is a range of viscosity values between which uniform fibres are produced.

3.3.4 Volatility of Solvent

Evaporation of solvent is a vital phenomenon which takes place when the polymer jet leaves the tip of the needle and moves towards the collector. Fibre morphology is highly dependent on the volatility of the solvent. If volatility of the solvent is low, electrospinning could lead to formation of thin polymer solution films instead of fibres of any sort [Seeram Ramakrishna and Fujihara, 2005; Nakagawa Yuya and Kim, 2010]. Volatility of a solvent is not a quantifiable property but it is indicated by factors like vapor pressure and boiling point. A high boiling point indicates low volatility whereas high vapor pressure indicates high volatility. However, other factors like specific heat, heat of vaporization, surface tension, interaction between solvent and solute molecules affect the volatility of a solvent [Seeram Ramakrishna and Fujihara, 2005]. Nakagawa Yuya and Kim [2010] observed the effect of solvent volatility by electrospinning Polyvinylpyrrolidone (PVP) solution using four different solvents with varying boiling points. In increasing order of boiling point and decreasing order of volatiliy, ethanol, methanol, water and DMF were the chosen solvents. Due to high evaporation rate, the solutions in ethanol produced uniform solid fibres. Electrospinning of solutions in DMF, owing to the low volatility of the solvent, lead to formation of film-like morphologies instead of fibres. Low volatility of the solvent also leads to the fusion of wet fibres, resulting in fibre junctions to be formed [Chidchanok Mit-uppatham and Supaphol, 2004b]. In contrast, highly volatile solvents could lead to drying up of polymer solution at the tip of the needle itself, that is, even before jet initiation, which makes the electrospinning process sporadic. Researchers have attributed the occurrence of different types of morphological features to solvent evaporation rate. Formation of fibres with flat ribbon-like cross section has been observed and been credited to the high volatility of the solvent [Sureeporn Koombhongse, 2001; M. Dhanalakshmi, 2008]. Figure 3.5 shows fibres with flat ribbon-like cross section. Celebioglu and Uyar [2011] used a solvent mixture of two highly volatile solvents, dichloromethane and acetone, in different ratios to study their effect on fibre morphology. The fibres acheived from majority of their solutions had a flat ribbon-like cross-section. The reason for this is the formation of a polymer skin due to rapid vaporization of the solvent. The uneven evaporation of the solvent from core to surface and the formation of the polymer skin causes the atmospheric pressure to collapse the fibre and give it a flat cross-section [Sureeporn Koombhongse, 2001]. Porous fibres can be prepared by using highly volatile solvents which induce phase separation in the solution jet [Celebioglu and Uyar, 2011; Silke Megelski, 2002; Yasuhiro Miyauchi and Shiratori, 2006]. Silke Megelski [2002] electrospun polystyrene in various solvents and found that as the solvent got more volatile, more pores began to form on the fibres. THF and DMF are both commonly used solvents in electrospinning, where THF is highly volatile and DMF has low volatility. Celebioglu and Uyar [2011] used a mixture of the two in different ratios and found that as the amount of DMF increased the porosity of the fibres formed decreased. When the solution was completely made from DMF as the solvent, no pores were observed. The rapid evaporation of the solvent before the jet had erupted from the droplet caused a decrease in temperature of the solution jet due to evaporative cooling [Silke Megelski, 2002]. Phase seperation due to this drop in temperature takes place and gives a polymer-rich phase and a solvent-rich phase. The polymer-rich phase solidifies to form the fibre bulk whereas the solvent-rich phase evaporates to form pores. Rapid solvent evaporation could also lead to high viscosity of the solution jet by increasing the polymer concentration in it which in turn leads to fibres with larger diameter [Holly McIlwee Golecki, 2014]. From research it has been made clear that optimum volatility of the solvent is critical to the electrospinning process.

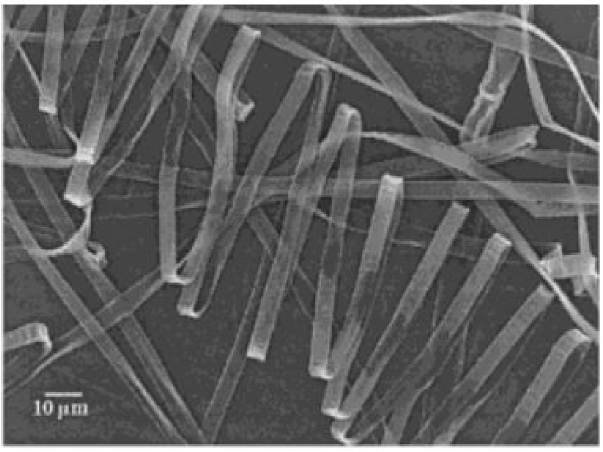

Figure 3.5: Fibres with flat ribbon-like cross section formed due to rapid solvent evaporation [Sureeporn Koombhongse, 2001]

3.4 Process Parameters

3.4.1 Applied Voltage

Electrostatics is the foundation on which the process of electrospinning is built. The process is possible only when there is a potential difference between the needle and collector. Applying voltage induces charges in the solution which creates the potential difference. The first influence of the applied voltage is in overcoming the surface tension to form the Taylor cone, from which the jet initiates. Since the electrostatic forces due to the charges and external electrical field cause stretching and acceleration of the polymer solution, the applied voltage also has an influence on the stability and shape of the Taylor cone [Xinhua Zong and Chua, 2002]. As the critical voltage is reached, the droplet deforms into a conical shape and jet is initiated. But depending on the feed rate, the nature of the conical deformation changes with the applied voltage. Even though the jet is initiated at the critical voltage, the taylor cone could cease to exist at irregular intervals of time. Xinhua Zong and Chua [2002] observed this by varying the applied voltage to the solution. For the poly(D,L-lactic acid) solutions in DMF, the critical voltage was 16 kV but a stable Taylor cone and uninteruptted electrospinning was not achieved until the voltage reached 20 kV. Furthermore, they observed that as the voltage was increased to 25 kV, the taylor cone began to recede and at 30 kV the spinning was initiated from inside the needle. The fibre morphology as a result of the very high voltages was that bead formation took place and the bead density increased with voltage. The reason for this is speculative but the fluctuations in the charge density due to the Taylor cone receding and change in shape of the surface from which the jet originates could facilitate the formation of beads [R. V. N. Krishnappa, 2003; Xinhua Zong and Chua, 2002; J.M. Deitzel, 2001]. A common observation regarding the applied voltage is the reduction in diameter of the fibres with increase in voltage [Silke Megelski, 2002; Larrondo and Manley, 1981; Joon Seok Lee, 2004]. The increase in applied voltage increases the strength of the repulsive forces between the charges which enhances the stretching of the polymer jet, leading to thinner fibres. Baumgarten [1971] had a similar observation on increasing the applied voltage for the electrospinning of a copolymer containing acrylonitrile, methyl acrylate and sodium styrene sulphonate in DMF. However, they also observed that on further increasing the applied voltage, the fibre diameter started to increase. Chunxue Zhang [2005] made the same observation when electrospinning polyvinyl alchohol in water. They attributed the increase in fibre diameter to the increase in amount of solution drawn from the needle. The higher applied voltage strengthens the external electrical field which increases the acceleration of the polymer solution while it leaves the needle, causing more mass to be drawn out. The change in acceleration of the polymer jet due to the applied voltage also alters its flight time, which in turn has an effect on the fibre diameter [Shengli Zhao, 2004]. A longer flight time allows the jet to experience more elongation which decreases the fibre diameter [Seeram Ramakrishna and Fujihara, 2005]. A voltage just above the critical voltage could be used with the aim of increasing flight time to obtain thinner fibres [Shengli Zhao, 2004]. Another influence of voltage on the electrospinning process that has been observed is the formation of secondary jets from the solution droplets. M.M. Demir [2002] found that a combination of low viscosity and high voltage could result in a number of jets erupting from the solution droplet, with the number of jets increasing at even higher voltages. Apart from the morphology of the fibres, the voltage has found to have an effect on their crystallinity. Shengli Zhao [2004] found that the increased stretching due to increased voltage induces crystallinity in the fibre. The crystallinity of the fibres increased with applied voltage upto 50 kV. The increased stretching of the jet allowed molecules to arrange themselves in an ordered manner. However, when the voltage was further increased from 50 kV, the reduced flight time due to increased acceleration at higher voltages did not give enough time for the ordering of molecules to take place and thus a reduction in crystallinity was observed. In electrospinning, DC voltage is applied to the process. Royal Kessick [2004] studied the effect of using AC voltage on the electrospinning of polyethylene oxide in water. The most critical difference in the electrospinning using AC was the reduction of bending instability. The use of AC voltage to charge the solution results in lesser net charge density on the jet as compared to DC voltage. Since, it is the strong electrical forces between charges that play a role in giving rise to the bending instability, it is significantly reduced when an AC voltage is used [Royal Kessick, 2004]. Royal Kessick [2004] observed the effect of the reduced bending instability due to the AC voltage on fibre formation. On comparison, the fibres produced using the AC voltage were perfectly aligned with each other whereas the ones produced using the DC voltage were randomly deposited with respect to each other, owing to the bending instabilites. Also, due to lesser bending, the fibres deposited using the AC voltage carried residual solvent and had larger diameter. The role of voltage on the process is vital and its effect on the fibre morphology reaches opposite extremes.

3.4.2 Feed Rate

The rate at which the solution is being fed towards the needle tip should be in accordance with the rate at which the jet is being drawn towards the collector, in order to have a smooth electrospinning process. If the solution is fed at rate such that the supply is more than the applied voltage can carry towards the collector, electrospinning is interrupted by solution dripping from the needle tip [Shamim Zargham, 2012]. For a particular value of applied voltage there is a range of solution feed rate for which the Taylor cone is stable and electrospinning of fibres takes place [Delaram Fallahi, 2009]. However, the value of the feed rate in this range does affect the fibre morphology that is obtained. At an optimum value of feed rate, electrospinning is continuous with a stable Taylor cone, which results in a narrow diameter distribution. Deviations from this optimum value gives a wide diameter distribution of the fibres obtained [Shamim Zargham, 2012]. Using a high solution feed rate has been found to produce fibres with large diameters [Xinhua Zong and Chua, 2002; Chi Wang, 2009]. At a high feed rate, the jet created is thicker since more volume of solution is being carried by it. This eventually leads to thicker fibres being collected. Chi Wang [2009] electrospun poly(D,L-lactic acid) in DMF at various feed rates. They reported that at high feed rate since the jet is thicker, the bending instability is reduced. The reduction in bending instability also then leads to fibres with larger diameter. Another effect of high solution feed rate is that since more volume of solution is being drawn, the high amount of solvent does not get enough time to evaporate and thus, wet fibres are deposited [Shamim Zargham, 2012; Raziyeh Ghelich, 2015]. Sheng-Han Chen [2014a] reported the formation of flat ribbon-like fibres due to high solution feed rate. The incomplete evaporation of the solvent due to insufficient time could cause the wet fibres to collapse on hitting the collector [Sheng-Han Chen, 2014a]. Shamim Zargham [2012] observed various defects like blobs and heavy branching of jets at high solution feed rates on electrospinning Nylon 6 fibres. Raziyeh Ghelich [2015] also reported junctions and branches of NiO-GDC fibres forming at high solution feed rate. They attributed this to wet fibres fusing together due to incomplete evaporation of the solvent. For a particular polymer-solvent, at any given voltage there is a corresponding value of feed rate at which stable electrospinning process will take place.

3.4.3 Tip - Collector Distance

The tip – collector distance influences the electrospinning process through two ways; flight time and applied electric field [Seeram Ramakrishna and Fujihara, 2005; Raziyeh Ghelich, 2015]. Christopher J. Buchko [1999] reported the nylon 6,6 fibre morphologies observed on varying the tip – collector distance. Flat ribbons and fused fibres were observed at low tip – collector distances. The less distance decreased the flight time, which was not enough for the solvent to evaporate and resulted in deposition of wet fibres [Christopher J. Buchko, 1999]. Raziyeh Ghelich [2015] studied the effect of varying the tip – collector distance on the electrospinning of NiO-GDC fibres and made a similar observation. At a tip-collector distance of 8 cm, a mat of branched and interconnected fibres were produced and on increasing this distance to 10 cm, the branches and junctions disappeared and individual fibres were produced. The shorter tip – collector distance reduced the time available for the solvent in the jet to evaporate which caused the deposited wet fibres to fuse together [Raziyeh Ghelich, 2015]. Furthermore, Raziyeh Ghelich [2015] reported that on increasing the tip-collector distance to 15 cm, the network of fused fibres was formed again and the diameter of these fibres was larger. This morphology was attributed to the weak electrical field and less stretching due to the large tip-collector distance. The less stretching could result in a thicker jet with more solvent, which does not evaporate completely, resulting in wet fibres. The influence of tip-collector distance on the electrospinning process by affecting the electrical field is similar to that of the applied voltage. At a constant voltage, the electrical field is inversely proptional to the tip-collector distance. A.R. Jabur [2017] carried out the electrospinning of PVA fibres at various tip-collector distances to study the effect on fibre diameter. They found that the diameter of the fibres decreased as the tip-collector distance increased from 4 cm to 20 cm due to more time for the solvent to evaporate and give thinner fibres. However, the fibre diameter increased when the distance was increased to 22 cm. At this large tip-collector distance the applied electrical field was weakened which lead to less stretching of the fibres [Joon Seok Lee, 2004]. Thus, increasing tip-collector distance can decrease the fibre diameter by increasing flight time but could also increase the diameter by weakening the electrical field.

3.4.4 Needle Diameter

The diameter of the needle used affects the electrospinning process via a number of ways. The diameter of the needle decides the size of the taylor cone and also the initial diameter of the jet [C.J.Thompson, 2007]. It has been extensively found that using a needle with larger diameter increases the diameter of fibres obtained [C.J.Thompson, 2007; Pirjo Heikkilä, 2008]. C. Wang [2006] observed the increase in diameter of poly (phenylene vinylene) fibres when the inner diameter of the needle was increased from 0.57 mm to 0.84 mm. However, they also observed that the fibre diameter increased when a needle of inner diameter 0.37 mm was used. They reported when the needle diameter is too small, the solution flow is restricted which reduces the number of charges on the polymer jet, which in turn reduces the amount of stretching [C. Wang, 2006]. Raziyeh Ghelich [2015] reported that use of a needle with smaller diameter creates a droplet which has higher surface tension which increases the critical voltage required to initiate the jet. Mo XM [2004] observed that needles with larger diameter were prone to clogging which resulted in formation of beads. Haijun He and Molnar [2018] studied the effect of the needle characteristics on the electrospinning of PEO and reported that the needle diameter changed the fibre diameter due to change in viscosity of the solution. The flowing of the solution through the needle is shear rate dominated and for a constant volume flow rate the shear rate will decrease with increase in diameter of the nozzle. For a fluid that experiences shear thinning, the decrease in shear rate increases viscosity of the solution which leads to larger diameter of the fibres [Haijun He and Molnar, 2018]. Jun-Wei Liang and Lu [2019] reported that decreasing needle diameter leads to porous fibres by increasing the solvent evaporation rate. As mentioned earlier, pore formation is facilitated when the solvent evaporation is fast. A needle with smaller diameter produces a jet with smaller diameter which gives the jet a larger specific area for the solvent evaporation to take place [Jun-Wei Liang and Lu, 2019]. This increases the solvent evaporation rate and leads to the formation of pores.

3.4.5 Type of Collector

In the electrospinning process, an electric field must be created between the needle and collector. Since the polymer jet moves towards the collector as a result of the potential difference, the collector has an influence on the way the fibres are deposited. The material, design and configuration of the collector affect the arrangement of the fibres on the collector by influencing the applied electric field [Liu L, 2008; Jonathan Stanger, 2009; Manuel A.Alfaro De Prá, 2017]. Jonathan Stanger [2009] placed a glass substrate over a grounded copper counter-electrode plate to use it as the collector. The use of an insulating material as the collector decreased the mass deposition rate significantly. HAIQING LIU [2002] made the same observation on using paper as the collector. The use of a non-conducting material as the collector causes build up of residual charges on the deposited fibres which causes the incoming fibres to be repelled, which results in lesser deposition as well as a loosely packed fibrous network [HAIQING LIU, 2002]. Manuel A.Alfaro De Prá [2017] performed electrospinning of polycaprolactone fibres on a rotating drum collector and static parallel copper wires. They found that for a static drum the fibre alignment was random whereas when the drum was rotated at 2000 rpm the fibres were aligned next to each other in an ordered manner. Furthermore, the fibres deposited on the rotating drum had a lower average fibre diameter which was attributed to the stretching force on the fibres due to the high-speed rotation of the drum. The static parallel copper wires also lead to an ordered alignment of the deposited fibres. A. Becker [2015] also demonstrated that using a rotating drum collector resulted in the parallel alignment of fibres and lower fibre diameter. Furthermore, they reported that the alignment of the fibres became more ordered with increase in rotation speed. Adomavičiūtė Erika [2011] used a cylindrical collector with diameter 70 mm and a wire collector of diameter 0.5 mm and found that size of collector influences the electric field. They observed that the electric field was weaker in the case of the wire electrode which resulted in a thinly populated deposition of fibres. The electric field generated using the cylindrical collector was higher and a densely packed fibrous mat was produced [Adomavičiūtė Erika, 2011].

3.5 Ambient Parameter

3.5.1 Humidity

The environmental conditions under which the electrospinning process is taking place have an effect on the fibre formation process [Tugrul Ogulata, 2013]. Various researchers have found that an increase in relative humidity of the area surrounding the setup affects the process by varying the solvent evaporation process and solution properties due to water condensation on the polymer solution jet [Htet Htet Htike, 2012; Baumgarten, 1971]. Baumgarten [1971] observed the effect of relative humidity on the solvent evaporation in the electrospinning of a copolymer of acrylonitrile, methyl acrylate and sodium styrene sulphonate in DMF. At 30-40% relative humidity the electrospinning was continuous and uniform fibres were produced. However, on reducing the relative humidity to below 5%, the solvent evaporation was so rapid that the solution droplet dried out and the electrospinning was short lived [Baumgarten, 1971]. In contrast, at a relative humidity above 60%, the fibres were wet when they reached the collector and appeared to dangle above it. Tugrul Ogulata [2013] found that the diameter of polyetherimide fibres increased with relative humidity. Tugrul Ogulata [2013] reported that the higher amount of water in the air lead to the addition water to the polymer solution which had 1-methyl-2-pyrrolidinone as the solvent. This caused the polyetherimide to precipitate which reduced the elongation of the jet, eventually resulting in thicker fibres [Tugrul Ogulata, 2013]. A study by Htet Htet Htike [2012] showed that the increase in relative humidity lead to a decrease in diameter of the PVA fibres. They reported that at low relative humidity the solution jet had absorbed less water which increased the evaporation rate and lead to thick fibres. Whereas at high relative humidity, due to high degree of water absorption the viscosity of the solution jet decreased which enhanced elongation and thus lead to thinner fibres [Htet Htet Htike, 2012]. Sureeporn Tripatanasuwan [2007] also reported the decrease in fibre diameter with increase in relative humidity due to decrease in solidification rate. However, they observed that at high values of relative humidity bead formation takes place along the fibres. Nakagawa Yuya and Kim [2010] made the same observation for poly(vinyl pyrrolidone) at values of relative humidity 50% and above. The increase in elongation due to lower evaporation rate as a result of the higher relative humidity increases the surface area of the solution jet, this decreases the surface charge density on the jet [Sureeporn Tripatanasuwan, 2007]. Due to lowered surface charge density, the Rayleigh instability begins to set in which causes the formation of beads. The effect of relative humidity on the solvent evaporation and jet elongation differs with the polymer-solvent system. Htet Htet Htike [2012] reported that the decrease in solvent evaporation rate was due to the presence of soluble egg shell membrane in the solution and their hydrophilic nature. Beside from influencing the fibre diameter, studies have found that increase in humidity leads to the formation of porous fibres [Hyun-Su Bae, 2013; Cheryl L. Casper, 2004]. Hyun-Su Bae [2013] demonstrated this by the electrospinning of polymethyl methacrylate (PMMA) fibres using a binary solvent system of dichloromethane and dimethylformamide under controlled humidity conditions. They reported that due to the higher volatility of DCM than DMF, its rapid evaporation caused cooling of the jet which lead to the condensation of the atmospheric water. These water droplets settle on the fibres which eventually on evaporation form pores, whose number increases with increase in humidity [Hyun-Su Bae, 2013]. Cheryl L. Casper [2004] made a similar observation on electrospinning polystyrene fibres in THF and found that the number of pores increased significantly with relative humidity but saturated after a certain limit. Below a relative humidity of 25% no pores were observed while from 31- 72% of relative humidity the number of pores increased. They also reported that since the number of pores increased with humidity, at high values of humidity the smaller pores coalesced to form larger pores. The pore depth also increased with relative humidity [Cheryl L. Casper, 2004]. Nezarati R.M. [2013] on electrospinning various solvents reported that a solution with a highly hydrophobic polymer and highly volatile water-miscible solvent facilitates vapor-induced phase separation, which is a mechanism behind pore formation in fibres. On electrospinning polyethylene glycol (PEG) solutions in chloroform, Nezarati R.M. [2013] found that the due to the hydrophilic nature of PEG no phase separation, and thus no pore formation took place. On the other hand, polycaprolactone, a hydrophobic polymer had pores on its fibres since it precipitated on water absorption from the atmosphere and the highly volatile chloroform evaporated rapidly. Whereas, fibres of poly(carbonate urethane) had no pores even though the polymer is hydrophobic. Nezarati R.M. [2013] reported the reason behind this observation was the low volatility of N,N-dimethylacetamide which was used as the solvent. Thus, the effect of relative humidity in the formation of pores is highly dependent on the polymer and solvent properties.

4 Preliminary experiments

One of the aims of this project is to correlate the characteristics of the fibres produced with the process and solution parameters. While the solution parameters like viscosity, surface tension and conductivity have more of an effect on the fibre morphology and can be altered by changing the composition of the solution, suitable values of process parameters like applied voltage, feed rate and tip-collector distance are vital to uninterrupted electrospinning. Furthermore, the solvent properties also affects the fibre production and in this project aqueous solution of sodium hydroxide is used as the solvent. Lastly, this project employs polyvinyl alcohol (PVA) as a binder polymer to blend with the lignin in order to give sufficient viscosity to the solution. This section provides information on the applied voltage, flow rate and tip-collector distance values used in the main experiment of this project. It also states the reasoning behind choosing aqueous NaOH and PVA as the solvent and binder polymer respectively.

4.1 Applied voltage

This project investigates the effect of changing the applied voltage on the fibre spinning process and their morphology. Thus, five values of voltage were chosen: 16.5 kV, 18 kV, 19.5kV, 21 kV and 22.5 kV. As mentioned in the earlier section, the surface tension of the solution plays a major role in deciding the critical voltage required to deform the droplet such that fibres are drawn from it. Taylor [1969] also states an approximate expression for calculating this critical voltage from the surface tension of the solution. However, this calculation was not possible to carry out since the surface tension of the solution could not be measured. The voltages were chosen based on the experiments performed in the previous semester. Those experiments used only one value of applied voltage which was 21 kV. This value was selected through conducting several runs of electrospinning of lignin-PVA solutions in aqueous NaOH with different values of applied voltage. It was observed that when the voltage used was below 19.5 kV, the taylor cone was unstable and the electrospinning was interrupted. At 21 kV, the taylor cone was much stable and so it was chosen as the value for the main experiments. However, since this project studies the effect of voltage a set of values had to be chosen. It was then decided to observe the result of the electrospinning at a much lower voltage than 21 kV and thus 16.5 kV was opted. While the electrospinning was still interrupted due to the unstable taylor cone, a fairly large amount of fibres were produced and since it is the characteristics of the fibres that are to be analysed, the interrupted electrospinning was considered trivial. Thus, 16.5 kV was chosen as the starting value and 22.5 kV the final.

4.2 Feed rate

The feed rate used in this project is fixed for all experiments which is 0.0025 ml/h. This was also decided based on few preliminary experiments conducted in the previous semester as well as during the course of this project. As mentioned in the earlier section, the feed rate should be such that the rate at which the solution is being drawn due to the voltage is equal to or close to it. To acheive this a voltage of 21 kV was set and the feed rate was changed accordingly. A flow rate of 0.2 was set to begin with but the it proved to be fast and the droplet on top of the needle grew during the electrospinning and eventually fell off of the tip of the needle. On a few more attempts a flow rate of 0.005 mlwas chosen for the main experiments done previous semester. However, on performing preliminary experiments for this project it was observed that even at 0.005 mlthe flow rate proved to be a bit fast and dripping of the solution took place. So, the flow rate was reduced to 0.0025 mlwhich turned out to be the optimum flow rate.

4.3 Tip - collector distance

The tip-collector distance should be such that it fulfills two criteria; first, the electric field between the two electrodes is sufficient for solution to be drawn to the collector and second, the solvent has enough distance and thus flight time to evaporate before the polymer deposits on the collector. Researchers have used various values of tip-collector distance ranging from 8-25 cm, depending on the polymer and solvent in use. Based on studies, the preliminary experiment was conducted with a tip-collector distance of 25 cm. It was observed that a stable taylor cone persisted and solution was being drawn from the droplet. However, the amount of fibres present on the collector was quite less and fibres could be seen on surfaces near the collector. Thus, it was decided to lower the distance. At 16 cm, the electrospinning took place continuously and even a large amount of fibres deposited on the collector. On characterizing the fibres produced at this tip-collector distance, no clear signs of insufficient evaporation was observed. Hence, the value of tip-collector was fixed at 16 cm for the main experiment.

4.4 Solvent selection

Solvent selection is an important step in production of fibres with desired morphology. The lignin used in this study is Kraft lignin. It has a hydrophobic nature and shows low solubility in water and common organic solvents [Javad Sameni, 2017]. Whereas, it shows high solubility in an alkaline solvent and DMF. DMF is a commonly used solvent in electrospinning but due to its toxic nature it was decided not to use it in this project. Thus, it was decided to use an alkaline solvent and so aqueous sodium hydroxide was chosen since researchers have utilized it as a solvent for spinning kraft lignin fibres. Vida Poursorkhabi and Misra [2015] electrospun Kraft lignin-PEO fibres using 0.5M aqueous NaOH as the solvent and it was decided to use the same concentration in this study. However, a rough solubility test was done by adding the lignin in hand to a 0.5M aqueous NaOH solution and continuously stirring it. It was found that when the concentration of lignin was roughly above 20 g/g of solution, the lignin precipitated. This might not be accurate since it was not a precise solubility test. Evstigneev [2011] reported that solubility of kraft lignin in aqueous NaOH increases with concentration of NaOH. Thus, to ensure all the lignin was soluble, solutions that required the concentration of lignin to be more than 20 g/g of solution, 1M aqueous NaOH was used as the solvent.

4.5 Polyvinyl alchohol

It was found from literature survey and few preliminary experiments that a binder polymer is needed to increase the solution viscosity to the required amount. PVA was chosen as the binder polymer since it is a biodegradable polymer. This project revolves around the study of an environmental friendly precursor and so it was decided to adhere to that motive. It is known that lignin and PVA are not miscible but researchers have used their blends to prepare electrospinning solutions and have achieved uniform fibres [Mariko Ago and Rojas, 2012].

5 | Main Experiment

This chapter includes information on the materials used in the main electrospinning experiment, the composition of the solutions used, and the procedure followed to prepare. Finally, a description of the electrospinning is included.

5.1 Materials

The lignin used in this study is softwood kraft lignin (BioPiva 300) purchased from UPM. The material data sheet of this lignin says that the weight % of kraft lignin in this product is 80-98% and the sodium sulphate content is 0.5-3%. The PVA used had an average molecular weight of 115,000 Da, a degree of hydrolysis of 86.5-89%, and was purchased from VWR Chemicals. The sodium hydroxide used was 98.3% NaOH pellets purchased from Eka Nobel. Distilled water was used to make aqueous solutions.

5.2 Solution preparation

The solution preparation procedure followed in this study is the one used by Vida Poursorkhabi and Misra [2015]. The reason behind this was their lignin was kraft lignin and solvent used was aqueous NaOH, like in this project. The procedure involves the preparation of two precursor solutions; an aqueous PVA solution, in order to completely dissolve the PVA and another solution consisting of lignin and aqueous NaOH. The two solutions were then mixed in the required amounts to form the final solution. This technique ensured complete solubility of the materials. The PVA solution was prepared by boiling distilled water and then adding the PVA gradually while also stirring the solution. Once all the PVA had dissolved, the solution was removed from the heat and left to stir overnight. For dissolving the lignin, the 0.5 aqueous NaOH solution was heated up to 70 °C and the lignin was gradually added while stirring the solution at 600 rpm. Once the required amount of lignin was added, the solution was stirred at 600 rpm for 2 hours. In the case of solutions 3 and 6, 1M aqueous NaOH was used to dissolve the lignin. Once the two precursor solutions were ready, the required amounts of each were mixed together for 10 minutes and thus the final solution was obtained.

5.3 Experiment matrix

The solution used in this project consisted of aqueous NaOH as the solvent, with PVA and kraft lignin dissolved in it. It was decided to study the solution properties and their resultant electrospinning with respect to change in the polymer content. Since the solvent was primarily water with small amounts of NaOH, the compositions of the solutions were characterized with a polymer% and a water%. The water % calculated in this study does not consider the weight of NaOH since it was quite small. In addition to that, since the polymer in the solution was in fact a blend of two polymers, it was also characterized using the proportion of lignin and PVA in the blend polymer. 3 combinations of polymer and water concentrations were chosen; 10% polymer - 90% water, 15% polymer - 85% water and 20% polymer - 80% water. Similarly, 3 lignin-PVA ratios were chosen; 85-15, 90-10 and 95-5. For each lignin-PVA ratio, solutions were prepared with the different polymer and water concentrations. Thus, giving a total of 9 solutions to be electrospun as a part of the main experiment. Table 5.1 shows the experiment matrix.

Solution number	Lignin prop.	PVA prop.	Amt. of PVA (g)	Amt. of lignin (g)	Polymer %	Water %	Wt. of final solution (g)
1	85	15	1	5.667	10	90	66.667
2	85	15	1.5	8.5	15	85	66.667
3	85	15	2	11.333	20	80	66.667
4	90	10	1	9	10	90	100
5	90	10	1	9	15	85	66.667
6	90	10	1.5	13.5	20	80	75
7	95	5	1	19	10	90	200
8	95	5	1	19	15	85	133.333
9	95	5	1	19	20	80	100

Table 5.1: Main experiment matrix showing the solutions used in this study and their compositions

Once the polymer concentrations and the lignin-PVA ratios were decided, the experiment matrix was prepared. First, a fixed amount of PVA in every solution was decided. This meant that when the polymer concentration had to be altered, it would be done by changing the amount of lignin and this was the intention behind fixing the amount of PVA. The fixed amount of PVA was decided to be 1g. However, it had to be altered in the case of some solutions (solutions 2, 3 and 6) in order to increase the weight and volume of the final solution. A particular volume of final solution was required in order to measure its viscosity accurately using the measurement device available. Since the PVA was added to the final solution in the form of an aqueous PVA solution, the volume of the final solution could be increased by a slight increase in amount of PVA. Once the amount of PVA was fixed, the amount of lignin required in the solution was calculated according to the lignin-PVA ratio. Knowing the amount of polymer, the amount of water required in the final solution could be calculated. Once that was known, since some water in the final solution was coming from the aqueous PVA solution, the concentration of the lignin in the aqueous NaOH solution was calculated accordingly. The aqueous PVA solution consisted of a PVA concentration of 12%. This concentration was chosen since the amount of water coming from the PVA solution in order to meet the water requirement in the final solution had to be kept at a minimum, due to lignin's limited solubility in the 0.5M aqueous NaOH. The weight of the two precursor solutions and the different concentrations of lignin in aqueous NaOH are shown in Table 5.2

Solution number	Wt. of aqueous PVA solution (g)	Wt. of lignin-NaOH solution (g)	Conc. of lignin in aqueous NaOH (g/g)
1	8.333	58.333	9.714
2	12.5	54.167	15.692
3	16.667	50	22.667
4	8.333	91.667	9.818
5	8.333	58.333	15.428
6	12.5	62.5	21.6
7	8.333	191.667	9.913
8	8.333	125	15.2
9	8.333	91.667	20.727

Table 5.2: Information on the precursor solutions used for the preparation of each of the 9 final solutions

5.4 Electrospinning

The electrospinning setup used in this project is a vertical one, with the collector fixed at a distance above the tip of the needle. With this kind of vertical setup the dripping of solution from the needle onto the collector plate is avoided. The setup also consisted of a syringe which was used to supply the solution into the needle. A pump did the job of pushing the solution out of the syringe and into the needle. The needle used in this experiment had an inner diameter of 2.3 mm and outer diameter of 3 mm. As mentioned in the previous section, the flow rate used was fixed throughout the main experiment, which was 0.0025 ml/h. The electrospinning began as the voltage supply was turned on and the voltage was turned on only once the solution had emerged out of the tip of the needle and had formed a hemispherical droplet. A fixed electrospinning time of 45 seconds was used for each electrospinning run. The supply voltage was turned off at the end of 45 seconds. On the surface of the collector plate, an aluminium foil was attached which was the deposition plane and technically the collector for the fibres. In order to make characterization of fibres using SEM and LOM simpler, a small silicon wafer was stuck in the middle of the aluminium foil. Lastly, while it was planned to conduct electrospinning of the 9 solutions shown in Table 5.1, the 9th solution was not electrospun since it was regarded redundant to the experiment, based on the results of electrospinning of the previous 8 solutions. These results are explained in the later sections.

6 | Characterization of Lignin

6.1 Thermal characterization

6.1.1 Differential scanning Calorimetry

DSC was conducted on the lignin sample in order to determine its glass transition temperature (T_g). Studies have found the T_g of Kraft lignin to fall within a wide range of 90 °C to 200 °C due to their complex structure [Akpan and Adeosun, 2019; Tayra Rodrigues Brazil and Rezende, 2018]. The DSC run took place in three cycles; heat, cool and heat. In the first heating cycle the sample was heated from 20 °C to 110 °C and held at 110 °C for 30 minutes. The second cycle was a cooling one in which the sample was cooled down from 110 °C, back to 20 °C. This was done because a broad endothermic peak denoting evaporation of water from the sample was present around 100 °C, which was overlapping with the glass transition process shown by the curve, making its determination difficult. The third heating cycle, was a modulated DSC on the sample where it was heated from 20 °C to 250 °C with a temperature modulation of 0.66 +/-C every 60 seconds. The modulation parameters were chosen from Hui Li [2014]. The DSC curve was obtained for this third heating cycle and the T_g was determined from it. Figure 6.1 shows this DSC curve.

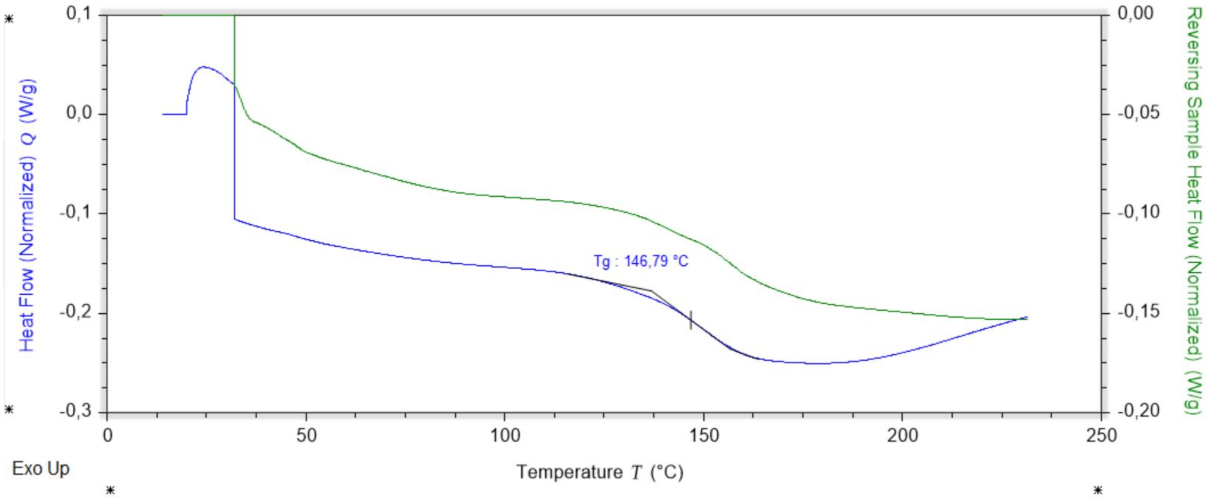

Figure 6.1: DSC curve of Kraft lignin sample

It can be seen from the curve that the change in the curve in the form of a downward step begins at around 115 °C, which ends at around 160 °C. On analysing the curve using the in-built TRIOS software, a T_g of 146.79 °C was calculated for this Kraft lignin sample. This value of T_g is in accordance with that determined in several studies [Javad Sameni and Sain, 2014; Hui Li, 2014]. Another observation associated with the T_g analysis via DSC is the broad downward step in the curve denoting the glass transition, that is, the difference between the onset temperature and glass transition temperature is high. Javad Sameni and Sain [2014] attributed this high difference to the presence of impurities in the lignin as a result of the extraction process it goes through and further stated that this difference was higher for lignin with higher amount of impurities. Hui Li [2014] conducted MDSC on Indulin AT Kraft lignin and found it to have a T_g of 143 °C. Further, they performed fractionation via solvent extraction on the lignin using methanol as the solvent. Then, DSC was performed on the soluble and insoluble fractions and it was found that the soluble fraction had a T_g of 118 °C and the insoluble had a T_g of 202 °C.

6.1.2 Thermogravimetric analysis

TGA was carried out on the lignin sample to analyse its thermal stability. The instrument used was Discovery SDT650 TA instruments thermogravimetric analyzer. The sample was heated from room temperature to 1000 °C at a heating rate of 10 °C/ min in nitrogen atmosphere. Figure 6.2 shows the TGA curve obtained. The curve follows a steep downward slope in the beginning itself and which ends just before the 100 °C mark. It is believed the evaporation of water from the sample is the reason of this initial mass loss. However, while this mass loss due to water evaporation has been observed by other researchers too, the amount of mass loss is much less compared to what is seen in the above curve. The behaviour of the curve after 100 °C is quite similar to that seen in literature. The onset of thermal degradation takes place close to 175 °C and continues gradually. The degradation becomes rapid from 300 °C and continues up to 600 °C. The DTG curve shows that the peak degradation takes place at 400 °C which is close to that found in literature for softwood kraft lignin [Javad Sameni and Sain, 2014; Hui Li, 2014]. The TGA curve also shows a residual weight of 35% at 1000 °C. Researchers have claimed that above 800 °C the mass loss is negligible and the residue is because of formation of highly condensed aromatic structures [Tayra Rodrigues Brazil and Rezende, 2018; Javad Sameni and Sain, 2014].

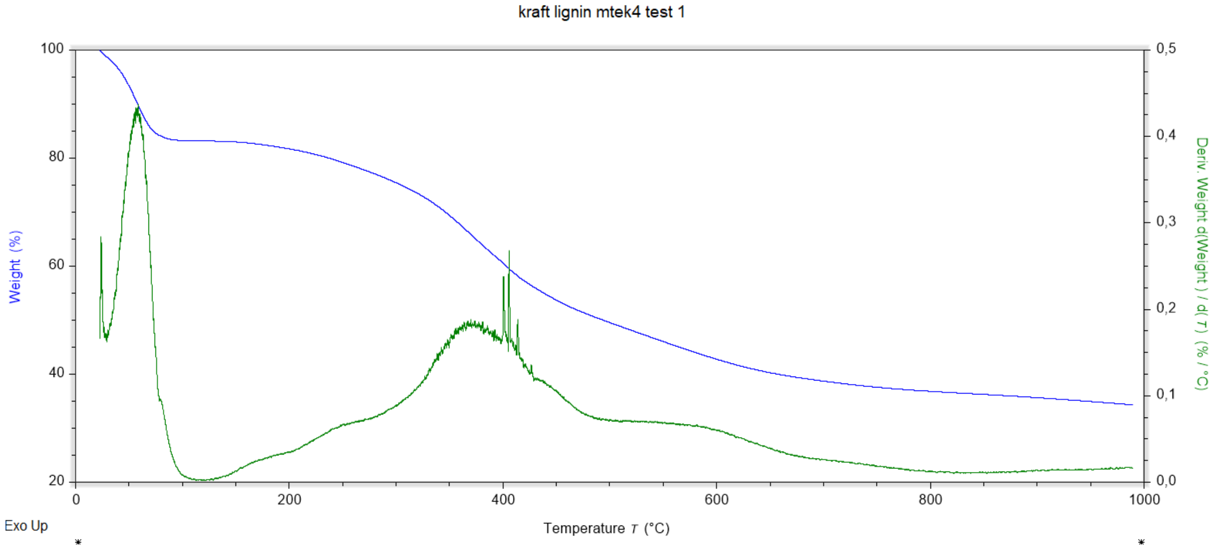

Figure 6.2: TG and DTG curves of the kraft lignin used in this study

6.2 Chemical characterization

6.2.1 Fourier-transform Infrared Spectroscopy

A Bruker Opus Infrared spectrometer was used to conduct FTIR on the softwood kraft lignin used in this study. IR spectrum of the kraft lignin sample is shown in Figure 6.3. The spectrum shows the characteristic absorbance peaks seen for Kraft lignin and they have been assigned based on FTIR characterization done on kraft lignin by researchers [Tayra Rodrigues Brazil and Rezende, 2018; Hui Li, 2014; Kubo and Kadla, 2005; Abd-Alla M. A. Nada and Kamel, 1998]. Table 6.1 shows the assignment of the absorbance bands seen in Figure 6.3.

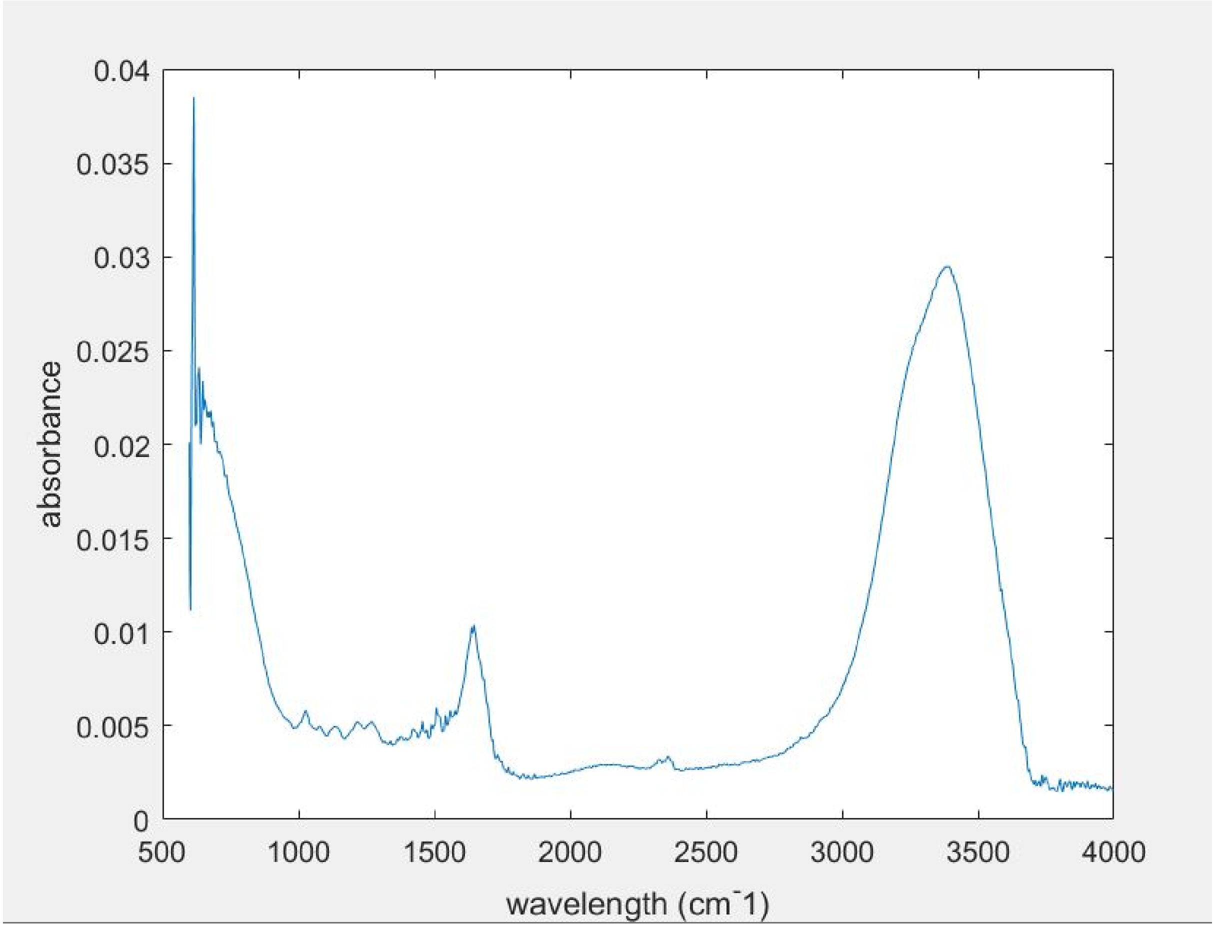

Figure 6.3: FTIR spectrum of the softwood kraft lignin used in this study

Number	Band position (cm^{-1})	Assignment
1	3345	O-H stretching
2	1727-1690	C=O
3	1645	Aromatic ring vibration
4	1508	Aromatic ring vibration
5	1457	C-H stretching in methyl and methylene groups
6	1421	C-H vibration of methyl groups
7	1269	C-O of the guaiacyl ring
8	1219	C-C plus C-O stretching
9	1136	O-H stretching in secondary alcohol
10	1027	Aromatic C-H in-plane deformation (G>S)
11	655	C-S vibration of sulphonic group
12	630	Broad band of C-S bond

Table 6.1: Assignment of absorbance bands seen in the FTIR specturm of softwood kraft lignin used in this study

While the IR spectrum in Figure 6.3 shows all the bands seen in the IR spectrum of softwood kraft lignin samples, there are quite a few differences seen in this IR spectrum. The most notable difference is the positions of two peaks, seen at 2362 cm^{-1} and 2325 cm^{-1} in 6.3. The shape of these two peaks is quite similar to those seen in the range 2940-2930 cm^{-1} and 2689-2880 cm^{-1}, respectively, in a majority of kraft lignin FTIR spectrums observed in literature [Tayra Rodrigues Brazil and Rezende, 2018; Hui Li, 2014; Kubo and Kadla, 2005; Abd-Alla M. A. Nada and Kamel, 1998]. These peaks seen in literature have been assigned to C-H stretching in methyl and methylene groups and C-H vibration in methyl and methoxyl groups, respectively. It looks as though the these two peaks have shifted from positions normally seen at to the ones seen in the spectrum for the kraft lignin in this study. Another difference that was observed is the C=O bond that has been assigned to the small peak seen between 1727-1690 cm^{-1}. The C=O bond peak seen for kraft lignin in most of the spectrums that were referred to is larger and more discernible compared to the one seen here. Another major difference is associated to peaks at 655 cm^{-1} and 630 cm^{-1} that have been assigned to the C-S vibration of sulphonic group and C-S bond, respectively. The absorbance shown by these peaks is much larger compared to that observed by a number of studies [Abd-Alla M. A. Nada and Kamel, 1998; Tayra Rodrigues Brazil and Rezende, 2018]. Furthermore, apart from these two peaks, a few more peaks can be seen lying in the range of 600-700 cm^{-1}. Larkin [2011] shows the IR spectrum of sodium suphate which has peaks at 639 cm^{-1} and 617 cm^{-1} which denote the assymetric bending of SO_4. Due to the high amounts of sodium and sulphur used in the Kraft process to extract lignin, sodium sulphite is a salt that is produced which could be present in the kraft lignin used in the study. Additionally, the high absorbance of the peaks at 655 cm^{-1} and 630 cm^{-1} could also mean there is a high amount of sulphur as impurities in this kraft lignin sample.

7 Solution characterization

This section contains the viscosity and conductivity measurements of the solutions along with their corresponding composition.

7.1 Viscosity

The viscosity of each solution was measured since it has a major effect on the electrospinning process. Viscosity has a role to play in the production of beads, beaded fibres and uniform fibres. A Viscolite 700 portable viscometer was used to measure the viscosities of the solutions. The measuring procedure involves immersing a probe into the solutions up to a certain depth. On doing so, the viscometer displays the dynamic viscosity of the solution in mPa.s. Table 7.1 shows the viscosities of the solutions. The value mentioned is the average of three measurements.

Solution	PVA proportion	Lignin proportion	Polymer % in solution	Water % in solution	Viscosity (mPa.s)
1	15	85	10	90	8.1
2	15	85	15	85	39
3	15	85	20	80	68.333
4	10	90	10	90	4.866
5	10	90	15	85	16.2
6	10	90	20	80	34.2
7	5	95	10	90	3.366
8	5	95	15	85	5.7

Table 7.1: Dynamic viscosity of the solutions used in this study

It can be seen from the table that the lowest viscosity measured was for the solution with lowest polymer content (10%) and lowest PVA to lignin ratio (5/95). This shows that the kraft lignin used in this study requires a binder polymer to form high viscosity solutions with aqueous NaOH. Furthermore, the composition of the blend polymer in the solution should be such that the PVA-lignin ratio is capable of forming the necessary molecular entanglements with the solvent that would significantly increase the solution's viscosity.

7.2 Conductivity

The conductivity of every solution was measured since the electrostatic forces that work to draw the solution towards the collector and elongate it in the process are affected by the amount of charge carriers in it. Furthermore, the solution contained NaOH which dissociates into ions which are charge carriers and the amount of NaOH in the solutions is different. The measurement was performed using a RS PRO 123-8777 Conductivity meter. The measuring procedure was similar to that of the viscometer. The conductivity meter consisted of a probe that was immersed into the solution up to a certain depth and a value of conductivity was displayed in mS/cm. The conductivity values are mentioned in Table 7.2.

Solution	Water % in the solution	Wt. of final solution (g)	Wt. of aqueous NaOH (g)	Amount of NaOH (g)	NaOH conc. (g/g)	Conductivity (mS/cm)
1	90	66.667	52.667	1.032	0.015	17.116
2	85	66.667	45.667	0.895	0.013	13.17
3	80	66.667	38.667	1.484	0.022	17.04
4	90	100	82.667	1.62	0.016	—-
5	85	66.667	49.333	0.966	0.014	14.843
6	80	75	49	1.881	0.025	—-
7	90	200	172.667	3.384	0.016	—-
8	85	133	106	2.077	0.015	15.153

Table 7.2: Conductivity of the solutions used in this study

The conductivity meter had a maximum measurable value of 20 mS/cm. The conductivity of solutions 4, 6 and 7 were above this value and thus the exact conductivity could not be measured. It can be seen from the table that solution 3 and 6 had a higher concentration of NaOH in the final solution, this was because the aqueous NaOH solution used for these solutions had a concentration of 1M while the other solutions were made using 0.5M aqueous NaOH.

8 | Characterization of fibres

8.1 Light Optical Microscopy

Light optical microscopy was performed on all the silicon wafers that were used to collect the fibres. LOM was done to get a general idea of the result of the electrospinning of each solution. Figures 8.1 to 8.8 shows the LOM images. Table 8.1 shows the results of electrospinning of each solution along with their viscosities.

Solution	Viscosity (mPa.s)	Resultant morphology
1	8.1	Beaded fibres
2	39	Uniform fibres
3	68.333	Uniform fibres
4	4.866	Beads
5	16.2	Beaded fibres
6	34.2	Beaded and uniform fibres
7	3.366	Beads
8	5.7	Beads

Table 8.1: Resultant morphology achieved from electrospinning of the solutions based on LOM images

The effect of viscosity on the morphology of the fibres produced is evident. Solutions 4, 7 and 8 did not have sufficient viscosity and break-up of the jet occurred due to Rayleigh instability which resulted in the formation of beads. Solution 1 and 5 had higher viscosities but still not sufficient to form uniform fibres and thus beads can be seen along the length of the fibres. However, on comparison the distance between the beads in the beaded fibres produced by solution 5 is much larger than that of solution 1, indicating the gradual transition from beaded to uniform fibres on increasing the viscosity of the solution. Solutions 2 and 3 had viscosities that lead to the electrospinning of uniform fibres. Solution 6 had a viscosity slightly lesser than that of solution 2 and the result was a mix of beaded and uniform fibres.

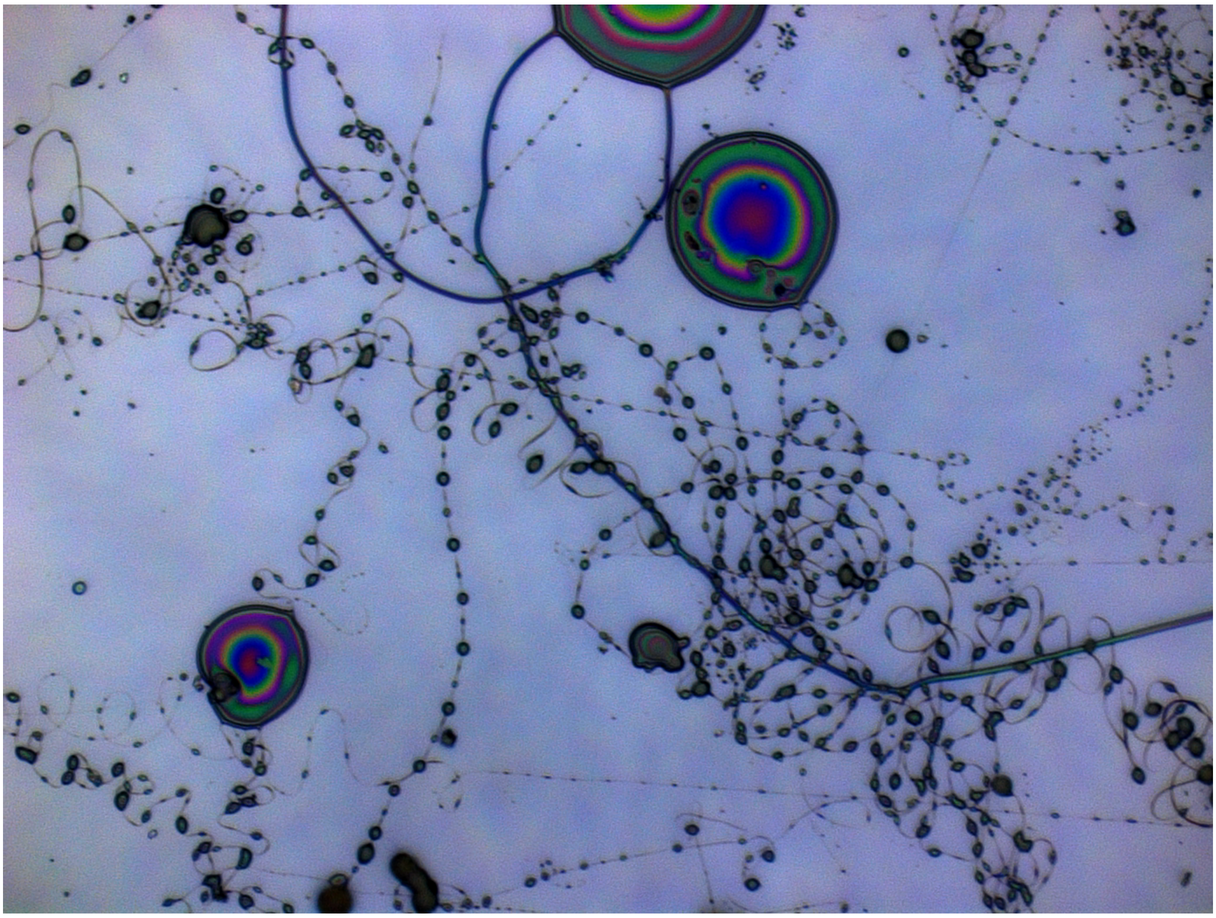

Figure 8.1: LOM image showing the beaded fibres produced from electrospinning of solution 1 (100X magnification)

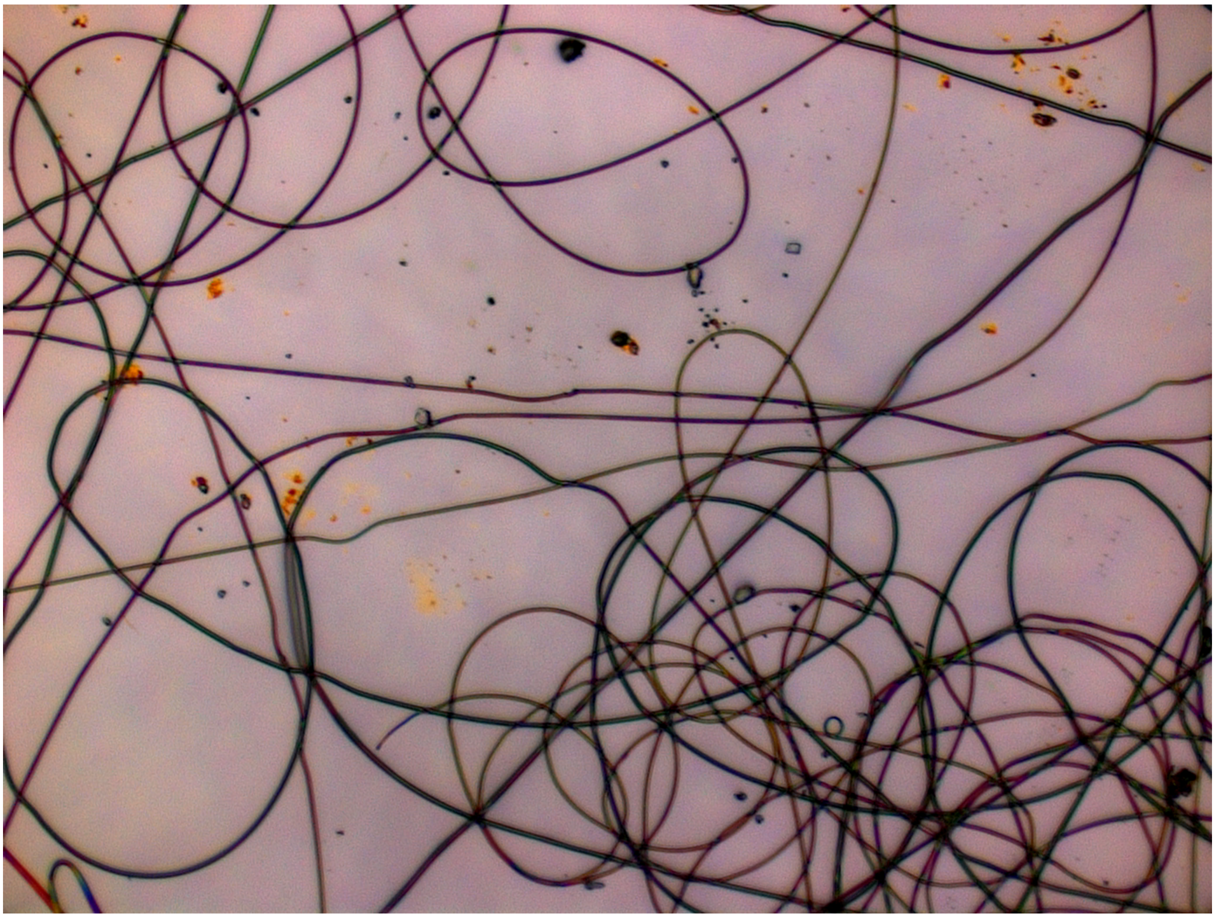

Figure 8.2: LOM image showing the uniform fibres produced from electrospinning of solution 2 (100X magnification)

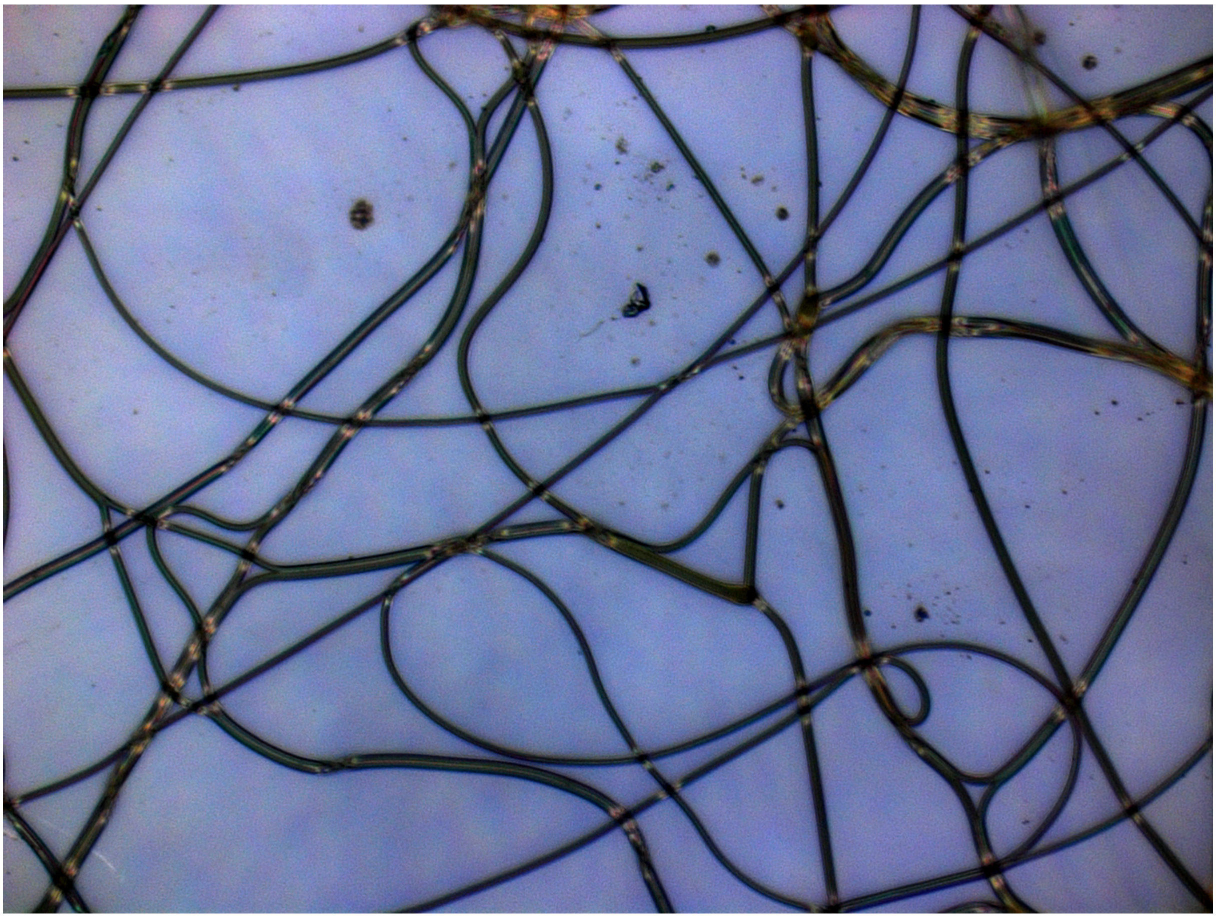

Figure 8.3: LOM image showing the uniform fibres produced from electrospinning of solution 3 (100X magnification)

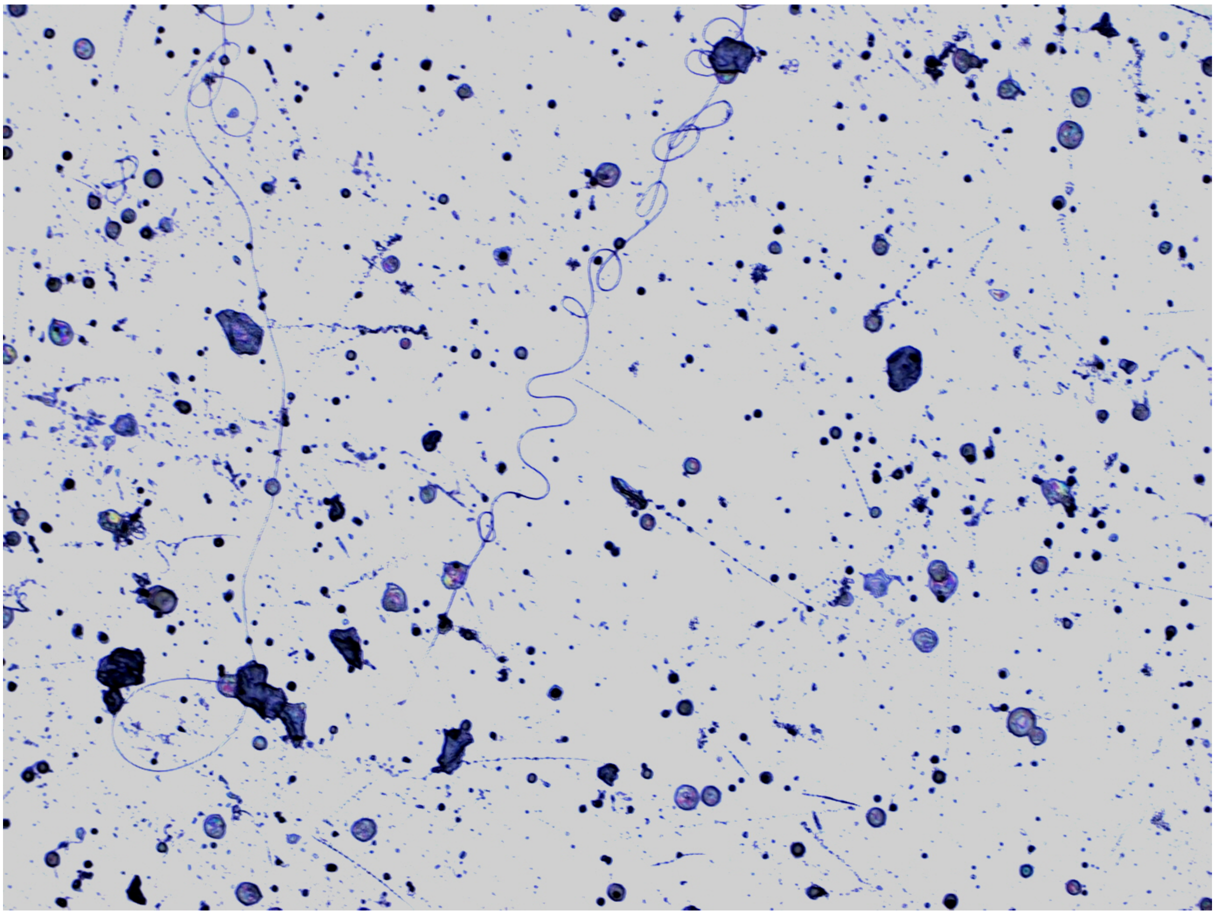

Figure 8.4: LOM image showing the beads produced from electrospinning of solution 4 (20X magnification)

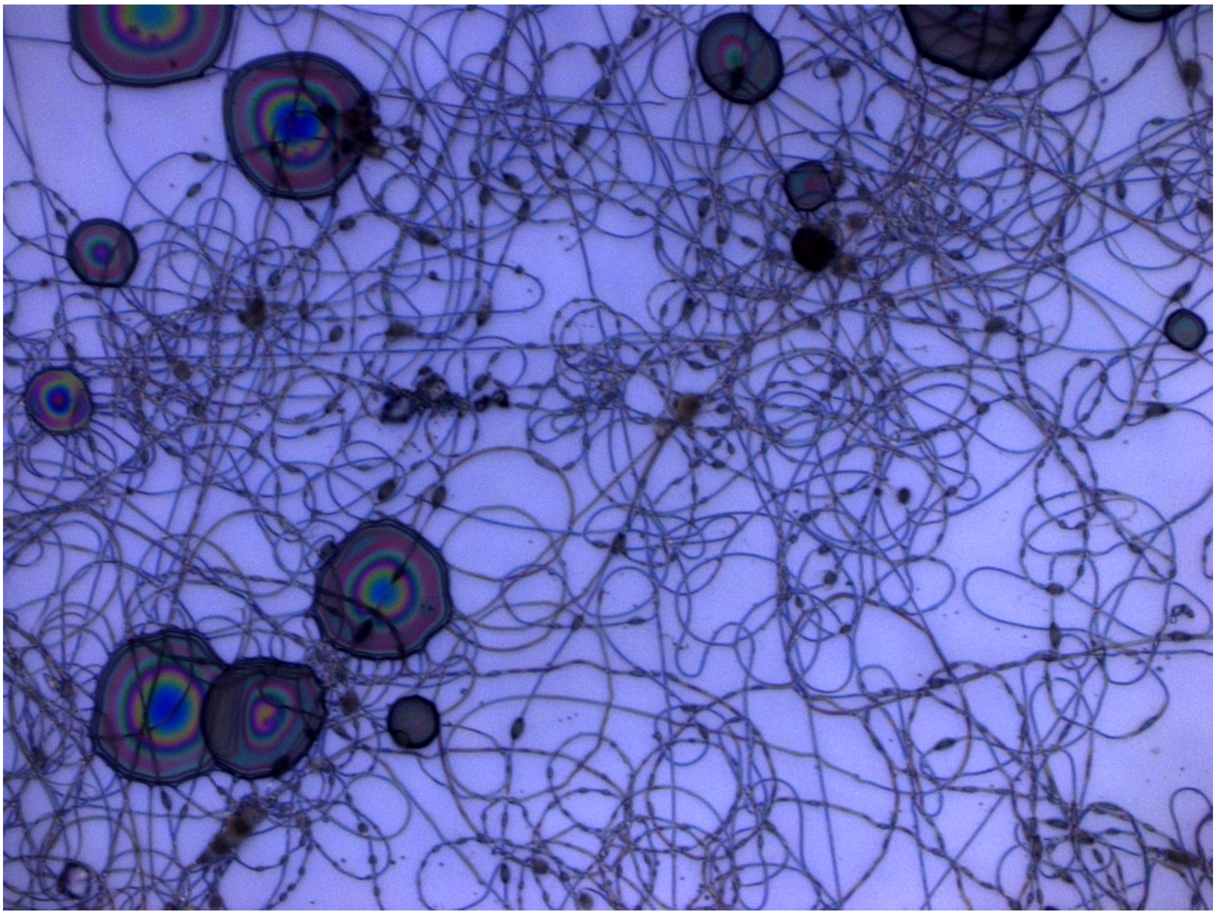

Figure 8.5: LOM image showing the beaded fibres produced from electrospinning of solution 5 (100X magnification)

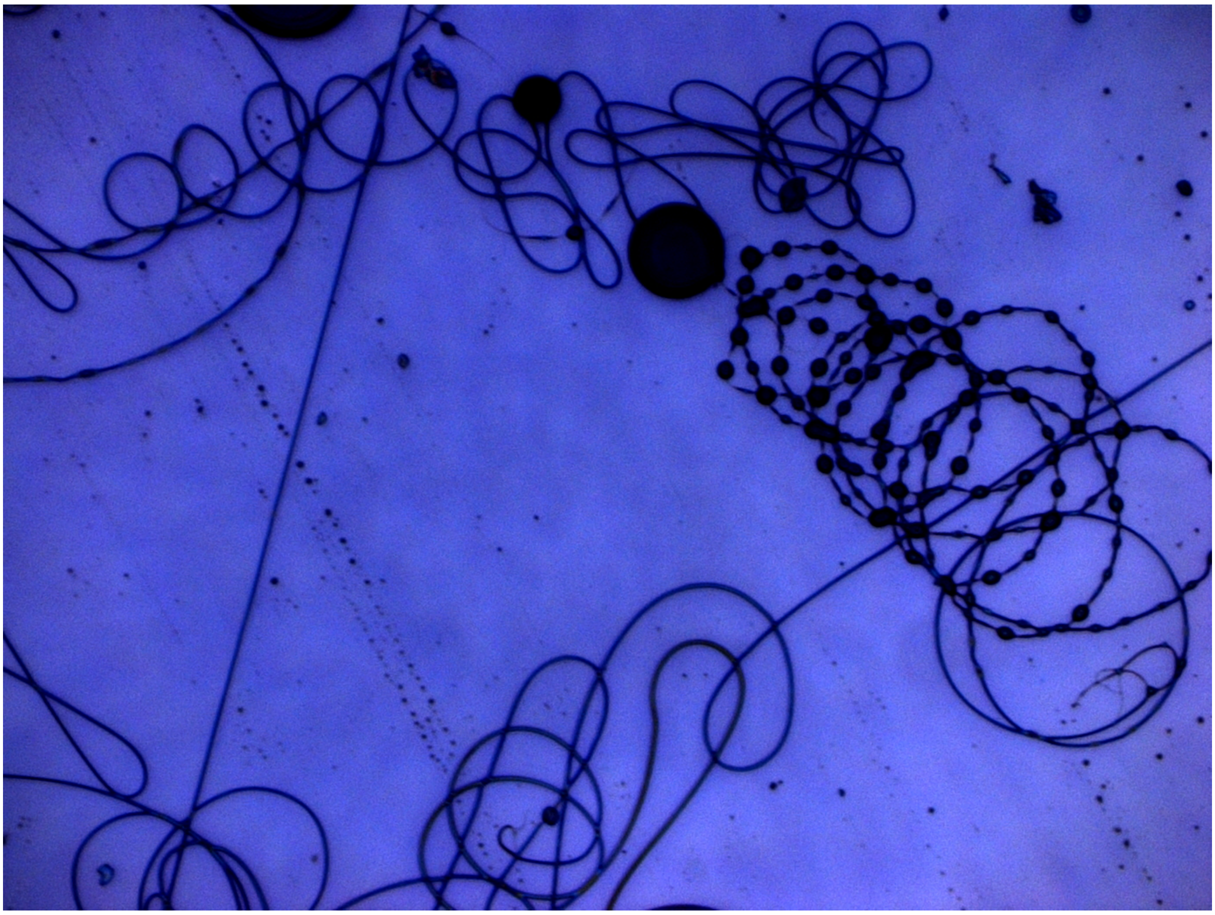

Figure 8.6: LOM image showing the beaded and uniform fibres produced from electrospinning of solution 6 (100X magnification)

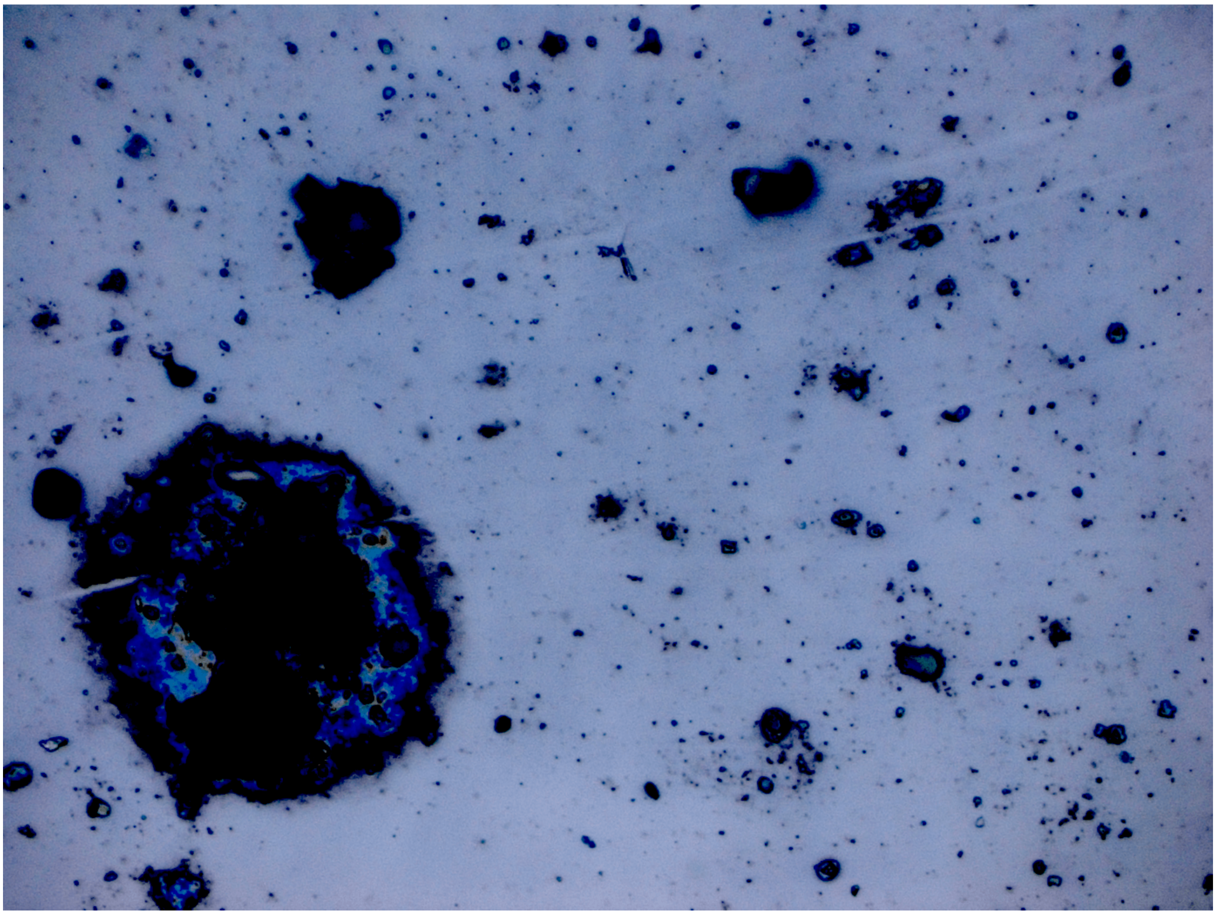

Figure 8.7: LOM image showing the beads produced from electrospinning of solution 7 (100X magnification)

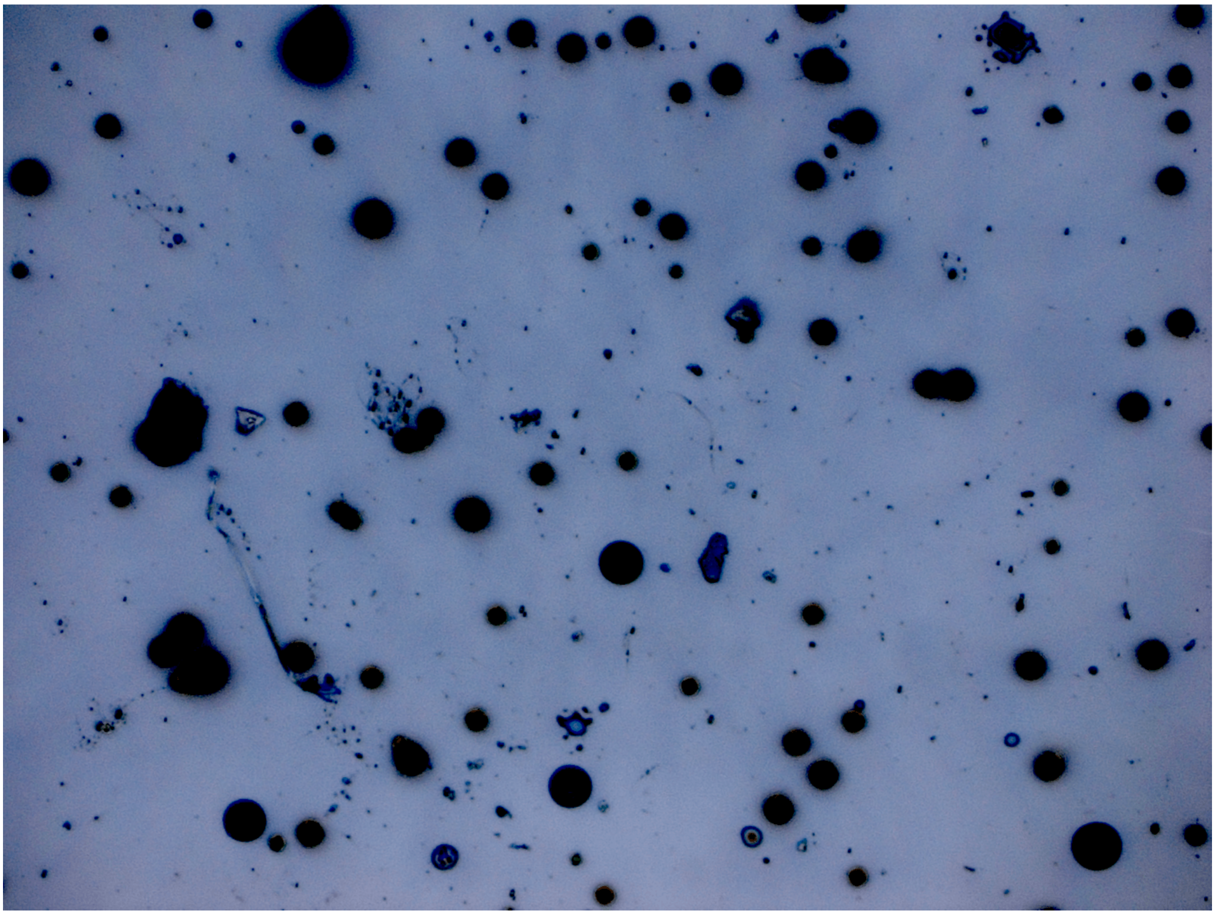

Figure 8.8: LOM image showing the uniform fibres produced from electrospinning of solution 8 (100X magnification)

8.2 Scanning Electron Microscopy

A Zeiss EVO 60 scanning electron microscope was used to carry out a SEM investigation of the fibres. On doing so, various fibre structures and shapes were observed. For the most part, the SEM investigation showed that the fibres produced were round and have a smooth texture. However, fibres have a flat morphology with a zigzag arrangement of the fibres could also be seen. Multiple fibres fused along their length were also observed. SEM images showing these various morphologies are in this section. An attempt has been made to correlate these fibre morphologies with the solution, process or material properties.

8.2.1 Effect of Viscosity

The two common effects of viscosity on the morphology of fibres that have been reported by researchers are; the transformation of beaded fibres to beadless fibres at a certain viscosity and the change in diameter of the fibres produced. The change from beads to beaded fibres and then to beadless fibres due to viscosity of the solutions has been mentioned in section 8.1 and can be seen in the LOM images. This section shows the SEM images of the beaded fibres produced by solutions 5 and 6 due to their lower viscosities and beadless fibres produced by solutions 2 and 3. These images can be seen from Figure 8.9 to 8.12 and have been arranged in decreasing order of the viscosity of the solution used. SEM investigation of the fibres produced by solutions 2, 3, 5 and 6 was done to observe the effects of viscosity. It was decided to perform a diameter investigation of the fibres using the SEM images and a software called DiameterJ but unfortunately that was not possible due to problems with the software.

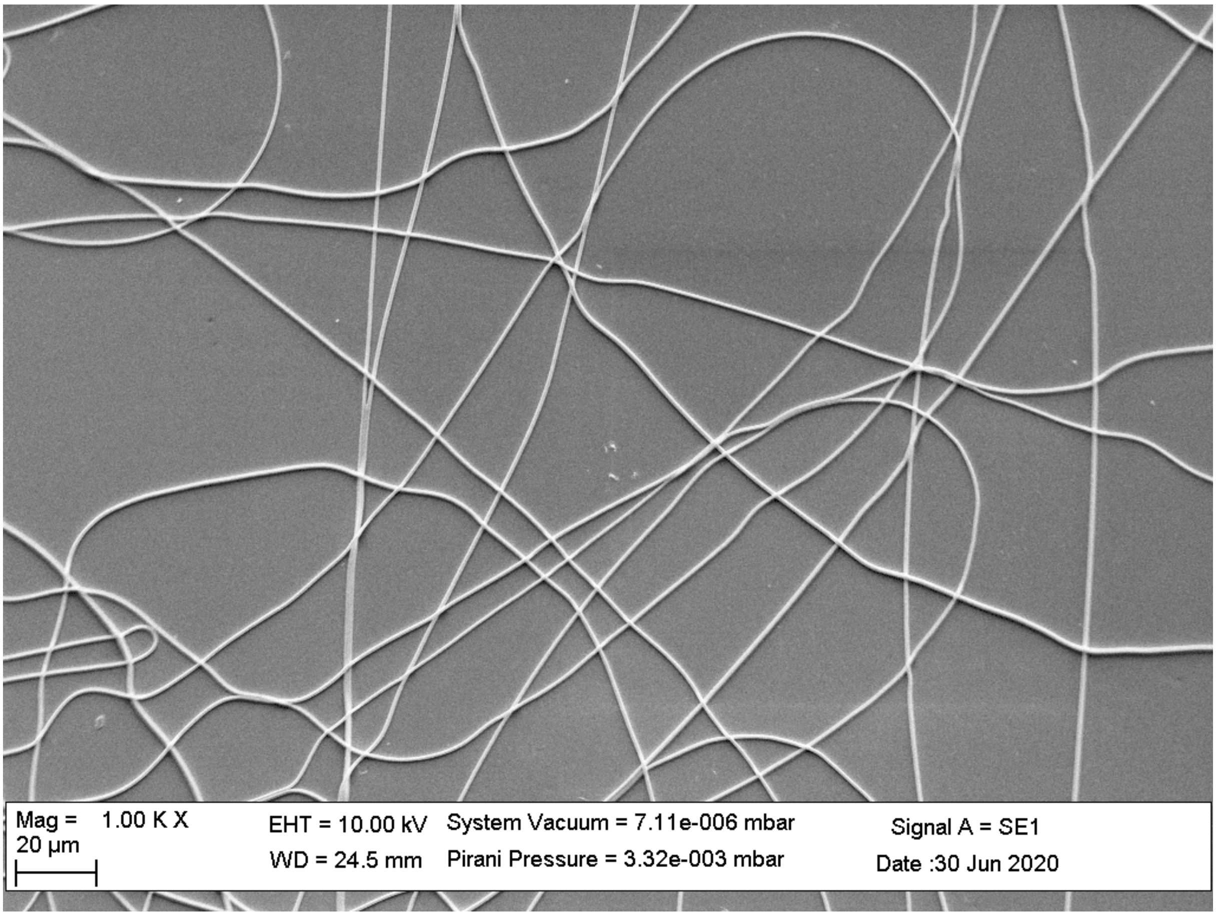

Figure 8.9: SEM image of beadless fibres produced from the electrospinning of solution 3 at 18 kV (1KX magnification)

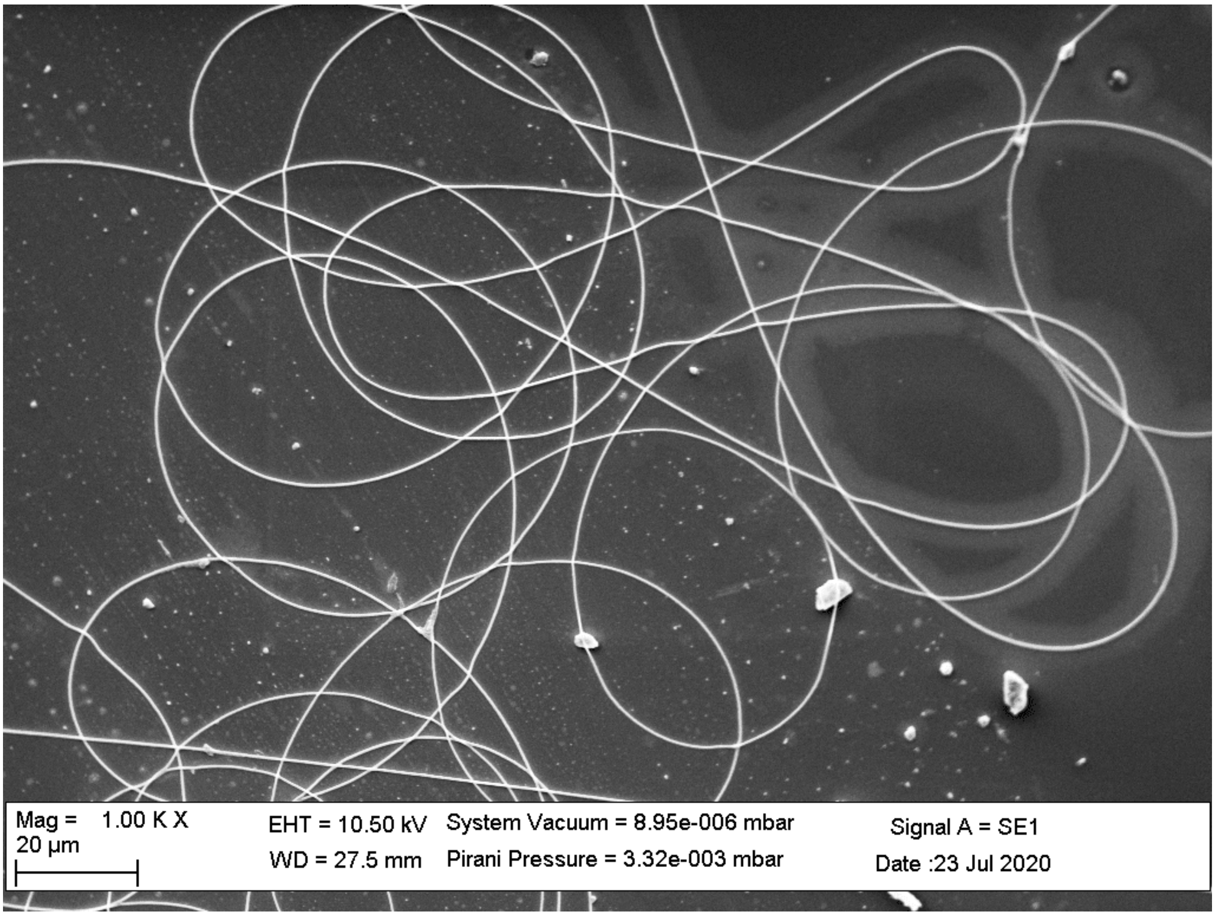

Figure 8.10: SEM image of beadless fibres produced from the electrospinning of solution 2 at 18 kV (1KX magnification)

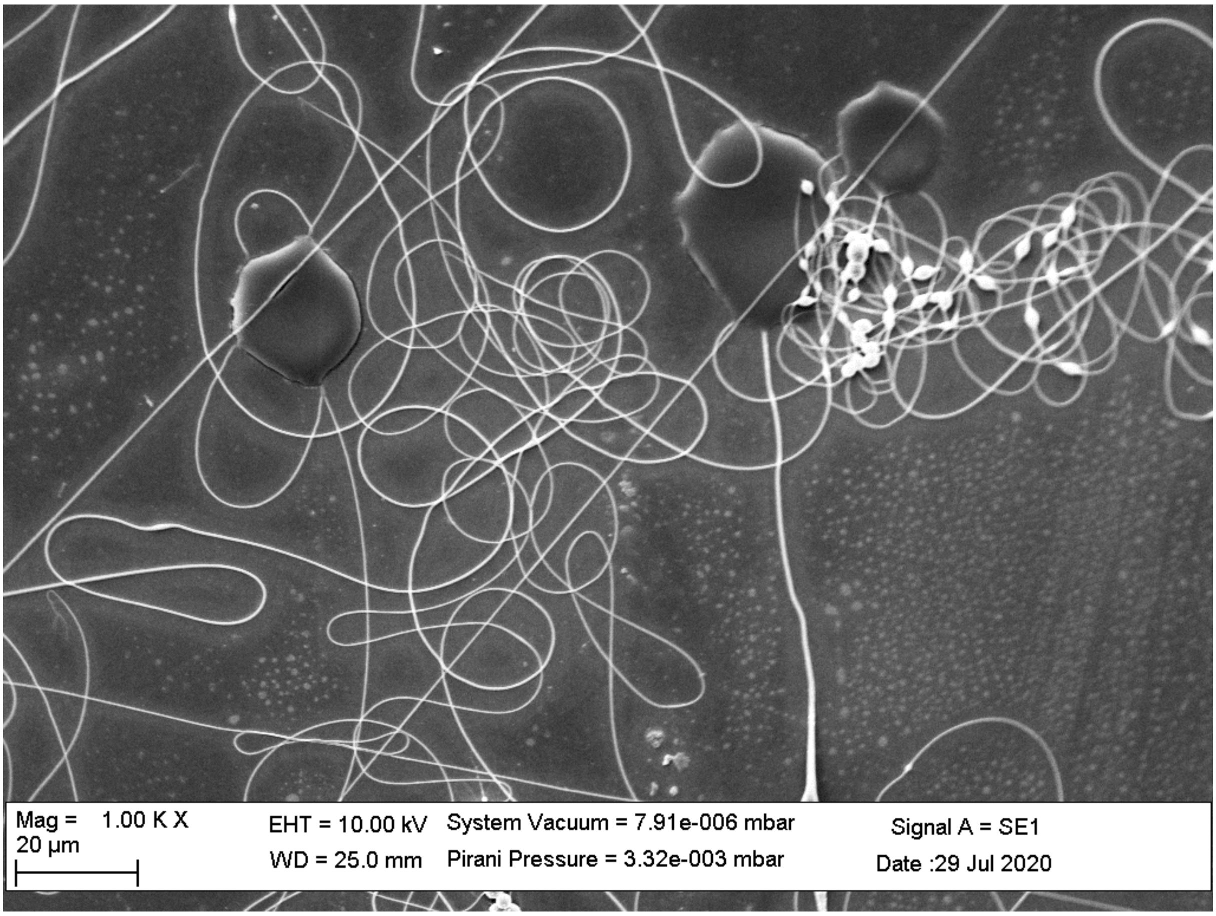

Figure 8.11: SEM image of beaded fibres produced from the electrospinning of solution 6 at 18 kV (1KX magnification)

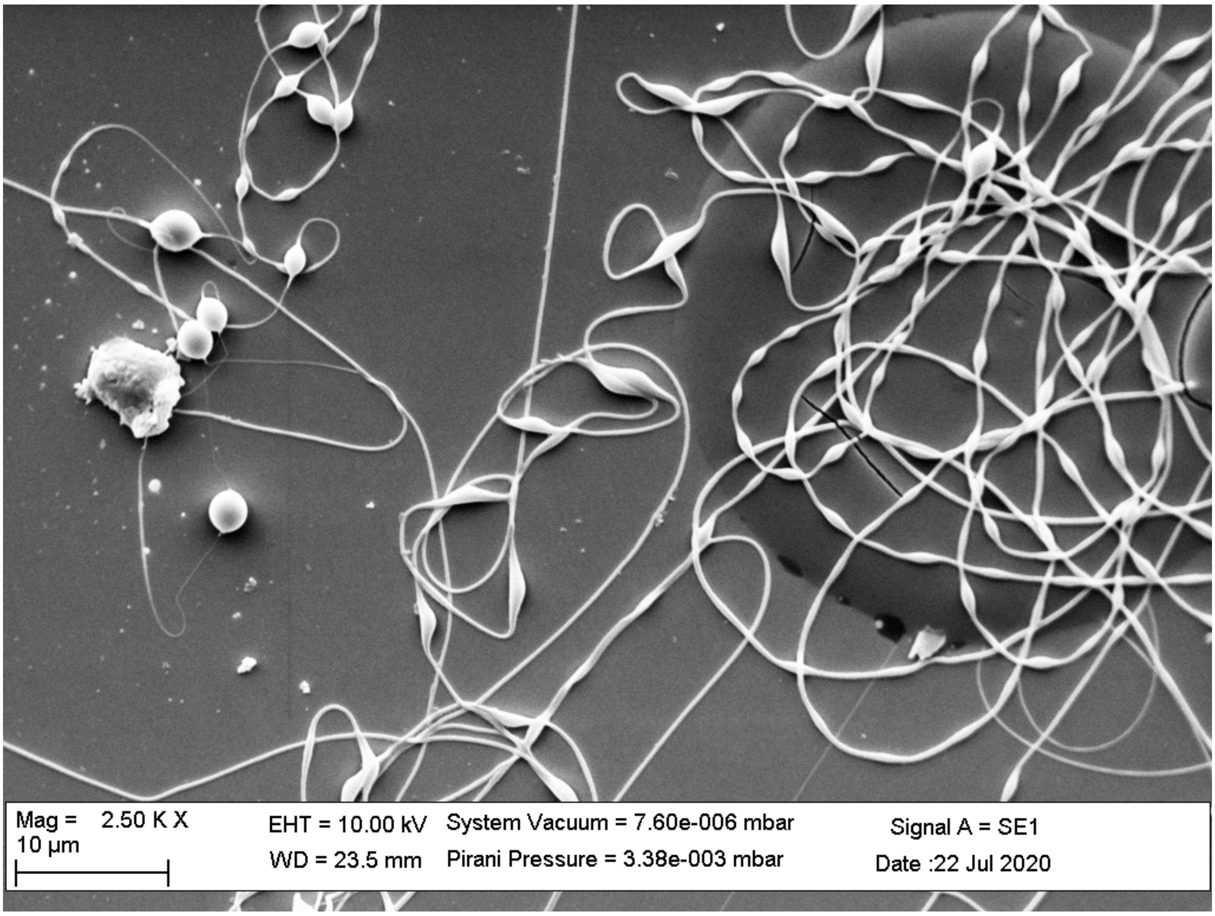

Figure 8.12: SEM image of beaded fibres produced from the electrospinning of solution 5 at 18 kV (2.5KX magnification)

8.2.2 Effect of applied voltage

An interesting effect of applied voltage on the fibre morphology was observed in the case of solution 6 (Viscosity 34.2 mPa.s). Electrospinning the solution at 16.5 kV lead to the formation of a beaded fibres, seen in Figures 8.13 and 8.14. When the voltage used was 18 kV, a mix of beaded and uniform could be seen when observed under the SEM (Figure 8.15). Some of the beaded fibres even looked like they had been elongated to a higher extent due to which the beads along the fibres were very spindle-like (Figure 8.16). At even higher voltages of 19.5 kV, 21 kV and 22.5 kV, the morphology of the fibres was uniform and the amount of beaded fibres had drastically decreased when compared to that seen in the case of 16.5 kV. Figures 8.17 to 8.22 show the SEM images of these fibres. Varvara Tserki [2006] made a similar observation when they electrospun fibres of poly(butylene succinate-co-butylene adipate) (PBSA) from its solutions in methylene chloride (MC) and MC / (N,N–dimethylformamide) mixtures, at different voltages. They achieved beaded fibres at voltages of 5 kV and 10 kV but at higher voltages of 15 kV and 20 kV they achieved uniform, beadless fibres. It has been reported that utilizing a higher voltage leads to stronger repulsive forces between charges which facilitates the elongation of the fluid jet [Teeradech Jarusuwannapoom, 2005]. It could be possible that when 16.5 kV was used, the surface tension could not be overcome which allowed the Rayleigh instability to set in and caused the formation of beads along the fibres. This changed gradually as the applied voltage was increased. Eventually, the stronger electrostatic forces overcame the surface tension and thus beadless fibres were formed. This effect of applied voltage also makes sense when the outcome of the electrospinning of the next greater viscosity solution is considered i.e. of solution 2. The viscosity of solution 2 was measured to be 39 mPa.s and its electrospinning produced beadless fibres for all the applied voltages used in this study. Whereas, despite the viscosity of solution 6 being only approximately 5 mPa.s lesser, its electrospinning at the lowest voltage produced beaded fibres. Thus, the morphology of the fibres, especially whether they will be beaded or beadless, is controlled by the solution viscosity, its surface tension, and to an extent the applied voltage used.

It is mentioned in the literature survey, section 3.1, applied voltage also has an effect on diameter of the fibres. This was decided to investigate but as mentioned earlier, errors with the software could not make this happen.

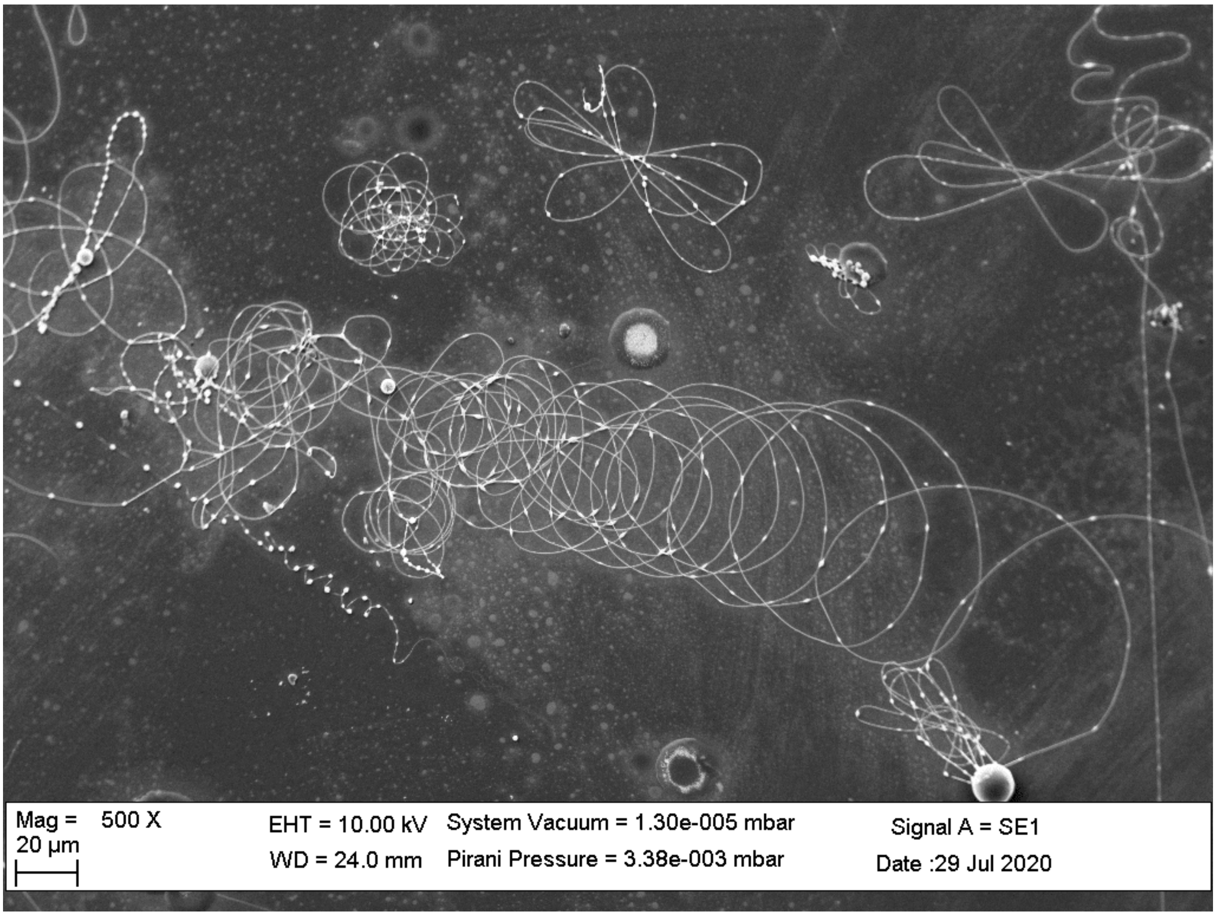

Figure 8.13: SEM image of beaded fibres produced from the electrospinning of solution 6 at 16.5 kV (500X magnification)

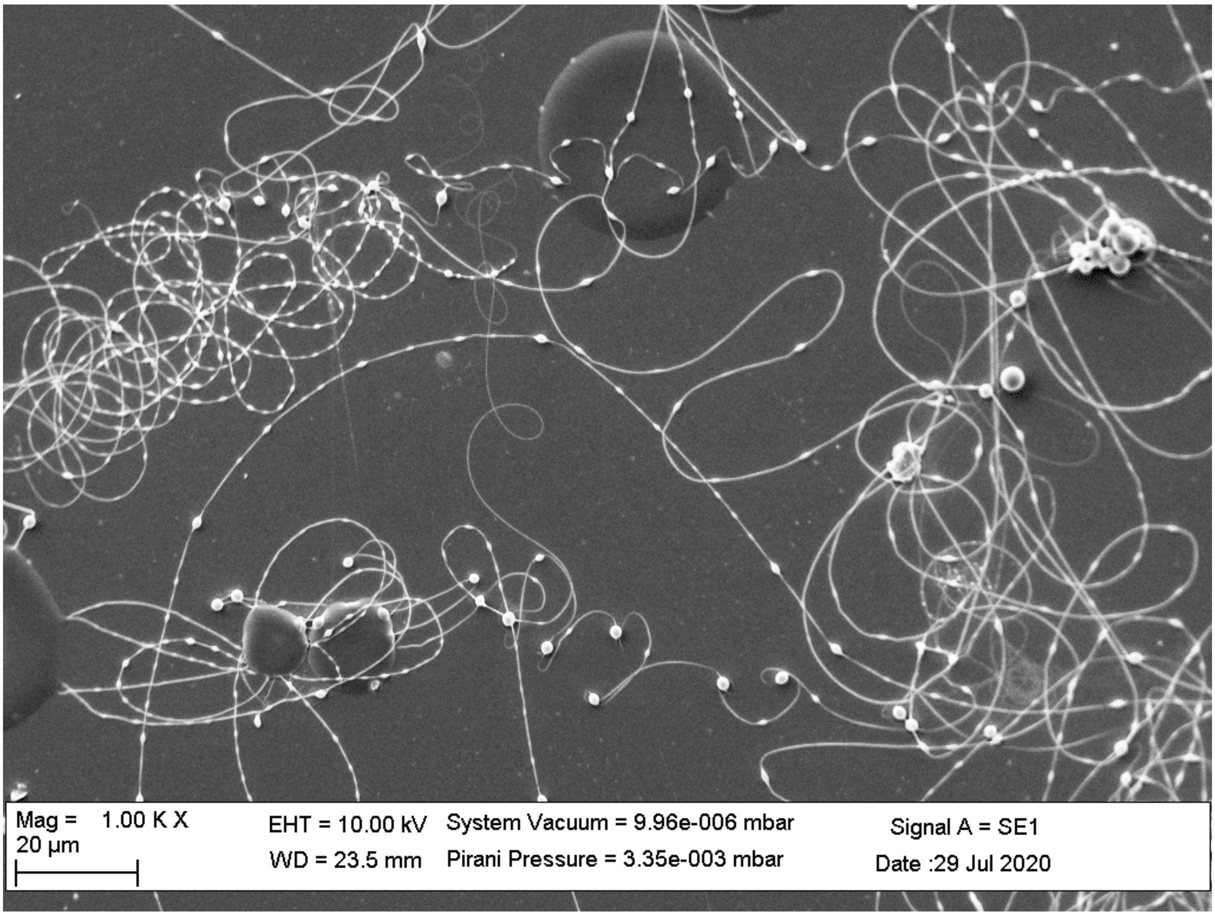

Figure 8.14: SEM image of beaded fibres produced from the electrospinning of solution 6 at 16.5 kV (1KX magnification)

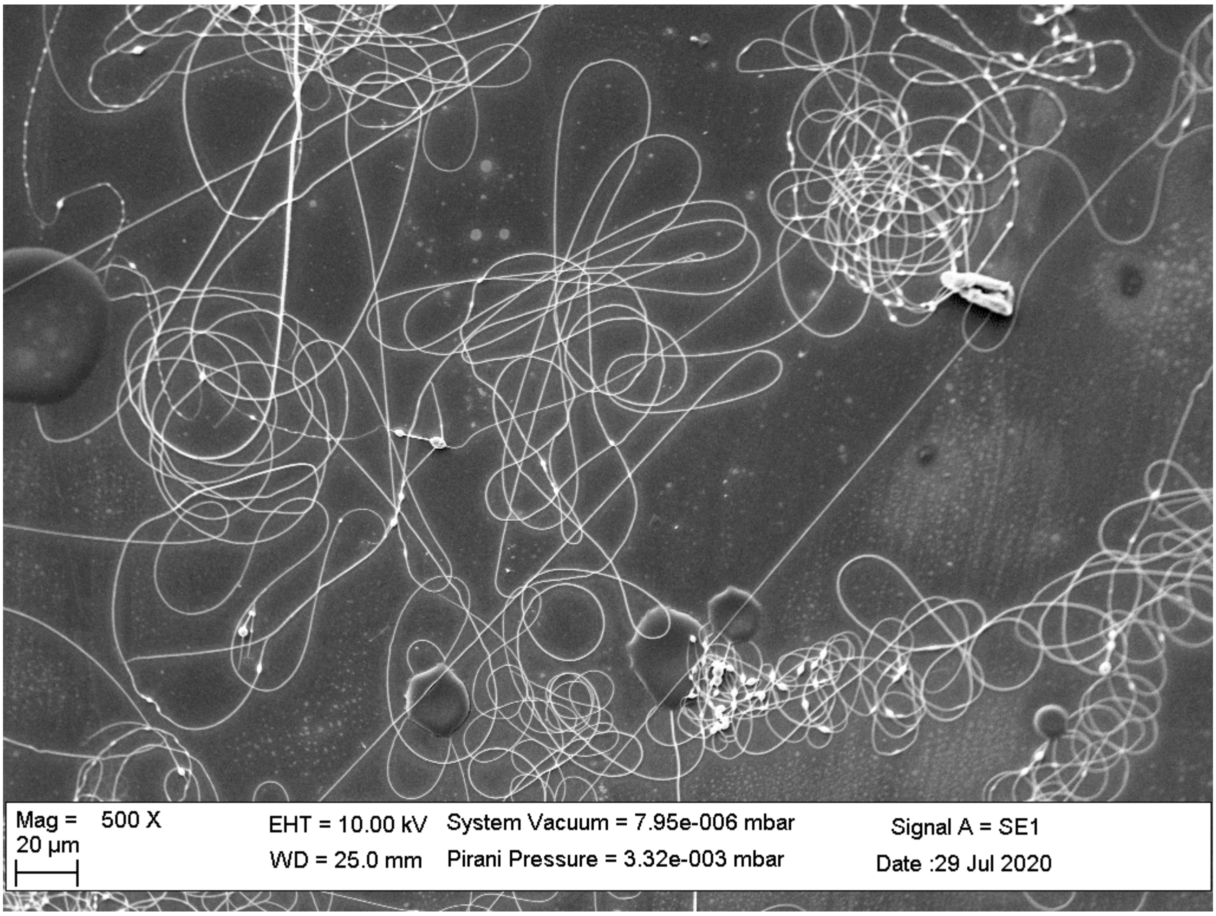

Figure 8.15: SEM image of beaded and beadless fibres produced from the electrospinning of solution 6 at 18 kV (500X magnification)

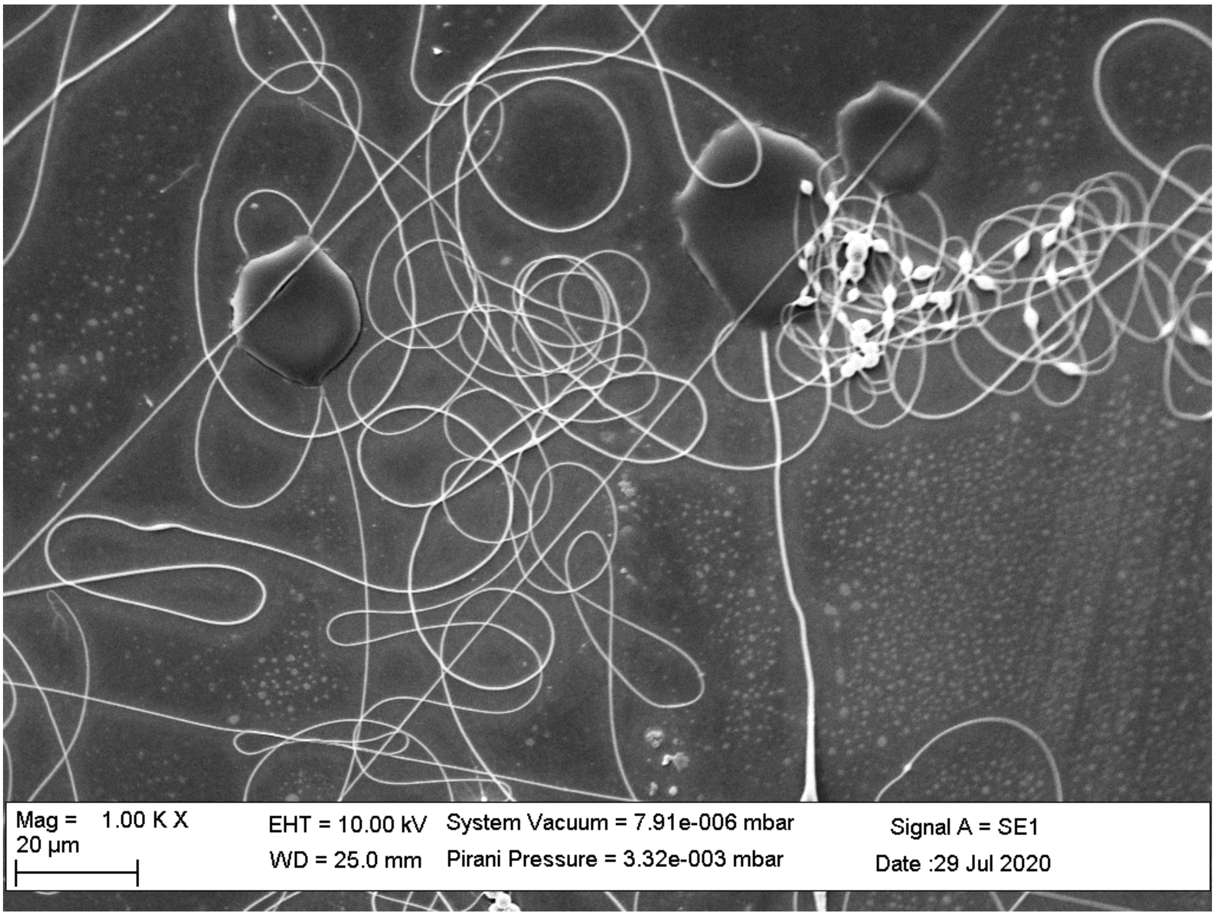

Figure 8.16: SEM image of slightly beaded fibres and some beadless fibres produced from the electrospinning of solution 6 at 18 kV (1KX magnification)

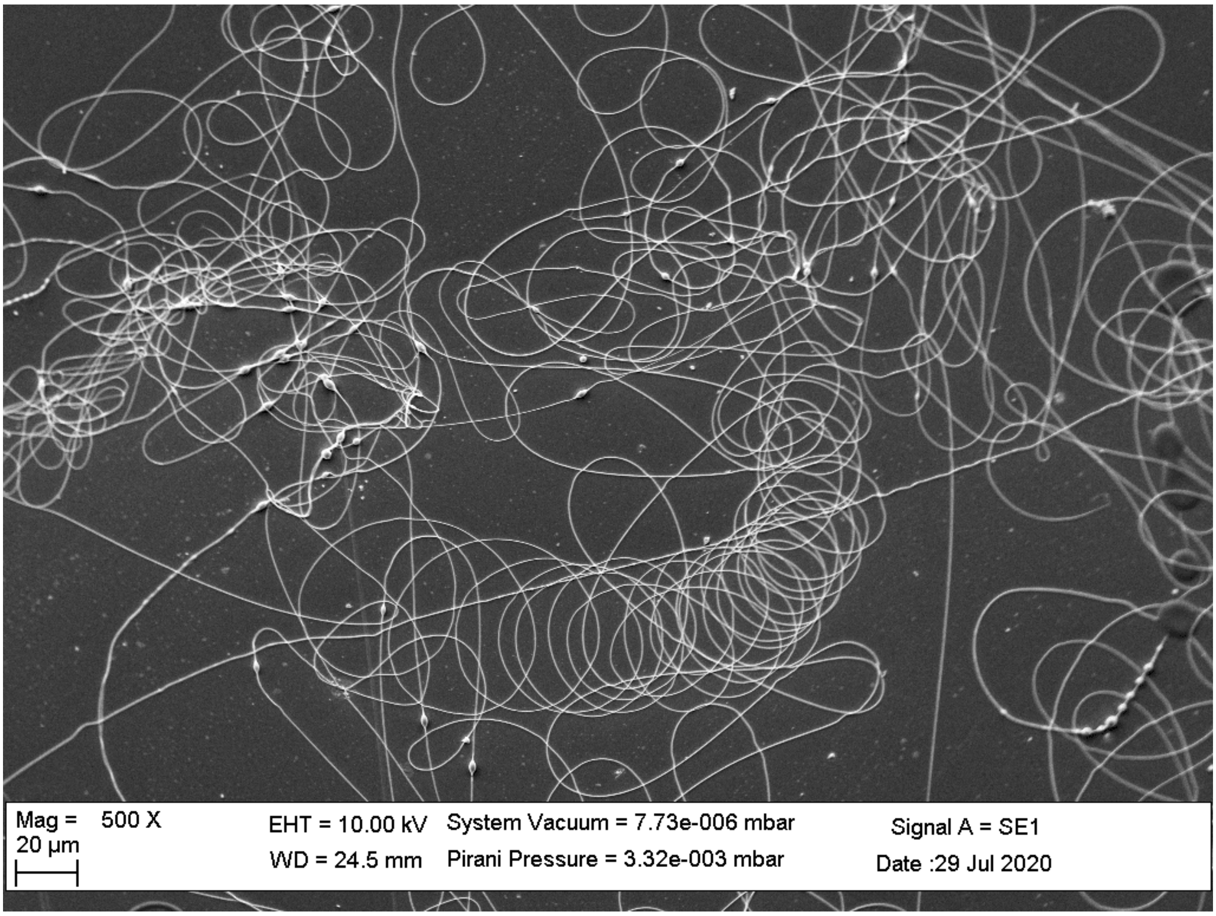

Figure 8.17: SEM image of fibres produced from the electrospinning of solution 6 at 19.5 kV (500X magnification)

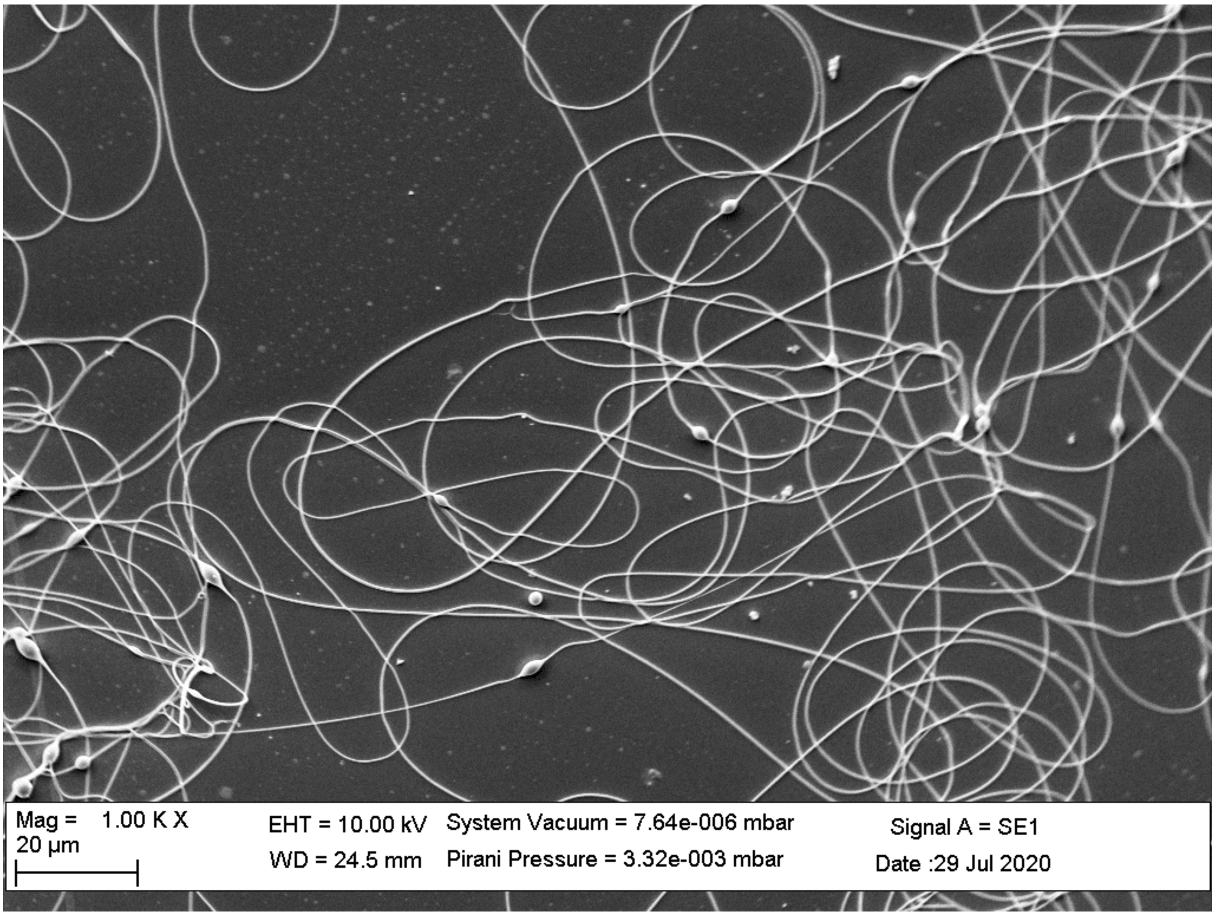

Figure 8.18: SEM image of fibres produced from the electrospinning of solution 6 at 19.5 kV (1KX magnification)

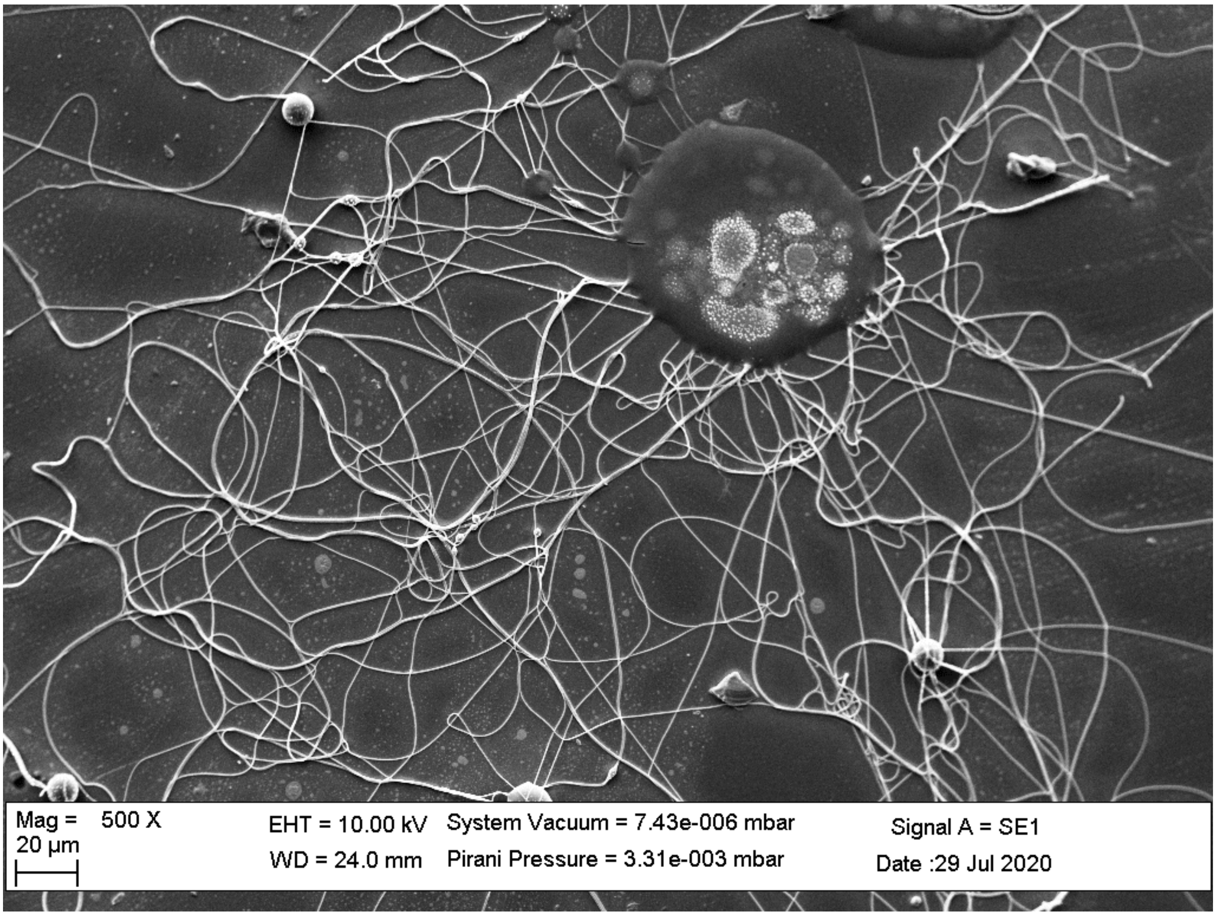

Figure 8.19: SEM image of fibres produced from the electrospinning of solution 6 at 21 kV (500X magnification)

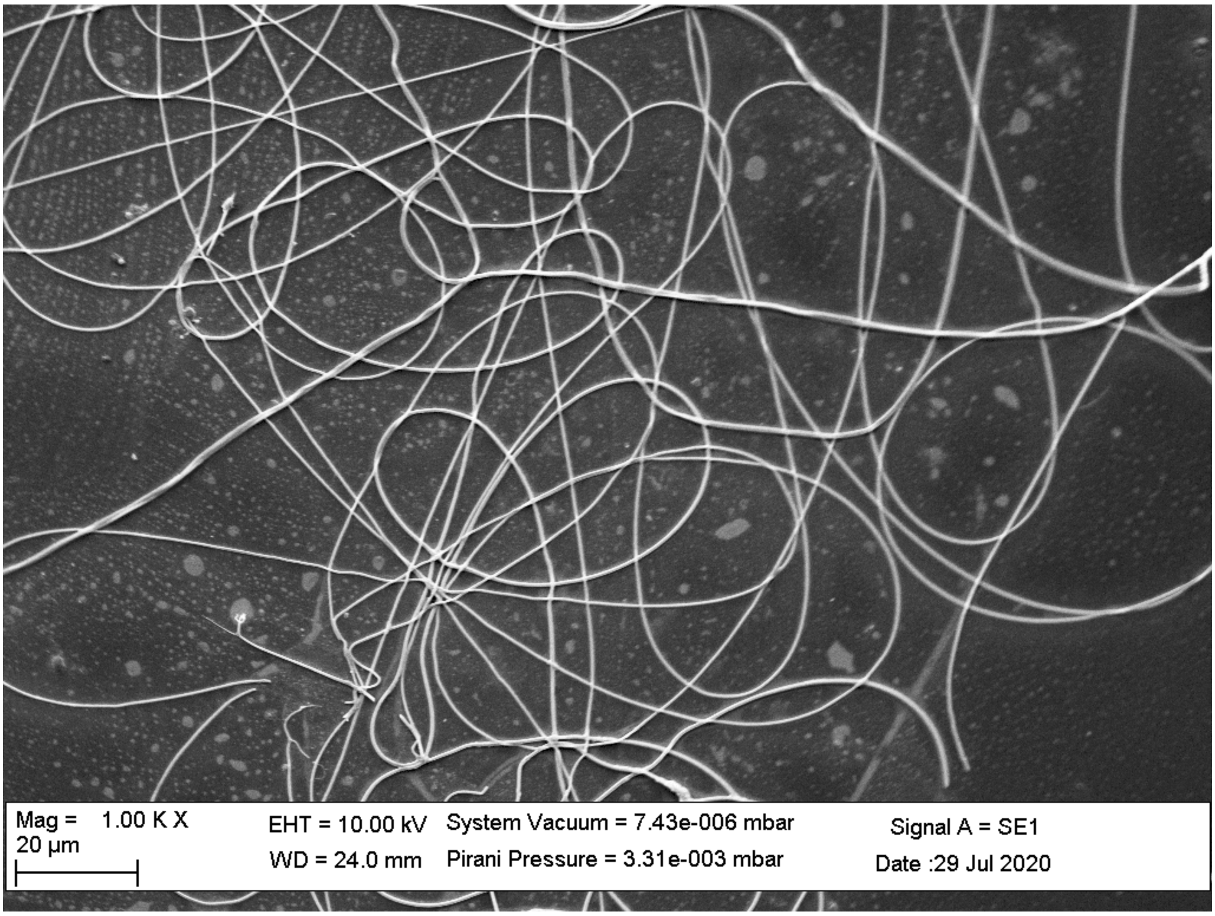

Figure 8.20: SEM image of fibres produced from the electrospinning of solution 6 at 21 kV (1KX magnification)

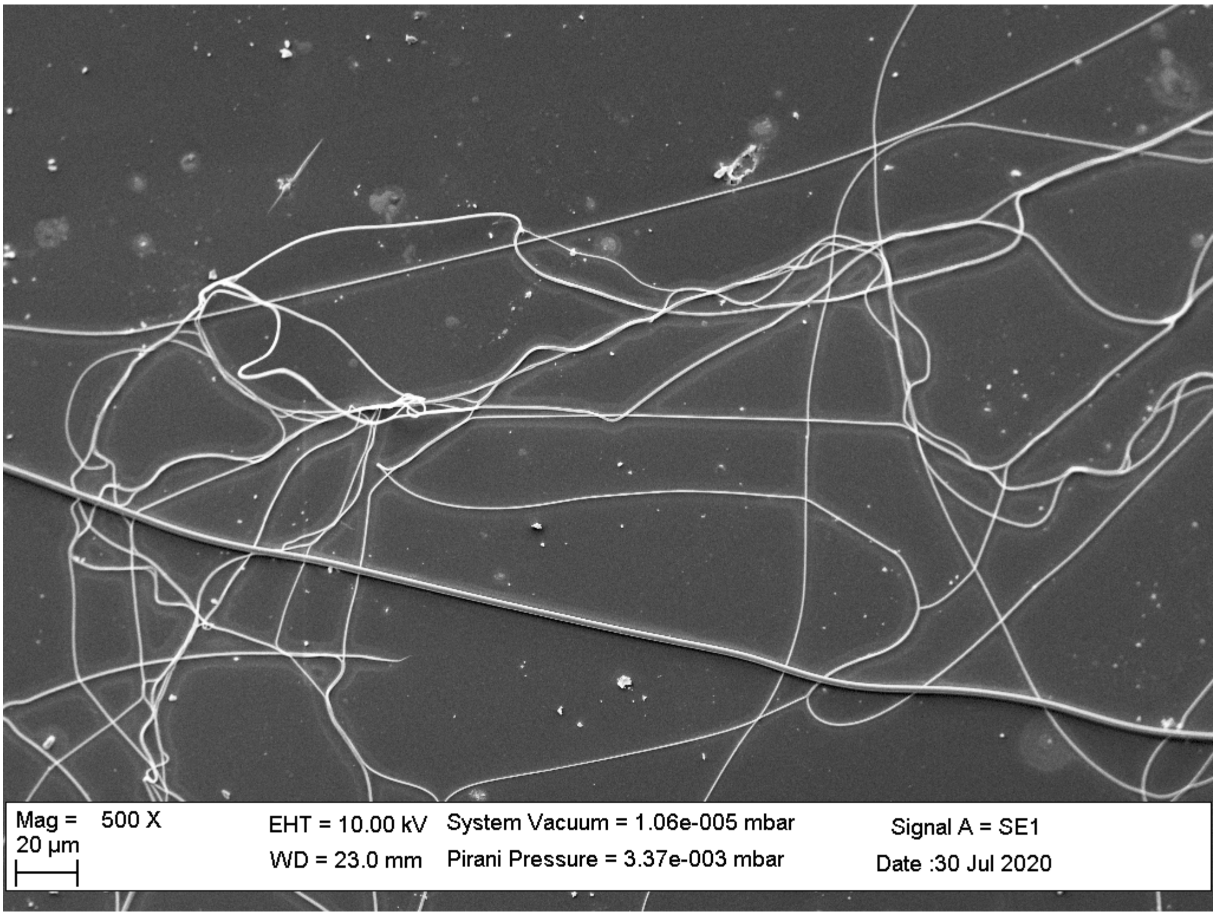

Figure 8.21: SEM image of fibres produced from the electrospinning of solution 6 at 22.5 kV (500X magnification)

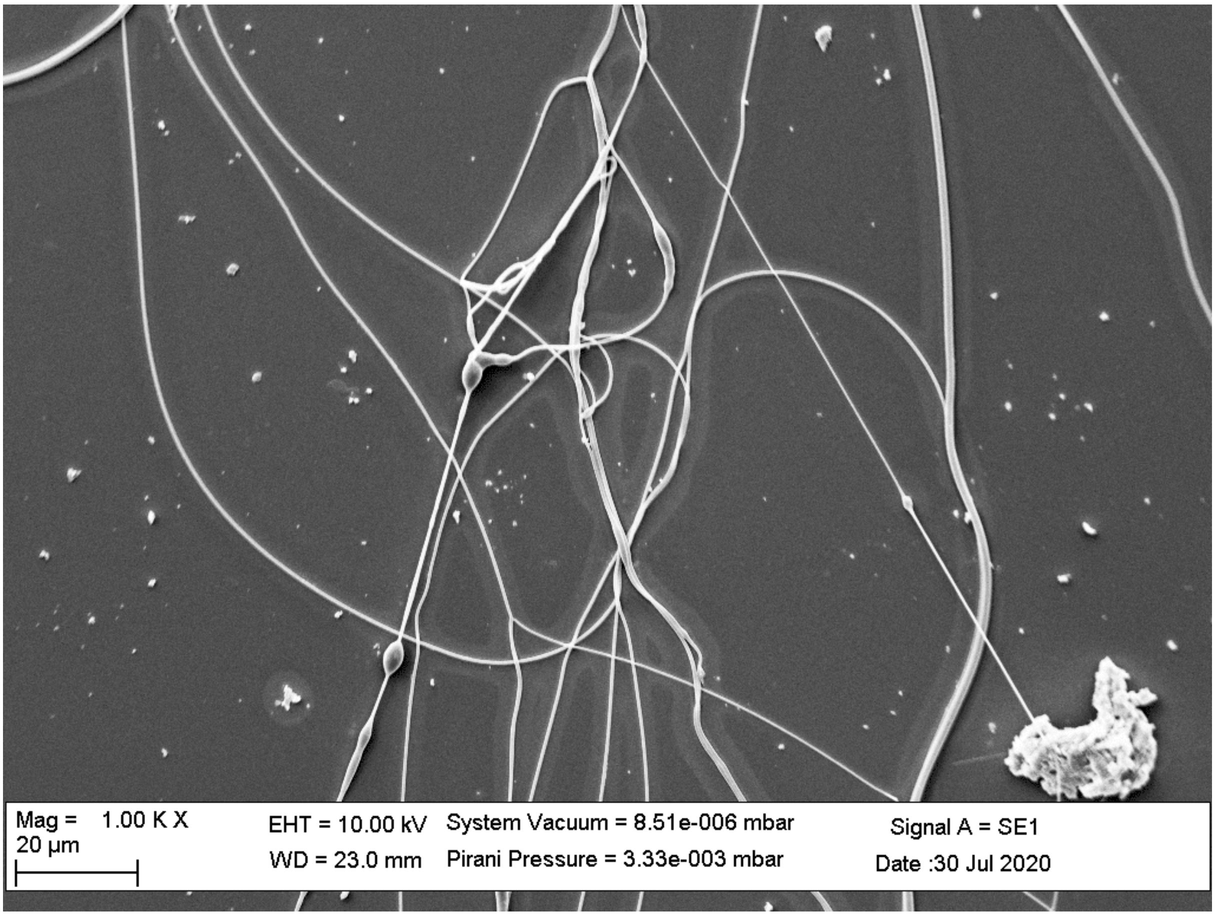

Figure 8.22: SEM image of fibres produced from the electrospinning of solution 6 at 22.5 kV (1KX magnification)

8.2.3 Flat fibres

Through the SEM images it was observed that the electrospinning of these solutions also lead to the formation of flat, ribbon shaped fibres. Figures 8.23 to 8.38 are SEM images at various magnifications showing these flat fibres. While the amount of these flat fibres are not a majority they were observed often during the SEM investigation. Furthermore, it was found that these flat fibres were produced by all solutions that produced fibres, both beaded and beadless. The production of electrospun flat fibres has been widely observed by researchers and have stated various reasons for this. Sheng-Han Chen [2014b] reported the contribution of solution feed rate to the formation of flat fibres. They found that on increasing the feed rate, the fibre diameter increases and as the feed rate is further increased, more solvent is trapped inside the fibres. Due to this, all of the solvent is unable to evaporate before the jet reaches the collector and thus the fibre collapses and attains a flat ribbon-like cross section [Sheng-Han Chen, 2014b]. This reasoning basically brings into picture insufficient flight time for solvent evaporation. That might not be the reason for the flat morphology of the fibres seen in this study. First, because compared to the round fibres the number of flat fibres is less. Applied voltage has an effect on the flight time, at a higher voltage the flight time is less due to the higher acceleration of the jet. In this study, the flat fibres were produced for all 5 applied voltage values and there were no major differences in the number of flat fibres produced between two voltages. Second, similar flat fibres were observed in the project done in the previous semester as well where the solvent-polymer system was the same and the flow rate used was a much higher value of 0.0622 ml/h compared to the 0.0025 ml/h used in this one. Again, there were no major changes in the proportion of flat fibres produced compared to the round fibres. From literature, a possible reason for the flat fibres produced in this project is the inhomogeneous and rapid evaporation of the solvent which leads to the formation of a solid polymer skin on the fibres [Darrell H. Reneker, 2008; Sureeporn Koombhongse, 2001; M. Dhanalakshmi, 2008]. Sureeporn Koombhongse [2001] on observing similar flat fibres reported that rapid evaporation of the solvent lead to the formation of solid thin polymer thin before all of the solvent inside coul evaporate. The remaining solvent then diffused through the skin and evaporated and then the atmospheric pressure collapsed the strong polymer skin which rendered the fibre flat. The skin is generally considered to be a gel phase formed by the solute, when the solute concentration near the surface becomes high. When the evaporation is rapid, the volume fraction of the polymer at the surface increases and at a certain volume fraction, a polymer skin is formed [Tohru Okuzono and Doi, 2006]. While no studies were found that used the polymer-solvent system used in this project, A. Koski [2004] electrospun aqueous solutions of PVA, having different concentrations and different molecular weight of PVA and found a transition from round to flat fibres when the concentration of PVA was increased. The concentration at which flat fibres were first observed was lower when the PVA used had a higher molecular weight, indicating that higher viscosity solutions could favour the formation of a polymer skin due to the rapid evaporation. Deng-Guang Yu and Wang [2014] conducted coaxial electrospinning of diclofenac sodium (DS) and Eudragit L100 (EL100) fibres using a mixed solvent of ethanol and N,N-dimethylacetamide. A mixture of ethanol and N,N-dimethylacetamide was used as a sheath fluid. On electrospinning the solutions without the sheath fluid, they observed flat fibres. But when more solvent was supplied using coaxial spinning, the fibres produced were round. The cross-sectional shape of a fiber that is created by evaporation of the solvent is dependent on the transport of solvent molecules through the drying surface of the jet [Darrell H. Reneker, 2008]. Some more interesting flat morphologies were observed. It was observed that some fibres had a cylindrical shape but changed to a flat one at some distance along their length. This can be seen in Figures 8.27, 8.32 and 8.33. Another observation was the occurrence of twisted flat fibres and can be seen in Figures 8.37 and 8.38. Finally, Figures 8.23, 8.25, **??** and 8.28 show a zigzag arrangement of fibres which is a result of the higher order bending instabilites experienced by the jet.

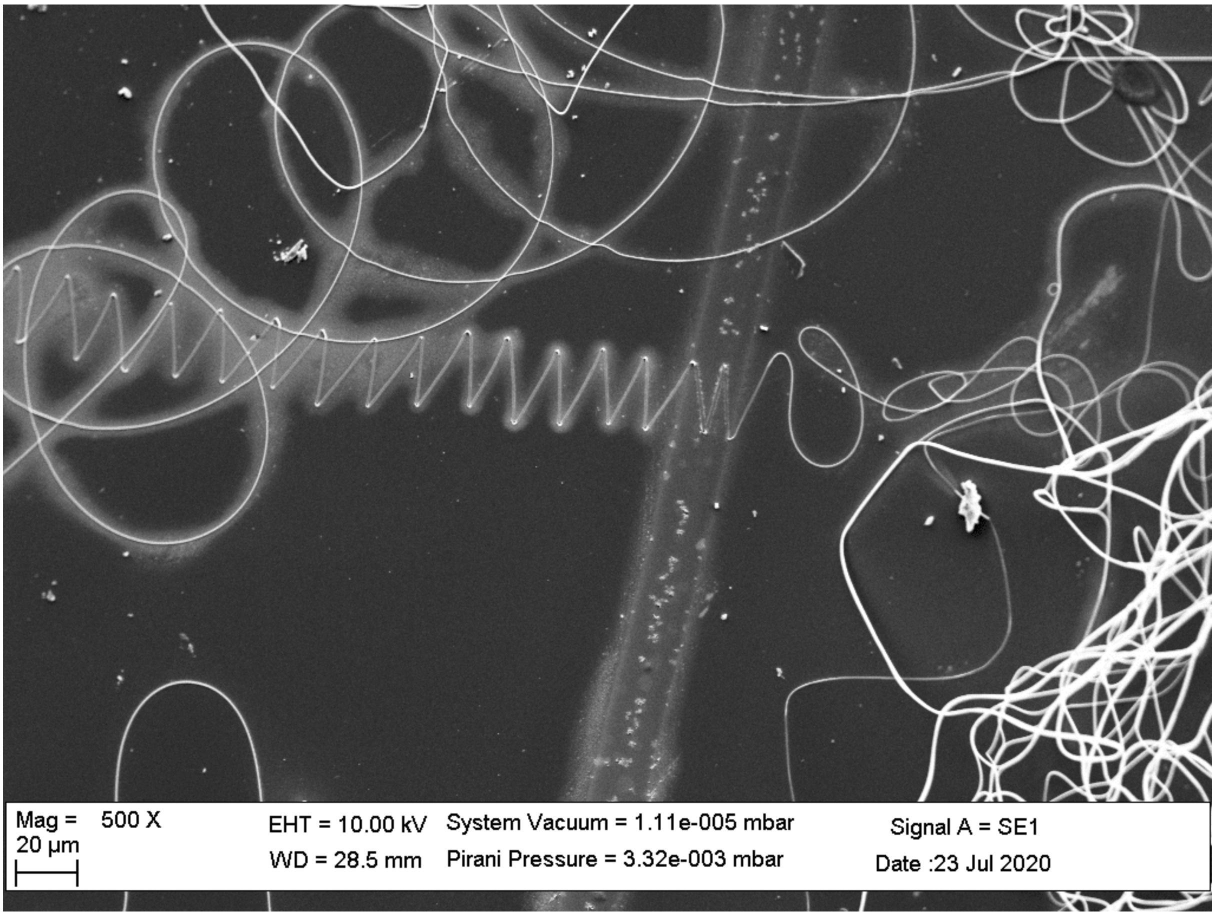

Figure 8.23: SEM image of flat fibres produced from the electrospinning of solution 2 at 18 kV (500X magnification)

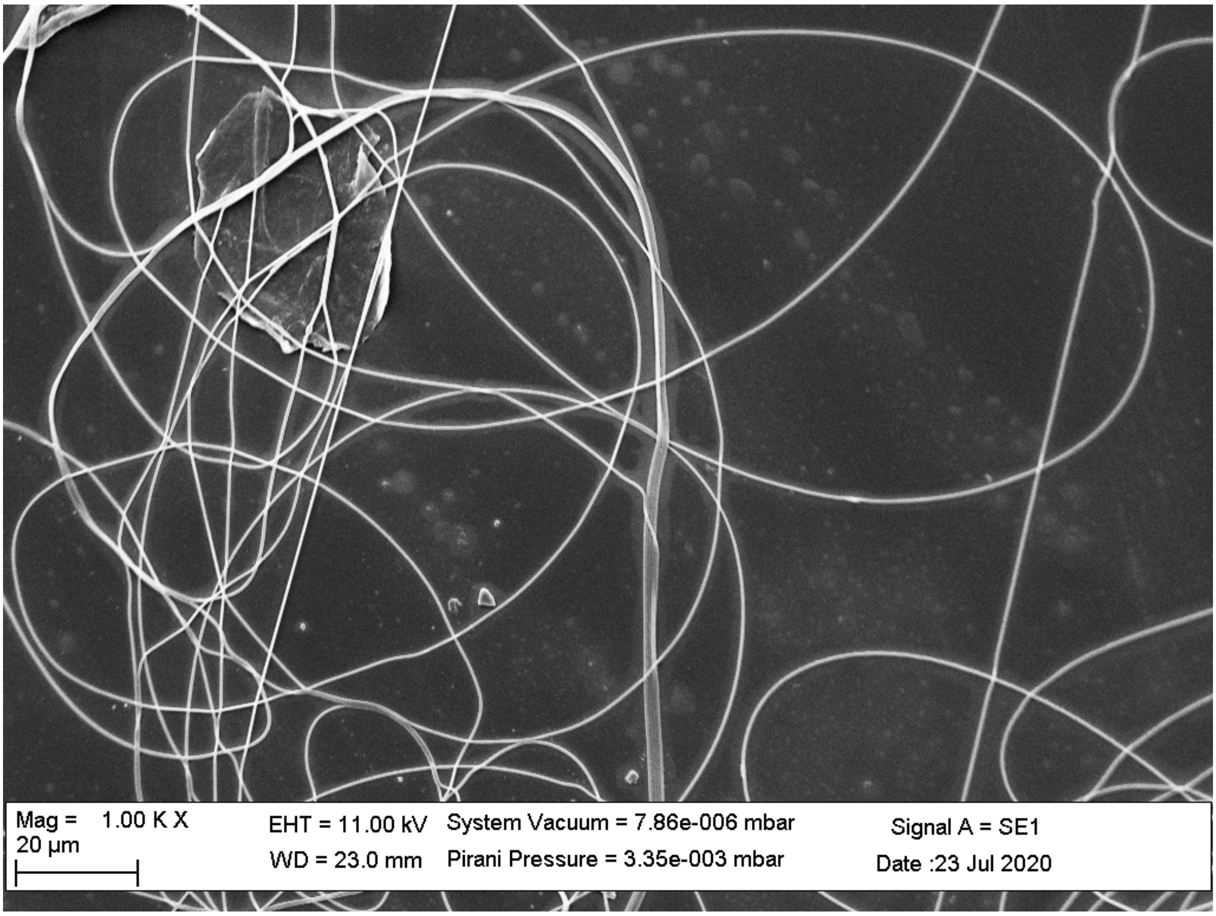

Figure 8.24: SEM image of flat fibres produced from the electrospinning of solution 2 at 19.5 kV (1KX magnification)

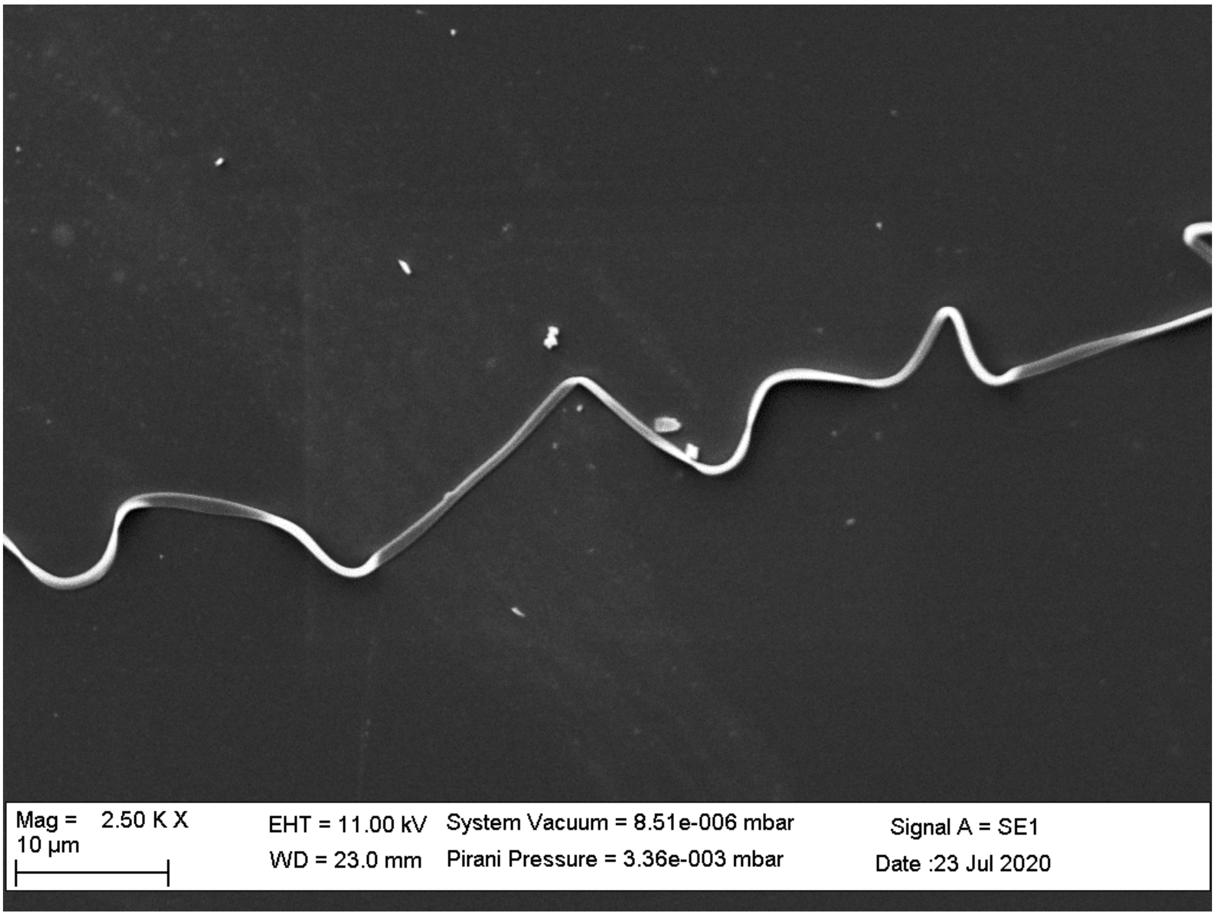

Figure 8.25: SEM image of a flat fibre produced from the electrospinning of solution 2 at 19.5 kV (2.5KX magnification)

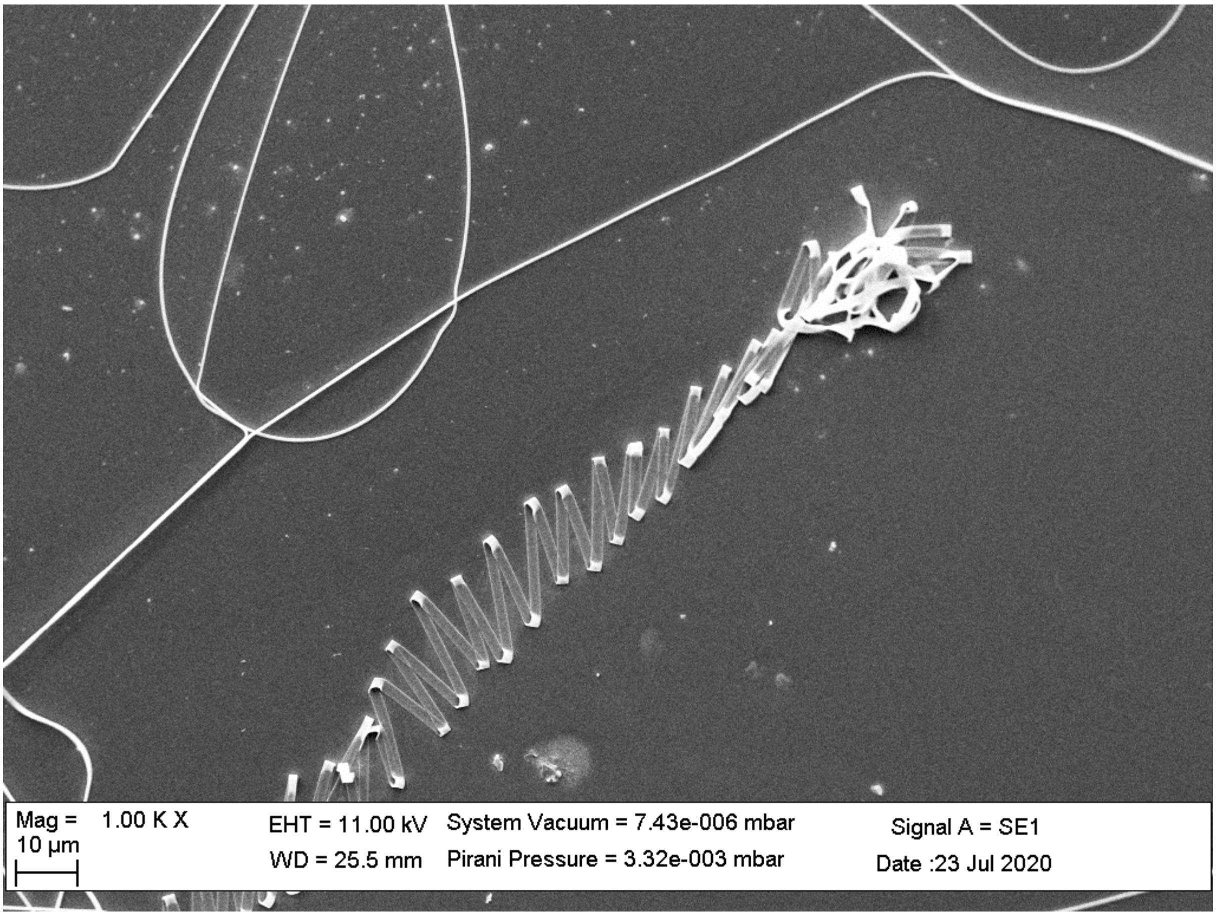

Figure 8.26: SEM image of flat fibres produced from the electrospinning of solution 2 at 21 kV (1KX magnification)

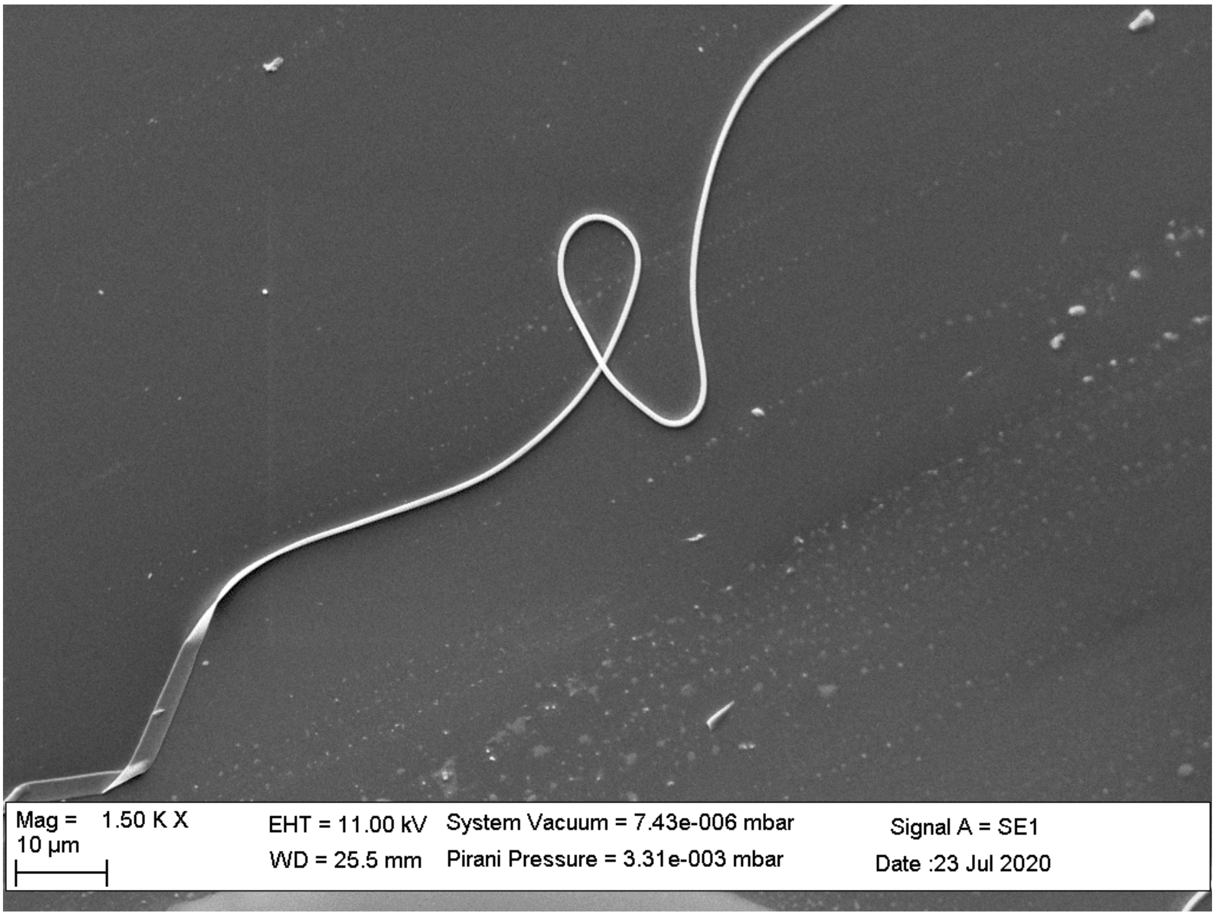

Figure 8.27: SEM image of flat and round fibre produced from the electrospinning of solution 2 at 21 kV (1.5KX magnification)

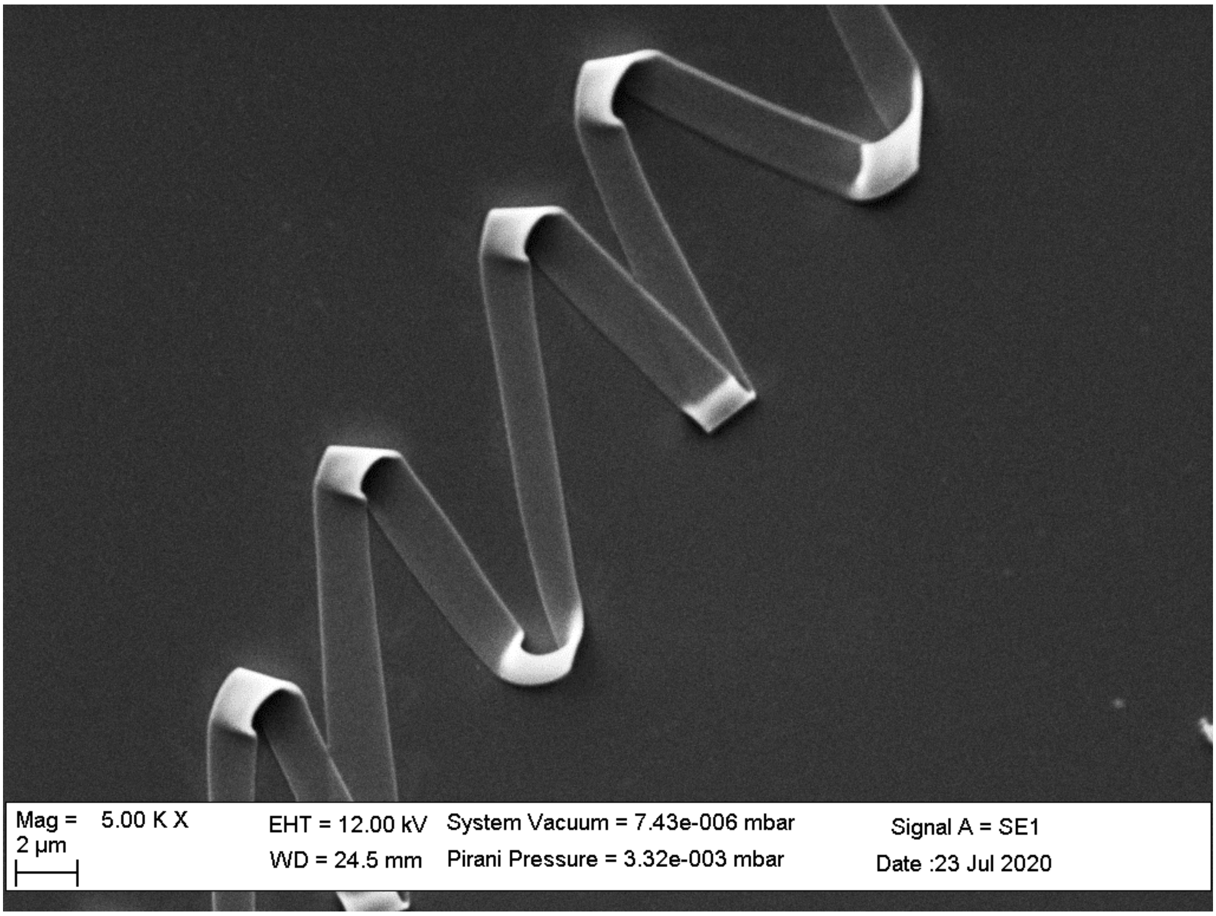

Figure 8.28: SEM image of flat fibres produced from the electrospinning of solution 2 at 21 kV (5KX magnification)

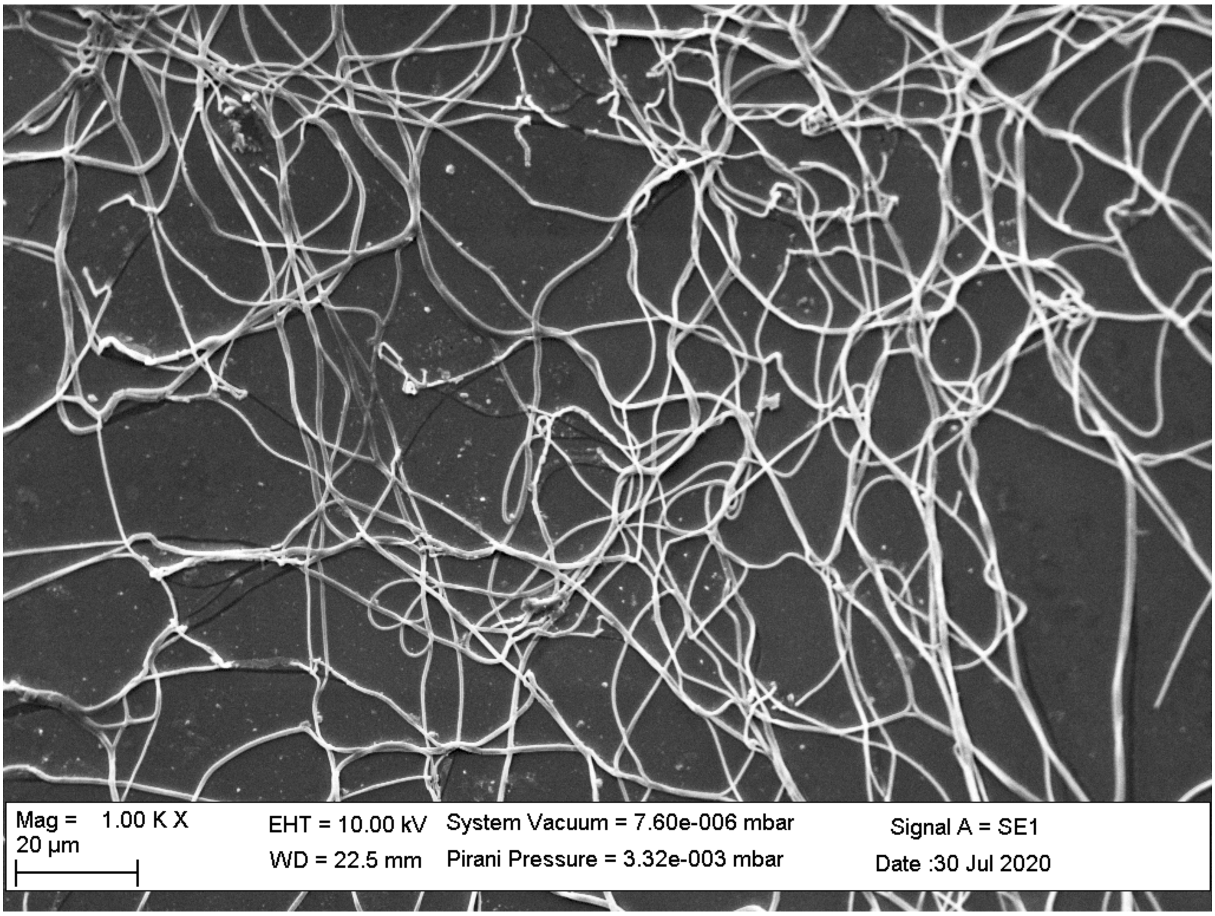

Figure 8.29: SEM image of flat fibres produced from the electrospinning of solution 2 at 22.5 kV (1KX magnification)

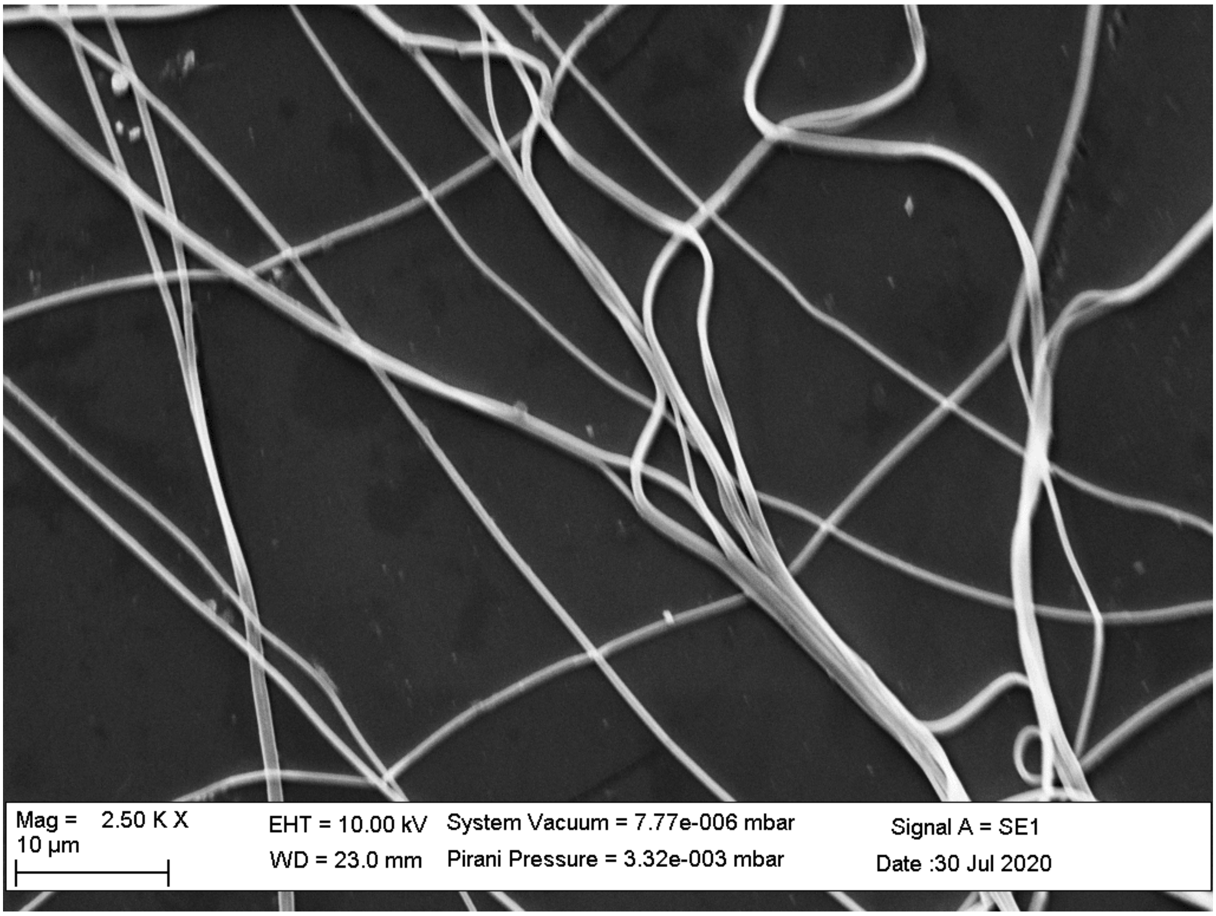

Figure 8.30: SEM image of flat fibres produced from the electrospinning of solution 2 at 22.5 kV (2.5KX magnification)

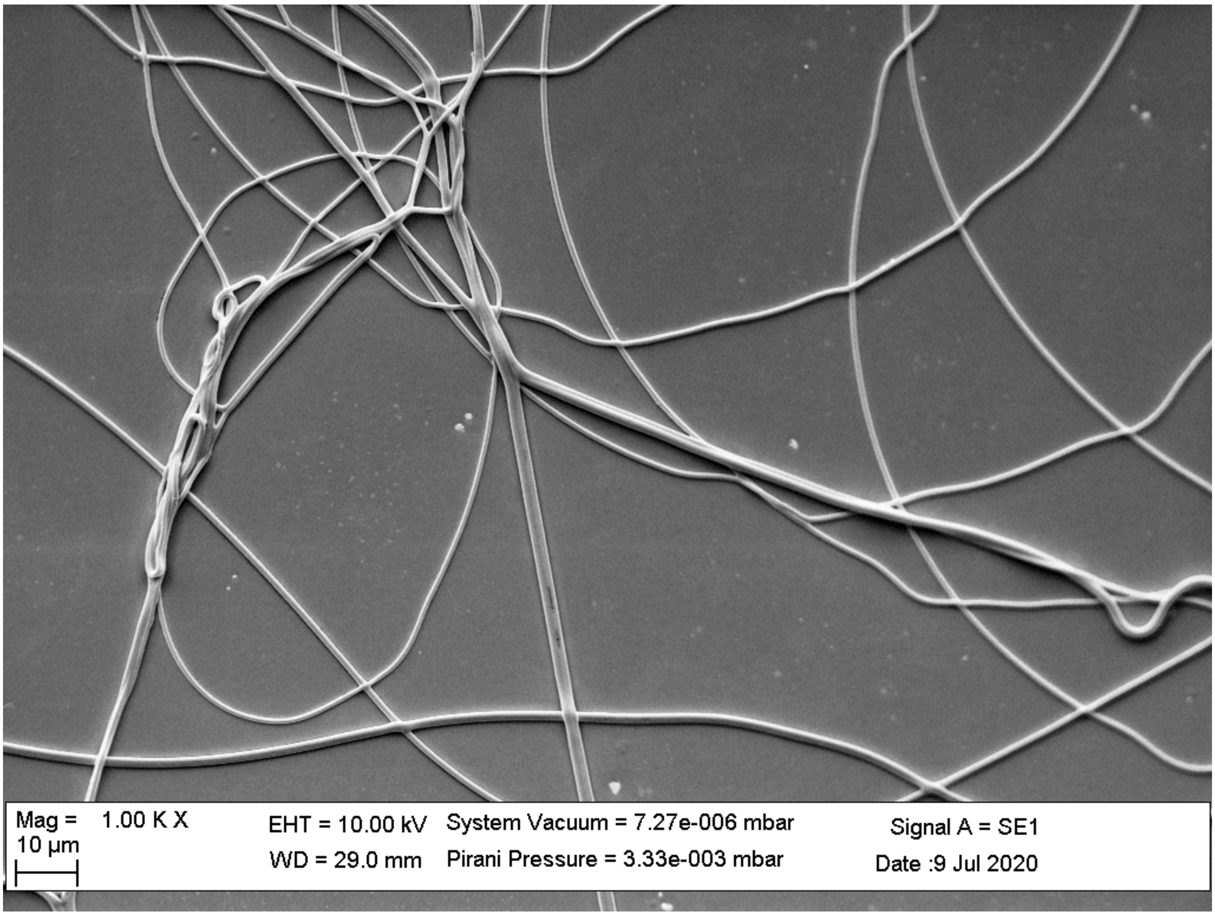

Figure 8.31: SEM image of flat fibres produced from the electrospinning of solution 3 at 16.5 kV (1KX magnification)

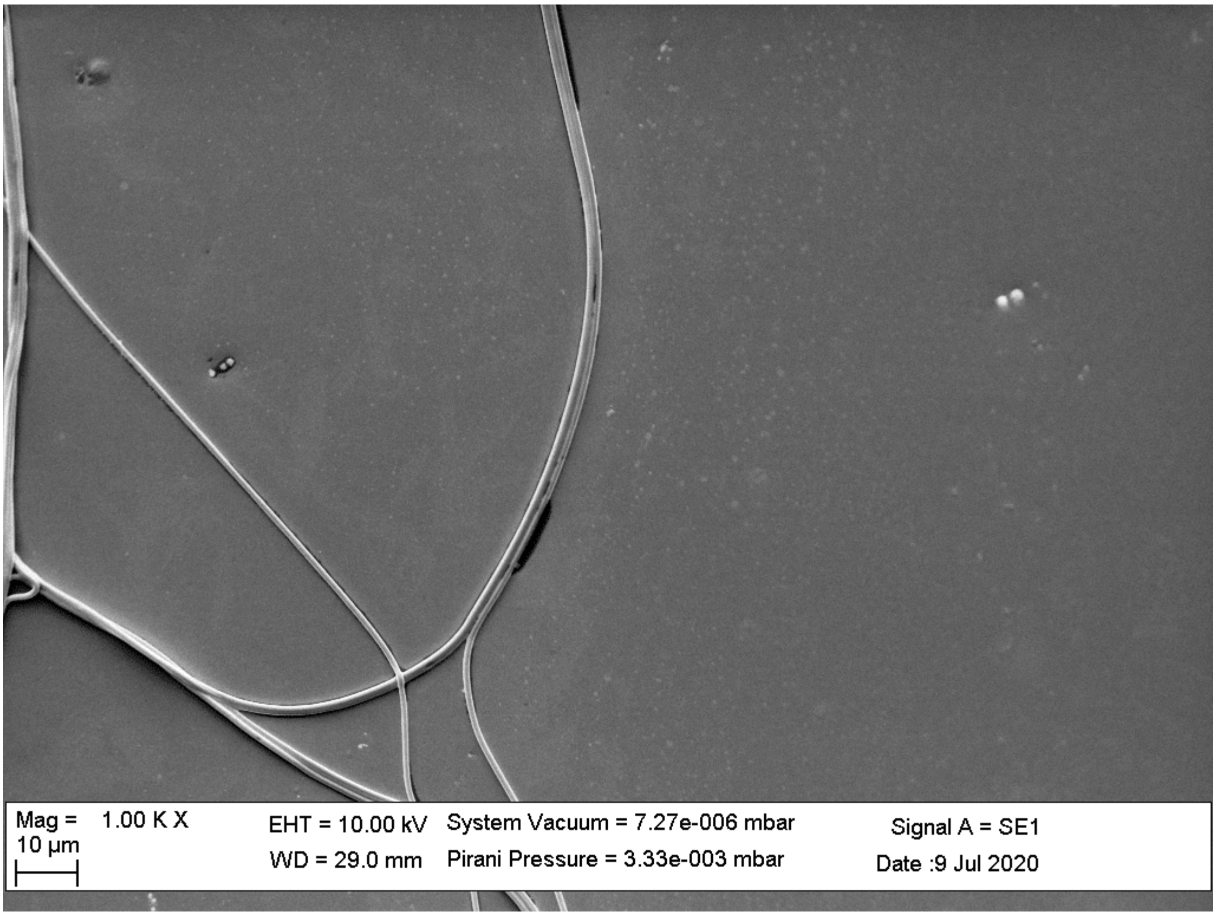

Figure 8.32: SEM image of a flat and round fibre produced from the electrospinning of solution 3 at 16.5 kV (1KX magnification)

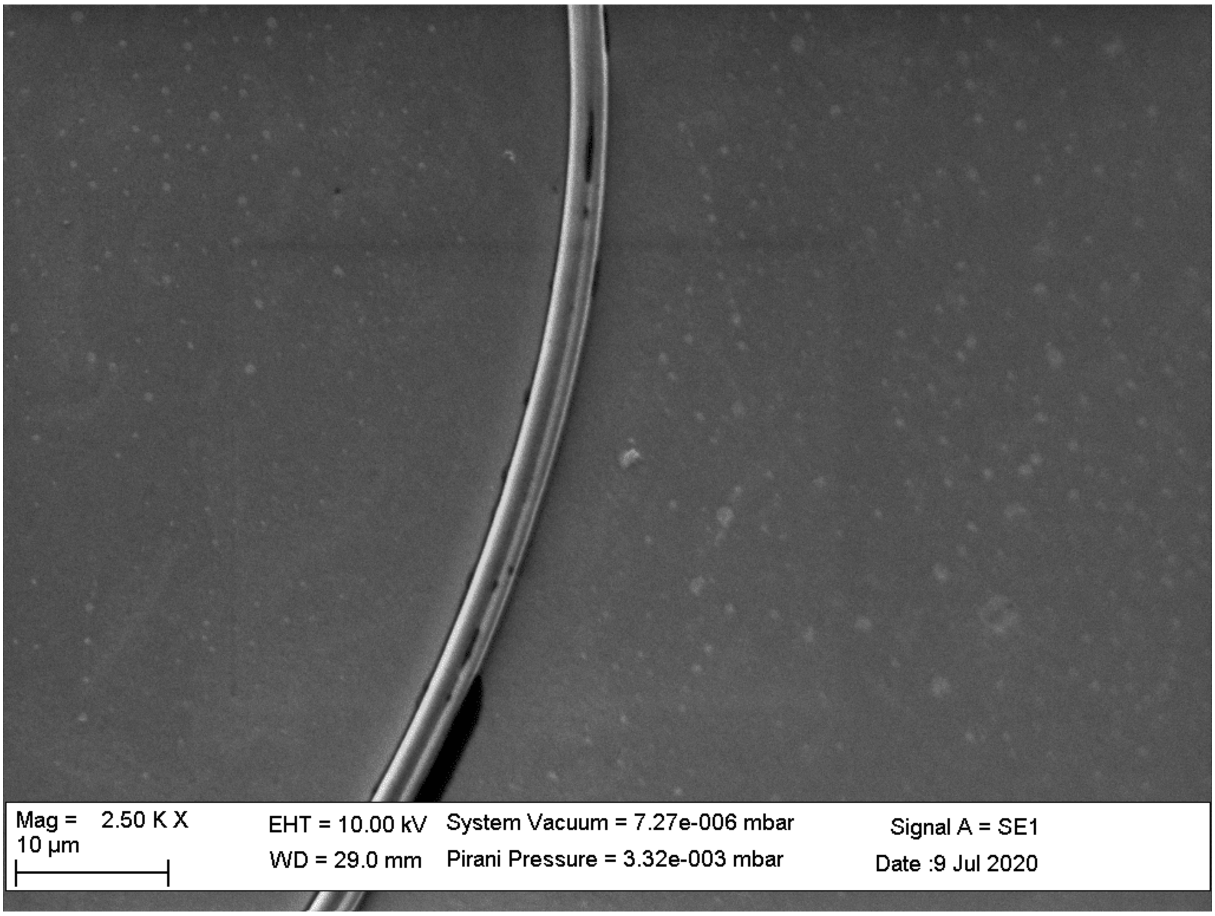

Figure 8.33: SEM image of the same fibre in 8.32 but at 2.5KX magnification

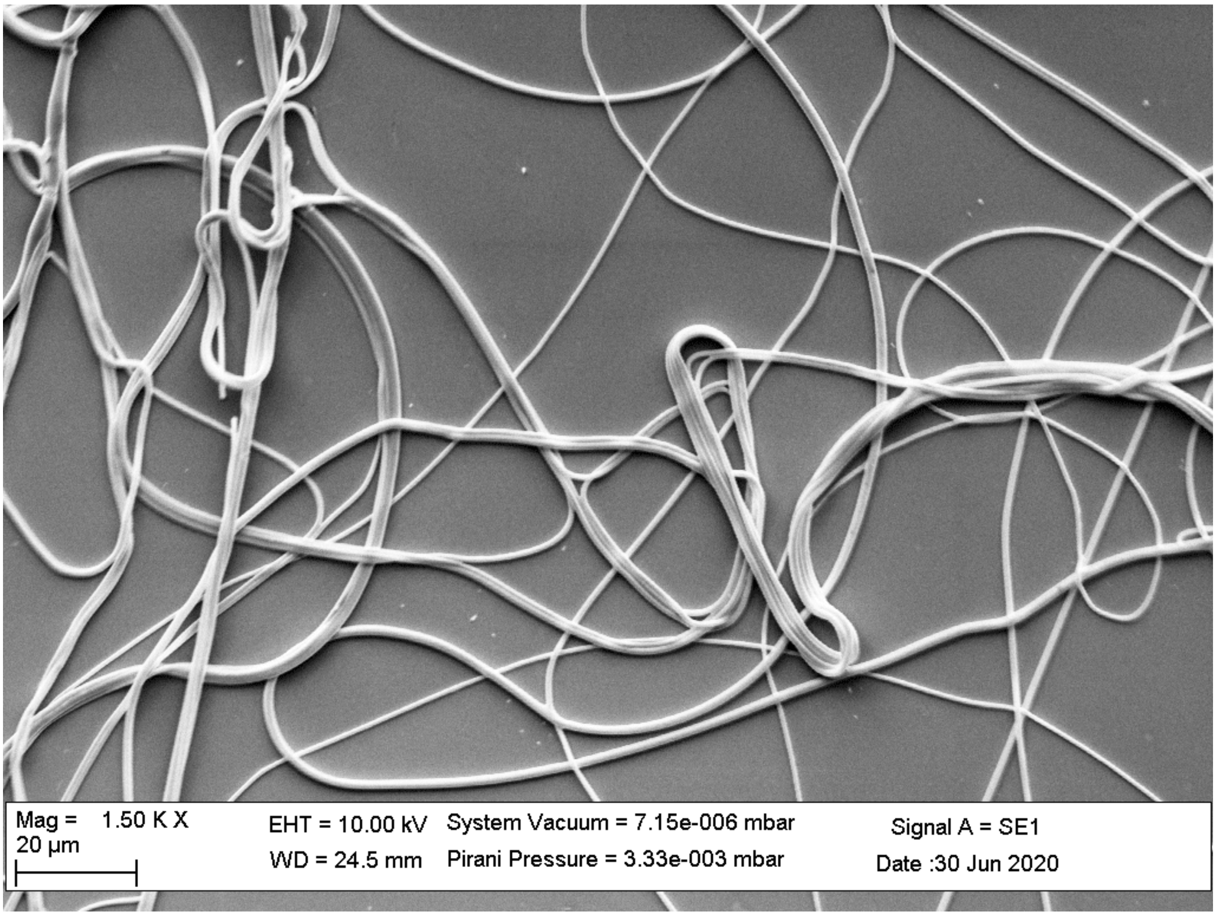

Figure 8.34: SEM image of flat fibres produced from the electrospinning of solution 3 at 18 kV (1.5KX magnification)

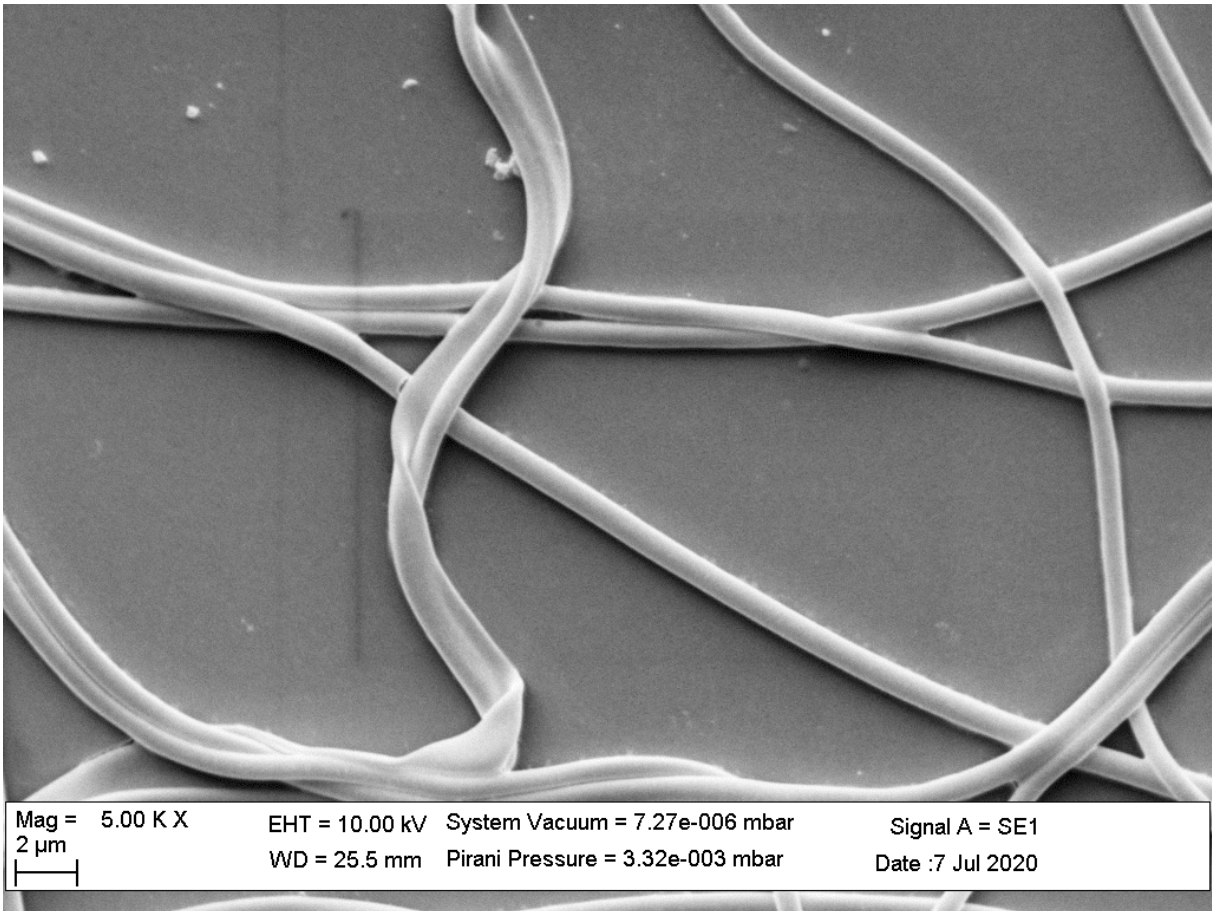

Figure 8.35: SEM image of a flat fibre produced from the electrospinning of solution 3 at 18 kV (5KX magnification)

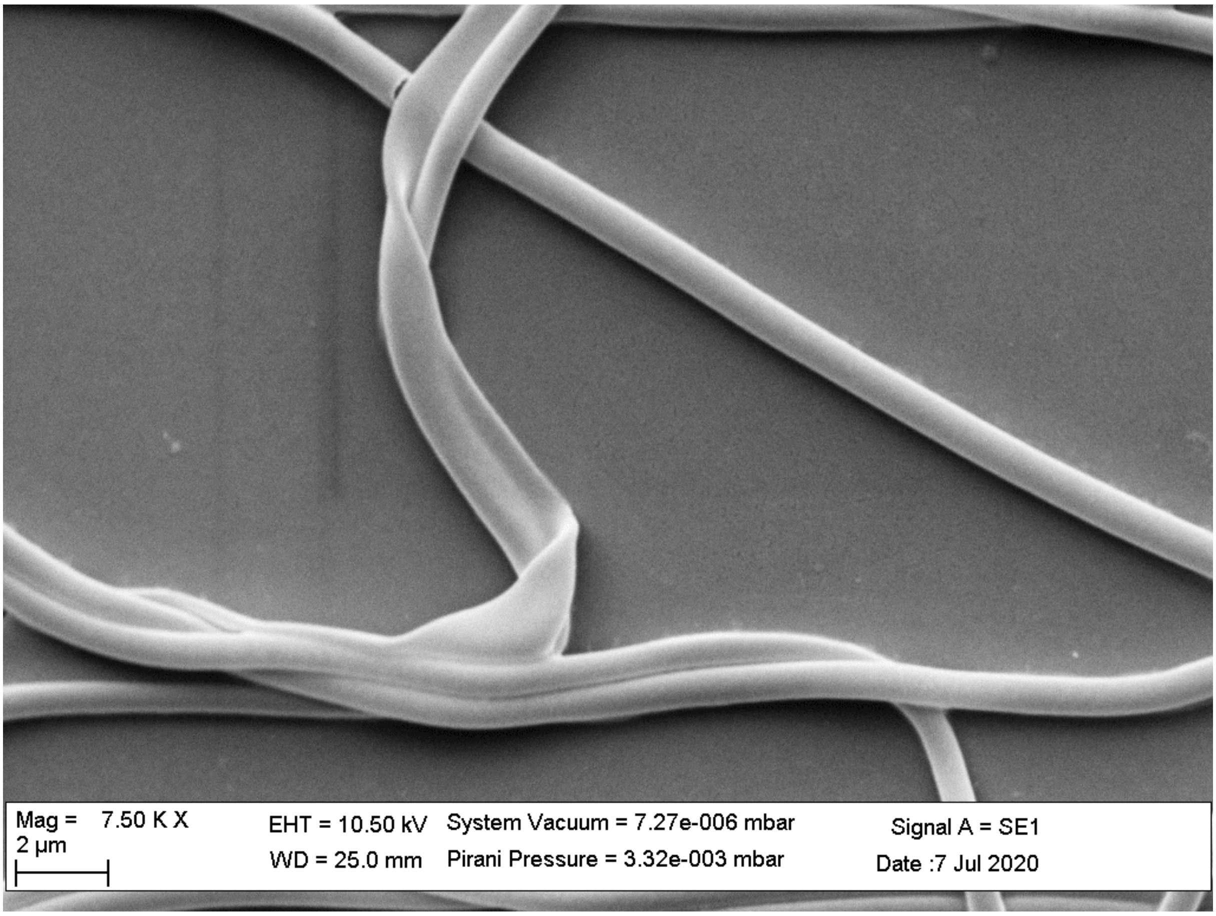

Figure 8.36: SEM image of the same flat fibre seen in 8.35 but at 7.5KX magnification

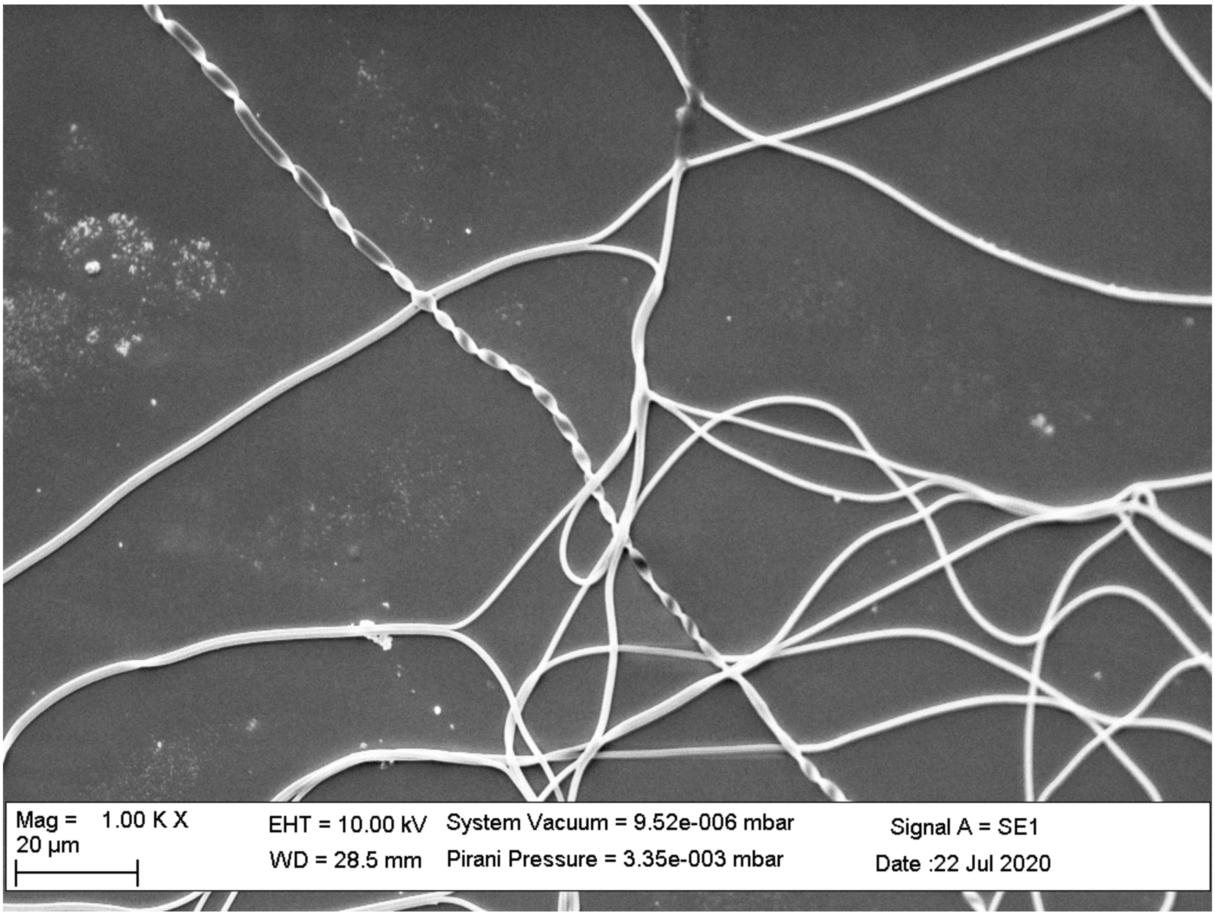

Figure 8.37: SEM image of a twisted flat fibre produced from the electrospinning of solution 3 at 22.5 kV (1KX magnification)

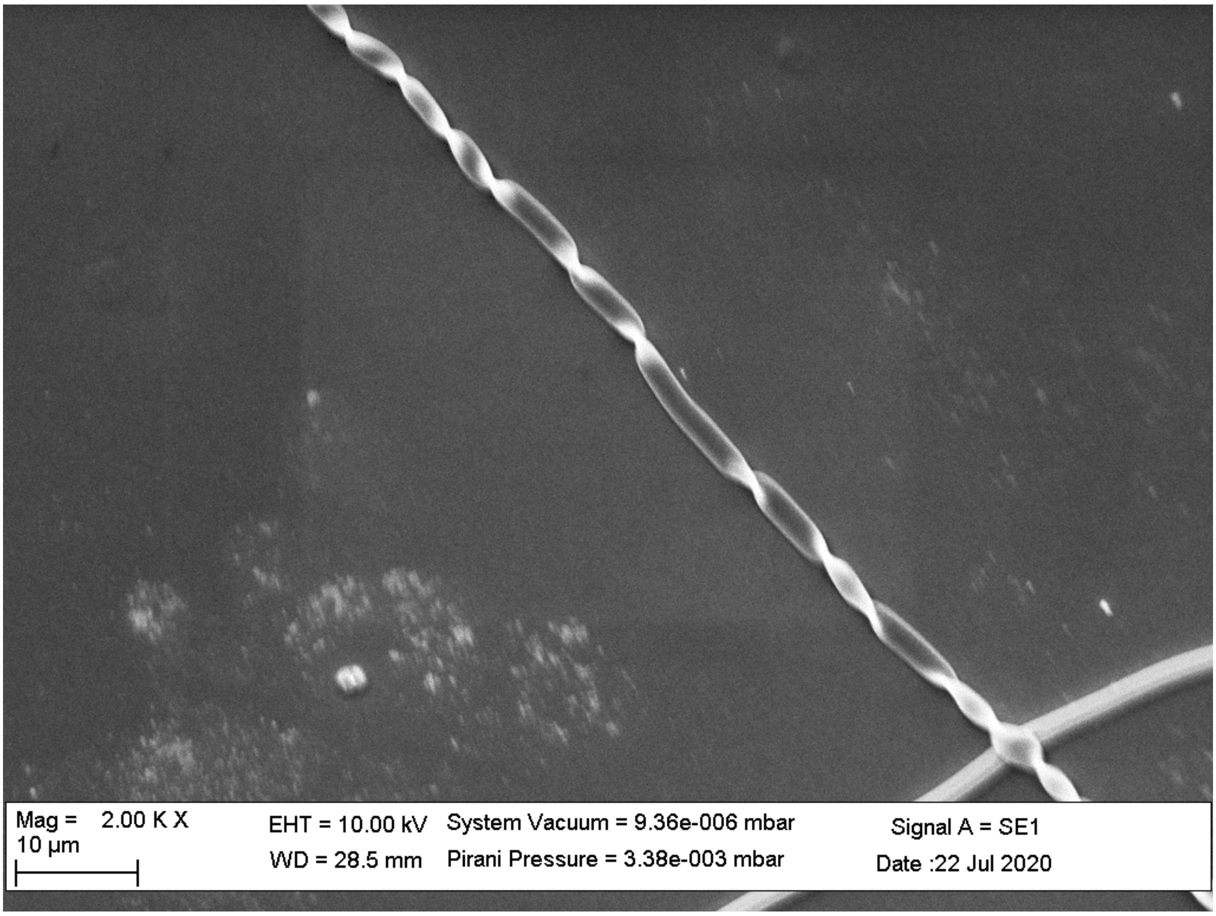

Figure 8.38: SEM image of the same twisted flat fibre seen in 8.37 but at 2KX magnification

8.2.4 Twin/Fused fibres

An interesting observation was made through the SEM investigation of the fibres produced. It was observed that a majority of fibres showed a tendency to be attached to each other along their lengths. This was a frequent observation and can also be seen in some of the SEM images that have been placed prior to this section. Figures 8.39 to 8.46 show these twin fibres and in some case even three to four fibres attached together. This was observed clearly for solutions 2 and 3. This arrangement of fibres could be observed clearly only when the magnification was quite high i.e at 2.5KX and above. At lower magnifications these fibres lined up together looked like one flat fibre. This can be seen in Figure 8.39. Thus, for solution 6 since the images were not clear at 2.5KX magnification it could not be differentiated whether the fibres and flat or just a group of fibres arranged very close to each other. ZENG Jing [2012] observed twin fibres when they electrospun solutions of poly(l-lactide) and poly(l-lactide-co-glycolide) in a mixed solvents of chloroform and acetone, loaded with rifampin. They observed that twin fibres were produced only when rifampin was present in the solution, that too at a certain concentration and above. They reported that the amount of twin fibres increased with increased loading of rifampin in the solution. They attributed the formation of twin fibres to the amphipathic nature of rifampin, whose hydrophillic part facilitated the formation of a sold skin layer due to rapid evaporation. However, in this case, the solvent evaporation is less rapid as compared to that described for the formation of flat fibres. Due to this less rapid evaporation the collapse of the fibre wall takes place only in the middle, which leads to the formation of twin fibres. This could be a possible explanation for the joined fibres observed in this study since PVA shares the same hydrophillic nature of rifampin. Another possible explanation for the formation of twin fibres has been reported by Li Meng-Meng and Zhi-Ming [2011]. They stated that since the fluid jet carries a large number of like charges, the coloumbic repulsion of charges on the surface of the jet could elongate the fibre in the radial direction and eventually split it into two fibres of smaller diameters. This could also be a likely explanation since the joined fibres show a tendency to split completely through the middle and change paths. This can be observed in Figure 8.43.

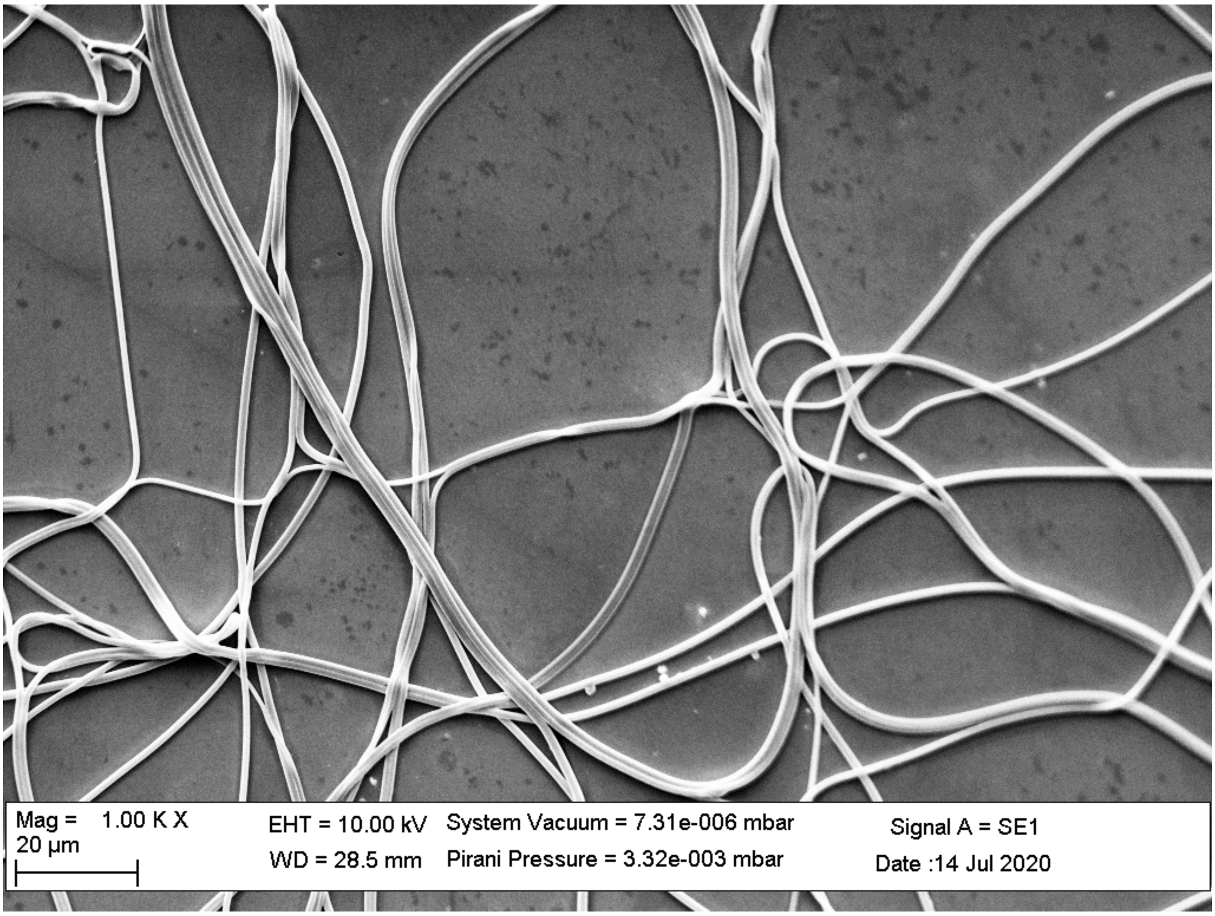

Figure 8.39: SEM image showing multiple fibres joined along their length making them look flat, produced from electrospinning of solution 3 at voltage 21 kV (1KX magnification)

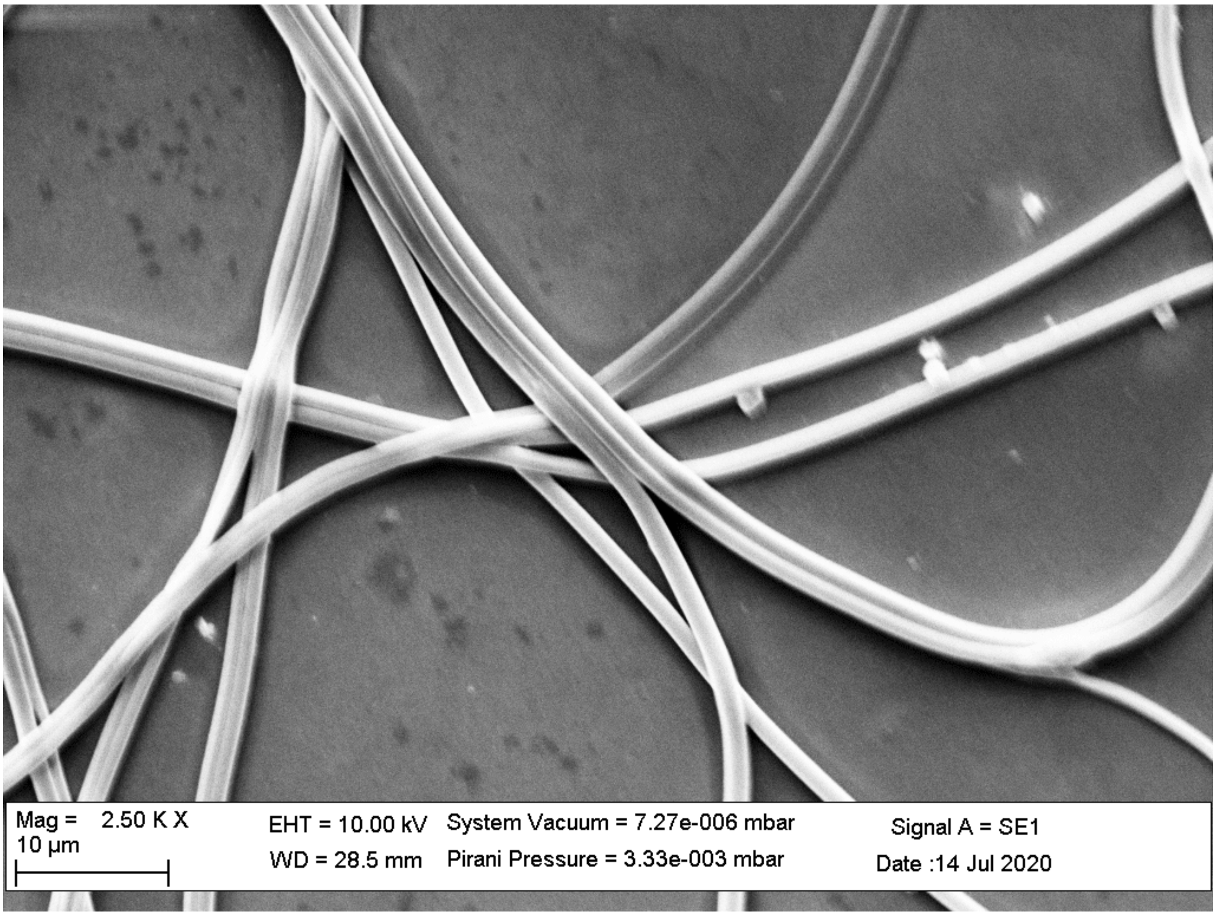

Figure 8.40: SEM image showing multiple fibres joined along their lengths produced from electrospinning of solution 3 at voltage 21 kV (2.5KX magnification)

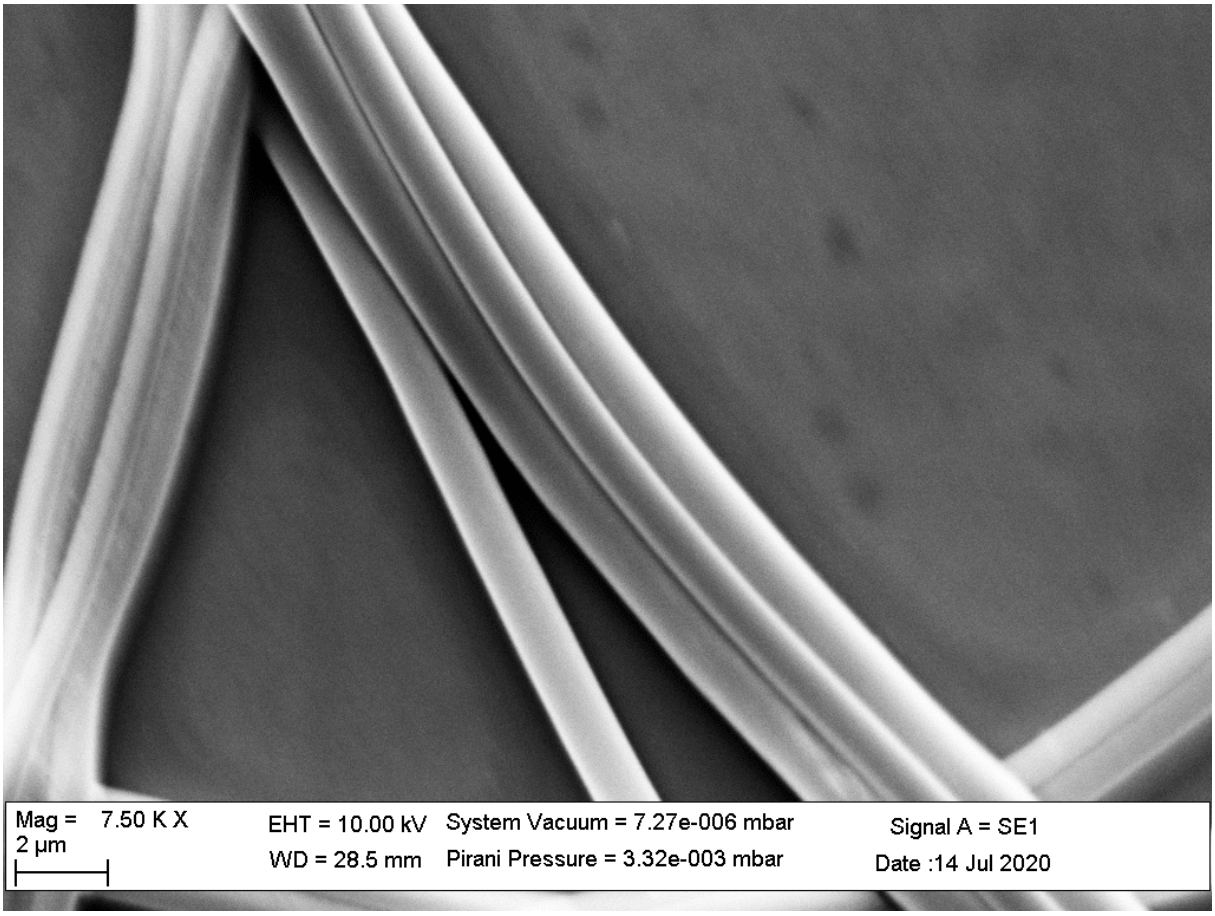

Figure 8.41: SEM image of fibres in Figure 8.40 but at 7.5KX magnification

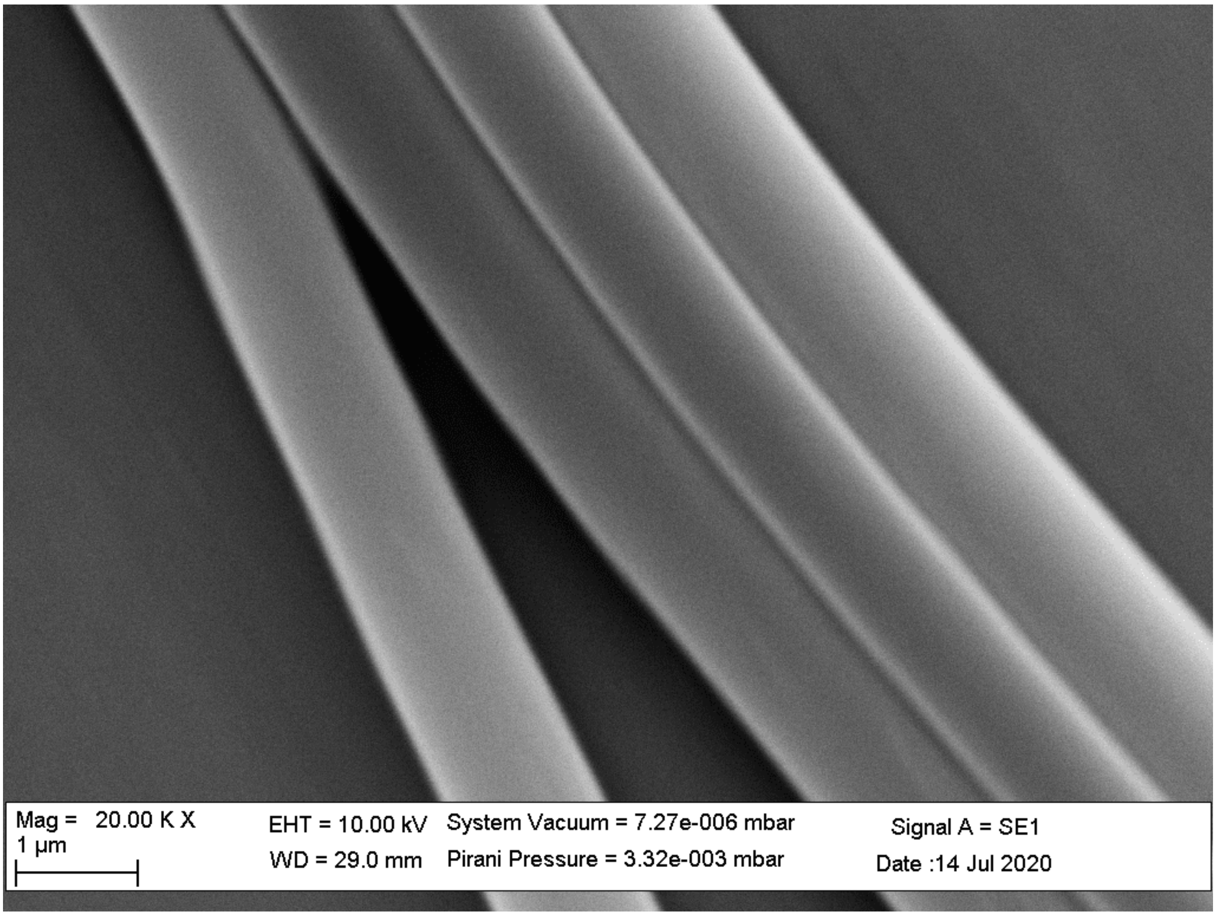

Figure 8.42: SEM image of fibres in Figure 8.41 but at 20KX magnification

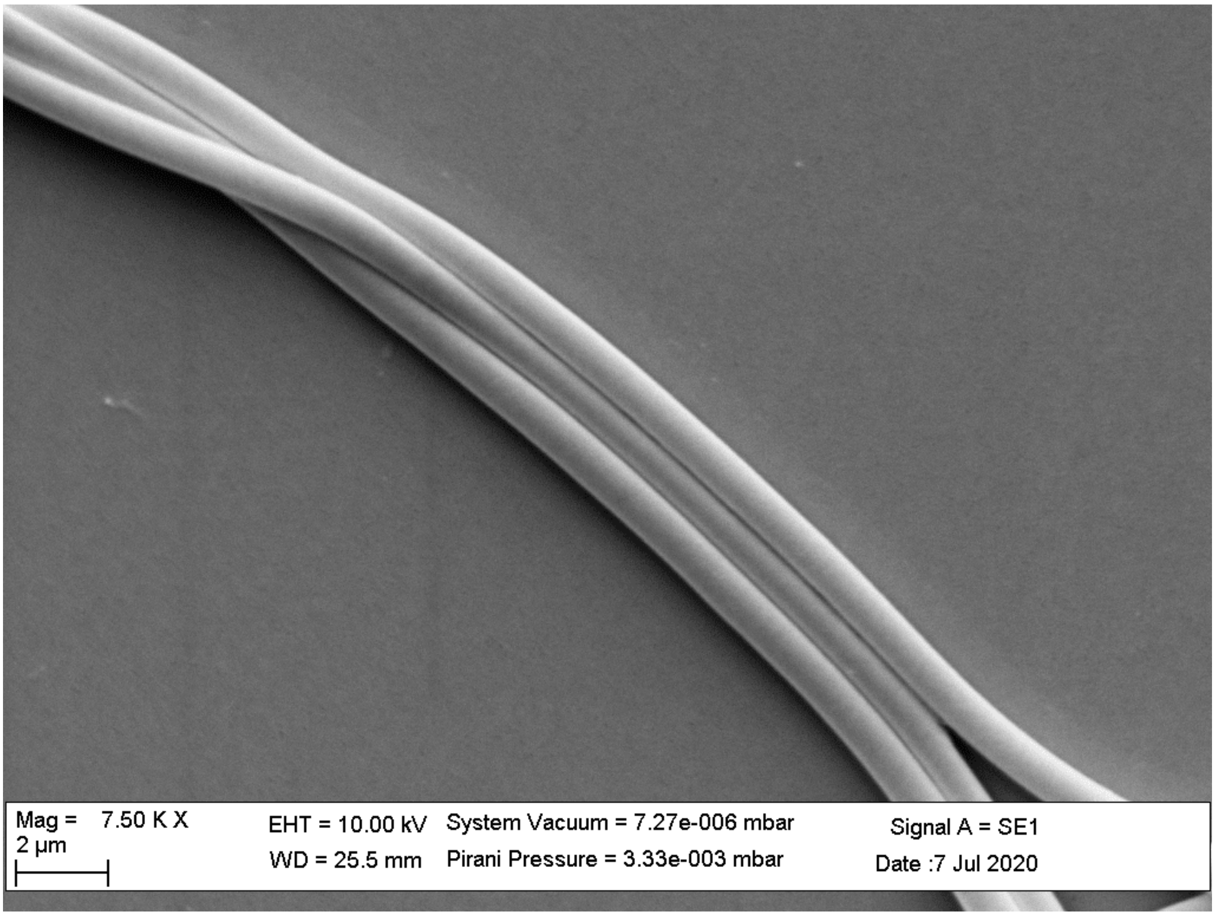

Figure 8.43: SEM image showing multiple fibres joined along their lengths produced from electrospinning of solution 3 at voltage 18 kV (7.5KX magnification)

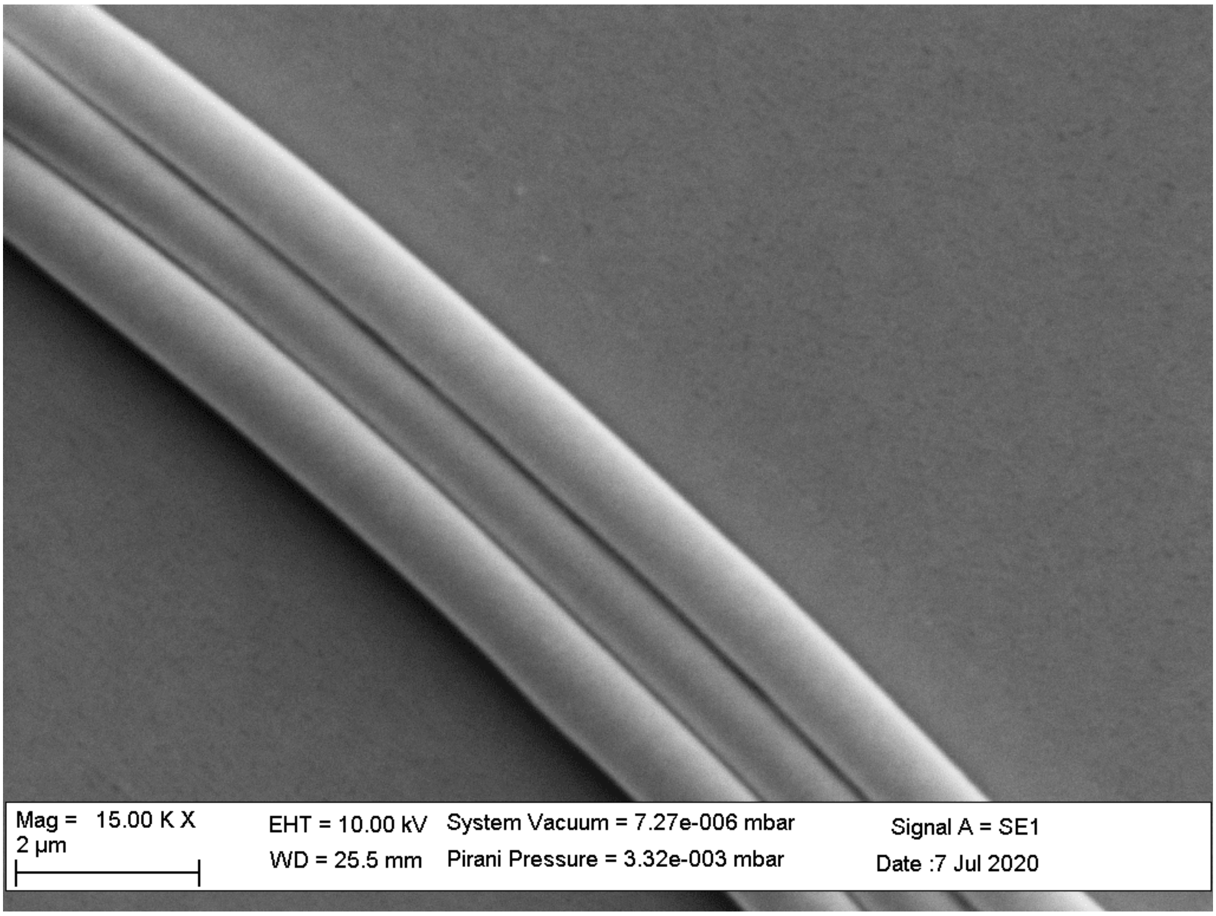

Figure 8.44: SEM image of fibres in Figure 8.43 but at 15KX magnification

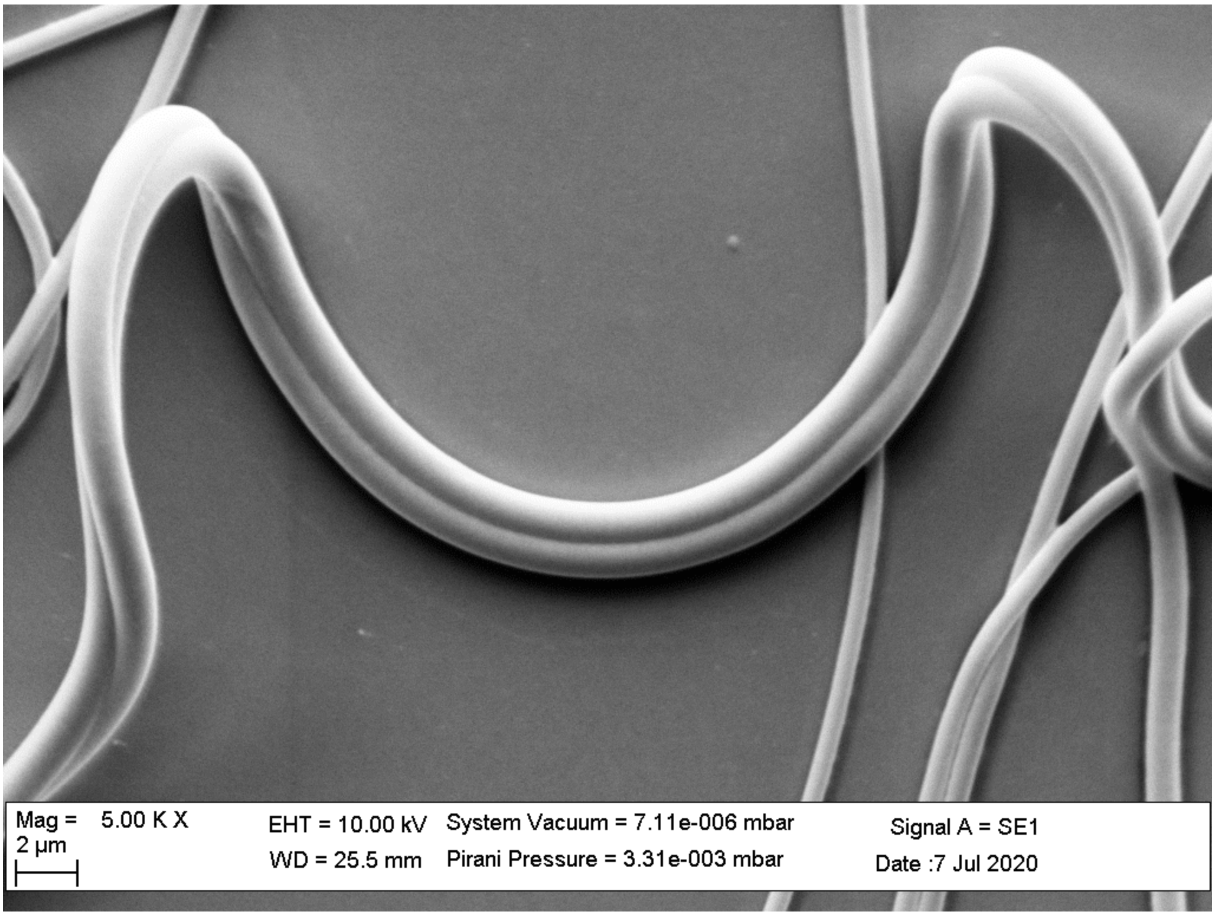

Figure 8.45: SEM image showing multiple fibres joined along their lengths produced from electrospinning of solution 3 at voltage 18 kV (5KX magnification)

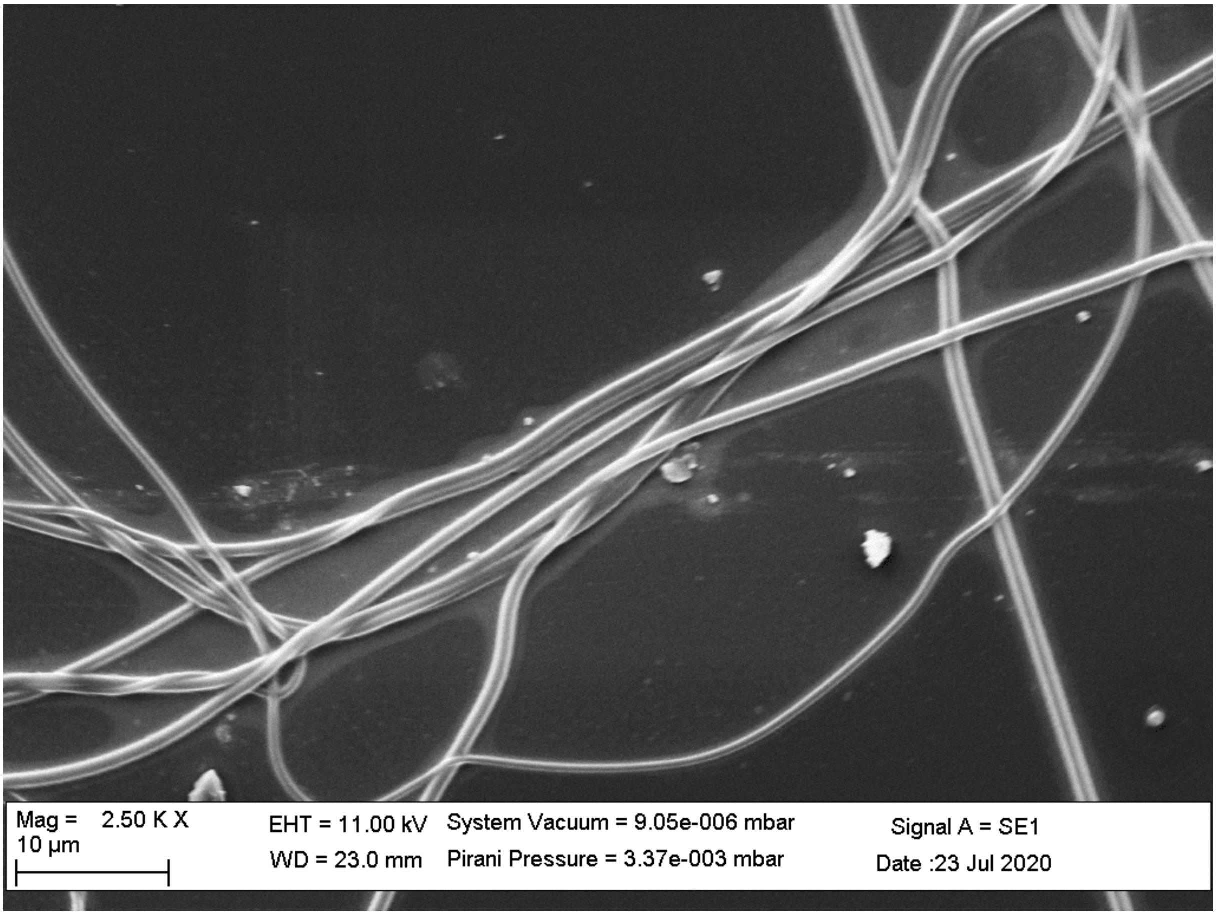

Figure 8.46: SEM image showing multiple fibres joined along their lengths produced from electrospinning of solution 2 at voltage 19.5 kV (5KX magnification)

8.3 Raman Spectroscopy

This section contains the analysis of Raman spectroscopy which was performed on lignin-PVA blend samples, their stabilized samples and finally carbonized samples. The instrument used was a Renishaw Raman spectrometer and the laser used was of wavelength 532 nm.

It has been mentioned in 2 that in order to obtain carbon fibres, the precursor fibres have to undergo heat treatment in the form of stabilization and and carbonization. While this project does not study the heat treatment step of producing carbon fibres it was decided to investigate this step briefly to get an insight on whether the lignin used in this study is able to attain the highly carbonaceous composition of carbon fibres. This was done by performing Raman spectroscopy on three samples. The Raman spectrums of these samples are shown in Figures 8.47, 8.48 and 8.49.

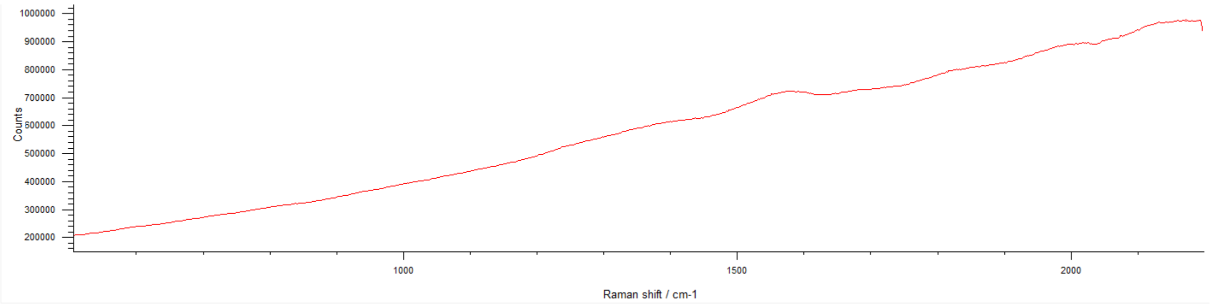

Figure 8.47: Raman spectrum of dried Kraft lignin-PVA blend sample

The first sample was a dried lignin-PVA blend. This was prepared by taking a few drops of one of the solutions mentioned in Table 5.1 and vacuum drying it at 100 °C in order to get rid of the solvent, leaving us with a sample that would represent the composition of the fibres produced during electrospinning. The Raman spectrum of this dried sample is shown in Figure 8.47. The atomic structure of a carbon fiber is similar to that of graphite wherein it consists of carbon atom layers arranged in a regular hexagonal pattern. Thus, the G band usually seen at 1585 cm^{-1} which is related to sp^2 C–C vibrations in graphite is present in all carbon fibers as well. It can be seen in Figure 8.47 that intense fluorescence has taken place. However, a small and broad peak representing the G-band can be seen at 1580 cm^{-1}. The broadness of the peak shows the lignin molecules lack ordered arrangement [Jiangling Li, 2013].

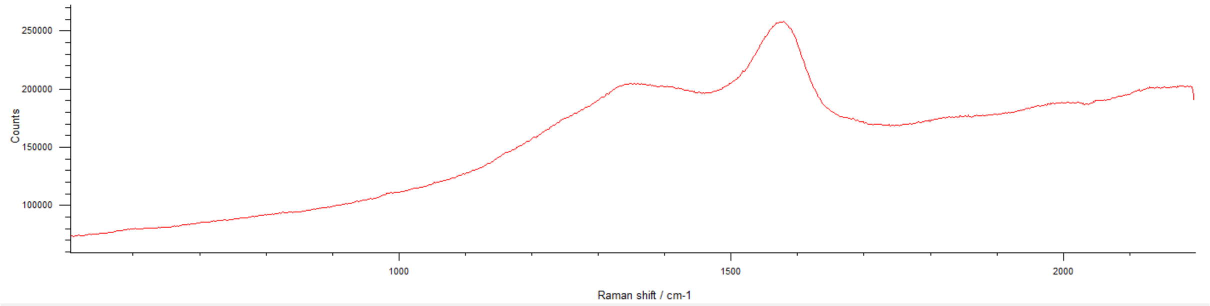

Figure 8.48: Raman spectrum of stabilized Kraft lignin-PVA blend sample

Figure 8.48 shows the Raman spectrum of the stabilized sample. The stabilization was carried out using a Discovery SDT650 TA instruments TGA machine. The dried sample was heated to 250 °C in air at a rate of 1 °C/ min and held for 1 hour. These stabilization parameters were chosen based on various literature and same goes for the carbonization parameters mentioned later. The flourescence is lesser in this spectrum and the G-band is clearly visible at a wavenumber of 1580 cm^{-1} . However, the peak is still small but narrower compared to that seen in the case of the dried sample. In addition to this a weak D-band can also be seen at approximately 1350 cm^{-1}. The D-band is associated with the disorder and defects in the structure. It is known that the ratio of the peak intensity of D band and G band, denoted as R-value, can be used to correlate the balance among the disorder and crystalline character in the carbon materials, where a higher R-value means lower crystallinity [Jiangling Li, 2013]. An R-value of lesser than 1 denotes high crystallinty of the sample under investigation [Jiangling Li, 2013]. The spectrum of the stabilized sample shows that the intensity of G-band is greater than that of D-band, which would give a low R-value and thus high degree of crystallinity. But due to the fluorescence, this observation is not credible.

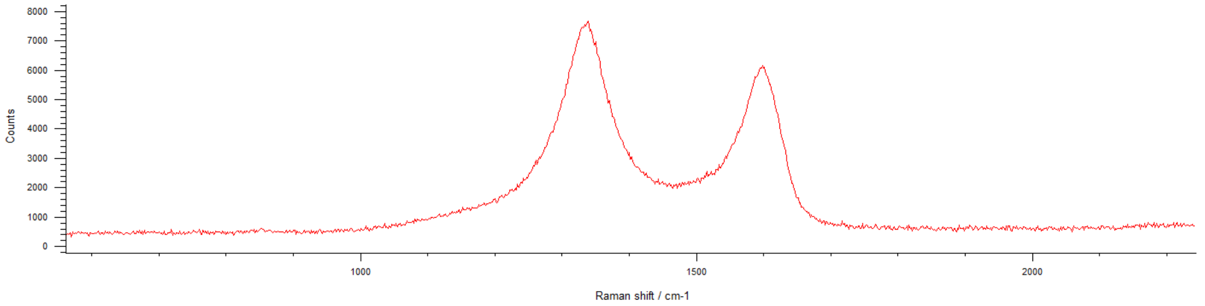

Figure 8.49: Raman spectrum of carbonized lignin-PVA blend sample

Figure 8.49 shows the Raman spectrum of the carbonized sample. The carbonization was carried out on a stabilized sample in the same Discovery TGA machine. It was heated to 1500 °C in nitrogen atmosphere at a heating rate of 1 °C/ min and held at that temperature for 30 minutes. The Raman spectrum obtained has no fluorescence and shows distinct D and G bands. On comparing the shape of the G band with that seen in the spectrum of the stabilized sample, it can be seen that the peak in this case is much narrower. However, the intensity of the D band is higher than that of the G band, denoting that the crystallinity of the carbonized sample is less. In addition to this, there is a slight shift in the position of the D and G bands to positions 1340 cm^{-1} and 1595 cm^{-1}, respectively.

9 Experimental Observation

This chapter contains an observation that was made while the electrospinning was taking place.

9.1 Formation of multiple jets

An interesting behaviour of the droplet on the tip of the needle took place when it was under the influence of the applied electric field. It was observed that as the voltage was applied, the deformation of the droplet into a conical shape took place and the eruption of a jet was visible, as it should when the voltage applied is above the critical voltage. However, interestingly at irregular intervals, the stretching suddenly stopped and an immediate formation of multiple jets could be seen on the surface of the droplet. These multiple jets were much smaller that the single jet observed earlier. The eruption of the multiple jets from the surface of the droplet took place in a random manner and made the droplet surface look like it was flickering heavily as these multiple jets emerged out of it. What was more striking was that when only a single jet emerged from the stretched droplet, no fibres were deposited on the collector plate, whereas a large amount of fibres were deposited when the multiple jets were formed. This was phenomenon was observed throughout the main electrospinning experiment, that is, for all solutions and at all values of applied voltage used. Thus, the fibre formation that took place in this study was intermittent. The change from a single jet to multiple jet was irregular and in some cases there was no change for the entire 45 seconds the experiment was run, which lead to no fibre formation in that specific run. The formation of multiple jets from a single droplet has been observed by researchers and it has been reported as an effect of high electric field [M.M. Demir, 2002]. M.M. Demir [2002] reported that higher applied voltages favoured the formation of multiple jets. Yoshihiro YAMASHITA [2007] reported that multiple jets can be produced from a single droplet by using a high voltage and a wide target area. From these literature studies and the observations made in this study it is possible that the applied external field was quite high. The absence of fibres despite the stretching of the droplet and formation of the jet could also be attributed to inconsistent electric field distribution. It is possible that the electric field in the fumehood in which the electrospinning setup was kept, was such that the jet deviated from its path to a high extent shortly after emerging from the droplet and deposited away from the collector. It was also observed that when a single jet was emerging out of the droplet, suddenly there was a production of sparks near the syringe pump which was kept about 30 cm to the side of the needle and collector. The sparks were produced for a few seconds and immediately after the sparks stopped, multiple jets from the droplet emerged and fibre deposition took place. The production of sparks took place when the applied voltage was 21 kv and 22.5 kV. Furthermore, a set of experiments were run in which the tip-collector distance was changed. At a tip-collector distance of 12 cm, the stretching of the droplet followed by no fibre depostion was observed. Whereas, at higher tip-collector distances of 20 cm and 24 cm, fibre deposition took place on the collector and interestingly even the formation of multiple jets decreased with increase of tip-collector distance.

Thus, it is speculated that the high electric field and its distribution in the fumehood and around the setup could be the reason behind the intermittent fibre formation that took place in this study.

10 Conclusion

The aim of this project was to study the electrospinning of lignin-PVA blend solutions since lignin fibres have the potential to be a sustainable precursor for carbon fibres. This was carried out by characterizing the lignin, performing electrospinning of solutions prepared from this lignin and then characterizing the fibres produced in order to correlate the results of the electrospinning with the process, solution or material properties.

The type of lignin used in this project is softwood kraft lignin. Thermal and chemical characterization of this lignin was done using DSC, TGA and FTIR.

MDSC was performed on this lignin to know of its glass transition temperature. The analysis gave a glass transition temperature of 146.79 °C. It was also observed that the glass transition step in the DSC curve was a broad one which could indicate that the lignin in hand has a high number of impurities.

TGA was performed in order to know the thermal stability of this lignin. The sample was heated up to 1000 °C The TGA curve showed that the decomposition of this lignin begins at 175 °C and the DTG curve showed that the maximum mass loss took place around 400 °C. The TGA curve showed a residual mass of 35% which could be as a result of impurities.

The FTIR spectrum of this lignin showed the characteristic peaks of softwood kraft lignin but with some differences when compared to those reported in literature. Two peaks were seen at positions 2362 cm^1 and 2325 cm^1. The shape of these peaks were similar to those seen in literature at positions 2940-2930 cm^1 and 2689-2880 cm^1 and no peaks were seen at these positions in the FTIR spectrum of this lignin sample. Another difference was that the bands that denote C-S bond and C-S vibration of sulphonic group showed very high absorbance as compared to that reported in literature. It is speculated that this could indicate the high number of impurities in the sample. The differences in the spectrum show that the structure of lignin heavily depends on its source and extraction technique.

Since the lignin used in this project was Kraft lignin, the solvent used in preparing solutions for electrospinning was NaOH, due to its alkaline nature. Polyvinyl alcohol (PVA) was added to the solutions in order to increase their viscosities.

9 solutions were electrospun and their properties were altered from each other by changing the polymer composition or concentration. 3 combinations of polymer and water concentrations were chosen; 10% polymer - 90% water, 15% polymer - 85% water and 20% polymer - 80% water. Similarly, 3 lignin-PVA ratios were chosen to change the polymer composition; 85-15, 90-10 and 95-5.

The viscosity measurements showed that an increase in polymer concentration increased the viscosity of the solution. Additionally, for the same polymer concentration, the viscosity of the solution was lower when the lignin-PVA ratio was higher.

The electrospinning was carried out at 5 different voltages to investigate the effect of applied voltage on the electrospinning process. These values were 16.5 kV, 18 kV, 19.5kV, 21 kV and 22.5 kV. Solution feed rate used was 0.0025 ml/h, tip-collector distance was 16 cm and the needle used had an inner diameter of 2.3 mm and outer diameter of 3 mm. Every electrospinning run was carried out for a fixed duration of 45 seconds.

The characterization of fibres was done using LOM and SEM. LOM images gave a general idea of the results of electrospinning of each solution. Electrospinning of solutions 4, 7 and 8 lead to formation of beads, owing to their low viscosities. Solutions 7 and 8 had low viscosities since the lignin-PVA ratio was high. This highlighted the role of PVA as a binder polymer. It would not be possible to produce beadless fibres using solutions prepared purely from the lignin in hand. Futhermore, a certain lignin-PVA ratio is required to significantly increase the viscosity of the solutions. Solutions 1 and 5 produced beaded fibres due to their slightly higher viscosities. Solution 2 and 3 produced beadless fibres due to their high viscosities. Solution 6 had a viscosity slightly lesser than that of solution 2 and the LOM images showed that its electrospinning produced beaded as well as beadless fibres. From these LOM images, the effect of viscosity on the electrospinning was evident. Viscosity plays a vital role in the keeping the fluid jet from breaking into droplets while it is being drawn from the droplet on the needle tip and accelerated towards the collector.

Through SEM investigation of the fibres produced by solution 6 at various voltages it was found that applied voltage also plays a role in keeping the fluid jet from breaking up. The fibres produced from the electrospinning at 16.5 kV were beaded. But the fibres produced at 19.5 kV, 21 kV and 22.5 kV were beadless. Some of the fibres produced at 18 kV were beaded and some were uniform.

Fibres with flat, ribbon shaped morphology were observed in the SEM images. These could not be correlated with the applied voltage since they were observed for all values of applied voltages and for all solutions that produced fibres. Studies have reported the formation of flat fibres and have attributed the solvent-polymer interaction to this morphology of fibres. They have reported that the rapid and non-uniform vaporization of solvent leads to the formation of a solid polymer skin which collapses the fibre, giving it a flat shape. The interaction between the PVA and solvent could be accountable for the flat fibres seen in this study. Another interesting observation made using the SEM images was the presence of multiple fibers joined along their lengths. Such fibres were present in a large amount and for all solutions that produced uniform fibres and for all values of applied voltage. Researchers have observed this tendency as well and have attributed it to charge repulsion on the surface of the fluid jet which causes it to split in to two fibres.

An observation was made during the electrospinning experiment. This was the formation of multiple jets from the droplet. The electrospinning of all the solutions and at all values of applied voltage took place via the formation of multiple jets from the droplet. This could also be a possible reason why a large number of fibres that were seen in the SEM images were attached to other fibres along their lengths. The multiple jets emerging from the droplet was seen as a result of the high applied electric field.

Raman spectroscopy was performed on the dried, stabilized and carbonized samples of lignin-PVA blends. Fibres were not used for this. It was found that the G-band became more evident and narrower as the sample went through the heat treatment. There was intense flouresence in the spectrums of the dried and stabilized samples, The Raman spectrum of the carbonized was accurate. In the Raman spectrum of the carbonized sample, the intensity of the D band was higher than that of the G band, indicating low crystallinity of the carbon material obtained. However, the result of the carbonization process is highly dependent on the carbonization temperature and holding times.

To summarize, the kraft lignin used in this study possibly has a high impurity content. The lignin requires a binder polymer in order to form chain entanglements with the solvent, which would help the solution attain the required viscosity for formation of uniform fibres. However, applied voltage can also be adjusted in some cases to obtain a transition from beaded fibres to beadless fibres. While the solvent-polymer system used in this study produces uniform fibres, it isn't the perfect solution since flat fibres were frequently observed. The electric field that was applied through the applied voltage was high and values lower than 16.5 kV should be tried for future electrospinning of these solutions. The Raman spectrums showed that the lignin used in this study does have the potential to form carbon-rich materials. Thus, it would be interesting to perform heat treatment on the fibres produced in this study and study the properties of the carbon fibres produced.

Bibliography

A. Becker, 2015. M. Mueller B. Glasmacher A. Becker, H. Zernetsch. *A novel coaxial nozzle for in-process adjustment of electrospun scaffolds' fiber diameter.* Current Directions in Biomedical Engineering, 1(1), 8456–8466, 2015.

A. Koski, 2004. S. Shivkumar A. Koski, K. Yim. *Effect of molecular weight on fibrous PVA produced by electrospinning.* Materials Letters, 58, 493– 497, 2004.

Abd-Alla M. A. Nada and Kamel, 1998. Mohamed El-Sakhawy Abd-Alla M. A. Nada and Samir M. Kamel. *Infra-red spectroscopic study of lignins.* Polymer Degradation and Stability, 60, 241–251, 1998.

Adomavičiūtė Erika, 2011. Stanys Sigitas Adomavičiūtė Erika. *Formation of Electrospun PVA Mats on Different Types of Support Materials Using Various Kinds of Grounded Electrodes.* FIBRES TEXTILES in Eastern Europe, 19(4), 34–40, 2011.

Akpan and Adeosun, 2019. Emmanuel Isaac Akpan and Samson Oluropo Adeosun. *Sustainable Lignin for Carbon Fibers: Principles, Techniques, and Applications.* Springer, 2019.

Allison Tolbert, 2014. Ratayakorn Khunsupat Amit K. Naskar Arthur J. Ragauskas Allison Tolbert, Hannah Akinosho. *Characterization and analysis of the molecular weight of lignin for biorefining studies.* Biofuels, Bioprod. Bioref., 2014.

Angammana and Jayaram, 2011. Chitral J. Angammana and Shesha H. Jayaram. *Analysis of the Effects of Solution Conductivity on Electrospinning Process and Fiber Morphology.* IEEE TRANSACTIONS ON INDUSTRY APPLICATIONS, 47, 1109–1117, 2011.

A.R. Jabur, 2017. S.M. Muhi Aldain A.R. Jabur, L.K. Abbas. *Effects of Ambient Temperature and Needle to Collector Distance on PVA Nanofibers Diameter Obtained From Electrospinning Technique.* Engineering and Technology Journal, 35 Issue:4 Part (A), 340–347, 2017.

Baumgarten, 1971. Peter K. Baumgarten. *Electrostatic Spinning of Acrylic Microfibers.* Journal of Colloid and Interface Science, 36(1), 71–79, 1971.

Brazel and Rosen, 2012. Christopher S. Brazel and Stephen L. Rosen. *Fundamental Principles of Polymeric Materials.* John Wiley Sons, 2012.

C. Wang, 2006. Zonghao Huang Y.H. Su C. Wang, W. Zhang. *Effect of concentration, voltage, take-over distance and diameter of pinhead on precursory poly (phenylene vinylene) electrospinning.* Pigment and Resin Technology, 35(5), 278–283, 2006.

Carroll and Joo, 2009. Colman P. Carroll and Yong Lak Joo. *Axisymmetric instabilities in electrospinning of highly conducting, viscoelastic polymer solutions.* Physics of Fluids, 21, 103101, 2009.

Celebioglu and Uyar, **2011**. Asli Celebioglu and Tamer Uyar. *Electrospun porous cellulose acetate fibers from volatile solvent mixture.* Materials Letters, 65(14), 2291–2294, 2011.

Cheryl L. Casper, **2004**. Nancy G. Tassi D. Bruce Chase John F. Rabolt Cheryl L. Casper, Jean S. Stephens. *Controlling Surface Morphology of Electrospun Polystyrene Fibers: Effect of Humidity and Molecular Weight in the Electrospinning Process.* Macromolecules, 37(2), 573–578, 2004.

Chi Wang, **2009**. Kuo-Wei Yan Chien-Lin Hung Kan-Lin Hung Chi Wang, Huan-Sheng Chien. *Correlation between processing parameters and microstructure of electrospun poly(D,l-lactic acid) nanofibers.* Polymer, 50(25), 6100–6110, 2009.

Chidchanok Mit-uppatham and Supaphol, **2004a**. Manit Nithitanakul Chidchanok Mit-uppatham and Pitt Supaphol. *Ultrafine Electrospun Polyamide 6 Fibers: Effect of Solution Conditions on Morphology and Average Fiber Diameter.* Macromolecular Chemistry and Physics, 205(17), 2327–2338, 2004.

Chidchanok Mit-uppatham and Supaphol, **2004b**. Manit Nithitanakul Chidchanok Mit-uppatham and Pitt Supaphol. *Effects of Solution Concentration, Emitting Electrode Polarity, Solvent Type, and Salt Addition on Electrospun Polyamide-6 Fibers: A Preliminary Report.* Macromolecular Symposia, 216, 293–300, 2004.

Christopher J. Buchko, **1999**. Yu Shen David C. Martin Christopher J. Buchko, Loui C.Chen. *Processing and microstructural characterization of porous biocompatible protein polymer thin films.* Polymer, 40(26), 7397–7407, 1999.

Chunxue Zhang, **2005**. Lili Wu Yue Han Jing Sheng Chunxue Zhang, Xiaoyan Yuan. *Study on morphology of electrospun poly(vinyl alcohol) mats.* European Polymer Journal, 41(3), 423–432, 2005.

C.J.Thompson, **2007**. A.L.Yarin D.H.Reneker C.J.Thompson, G.G.Chase. *Effects of parameters on nanofiber diameter determined from electrospinning model.* Polymer, 48(23), 6913–6922, 2007.

Darrell H. Reneker, **2008**. Alexander L. Yarin Darrell H. Reneker. *Electrospinning jets and polymer nanofibers.* Polymer, 49, 2387–2425, 2008.

Darrell H. Reneker and Koombhongse, **2000**. Hao Fong Darrell H. Reneker, Alexander L. Yarin and Sureeporn Koombhongse. *Bending instability of electrically charged liquid jets of polymer solutions in electrospinning.* Journal of Applied Physics, 87, 4531, 2000.

David Lukas and Pokorny, **2008**. Arindam Sarkar David Lukas and Pavel Pokorny. *Self-organization of jets in electrospinning from free liquid surface: A generalized approach.* Journal of Applied Physics, 104, 84309, 2008.

Delaram Fallahi, **2009**. Naser Mohammadi Behrooz Vahidi Delaram Fallahi, Mehdi Rafizadeh. *Effects of feed rate and solution conductivity on jet current and fiber diameter in electrospinning of polyacrylonitrile solutions.* e-Polymers, 104, 2009.

Deng-Guang Yu and Wang, 2014. Zan Li Lin-Ping Du Ben-Guo Zhao Deng-Guang Yu, Ying Xu and Xia Wang. *Coaxial Electrospinning with Mixed Solvents: From Flat to Round Eudragit L100 Nanofibers for Better Colon-Targeted Sustained Drug Release Profiles.* Journal of Nanomaterials, 967295, 2014.

D.S. Bajwa, 2019. A.H. Ullah S.G. Bajwa D.S. Bajwa, G. Pourhashem. *A concise review of current lignin production, applications, products and their environmental impact.* Industrial Crops & Products, 139, 111526, 2019.

Evstigneev, 2011. E. I. Evstigneev. *Factors Affecting Lignin Solubility.* Russian Journal of Applied Chemistry, 84(6), 1040–1045, 2011.

H. Fong, 1999. D. H. Reneker H. Fong, I. Chun. *Beaded nanofibers formed during electrospinning.* Polymer, 40(16), 4585–4592, 1999.

Haijun He and Molnar, 2018. Yahya Kara Haijun He and Kolos Molnar. *Effect of Needle Characteristic on Fibrous PEO Produced by Electrospinning.* Resolution and Discovery, 4(1), 2018.

HAIQING LIU, 2002. YOU-LOHSIEH HAIQING LIU. *Ultrafine Fibrous Cellulose Membranes from Electrospinning of Cellulose Acetate.* Journal of Polymer Science: PartB: Polymer Physics, 40, 2119–2129, 2002.

Heiko Lange, 2013. Claudia Crestini Heiko Lange, Silvia Decina. *Oxidative upgrade of lignin – Recent routes reviewed.* European Polymer Journal, 49, 1151–1173, 2013.

Holly McIlwee Golecki, 2014. Calla Glavin Benjamin Potter Mohammad R. Badrossamay Josue A. Goss Michael D. Phillips Kevin Kit Parker Holly McIlwee Golecki, Hongyan Yuan. *Effect of Solvent Evaporation on Fiber Morphology in Rotary Jet Spinning.* Langmuir, 30(44), 13369–13374, 2014.

Htet Htet Htike, 2012. Sachiko SUKIGARA Htet Htet Htike, Chen LONG. *The Effect of Relative Humidity on Electrospinning ofPoly-(vinyl alcohol) with Soluble Eggshell Membrane.* Journal of Textile Engineering, 58(1), 9–12, 2012.

Hui Li, 2014. Armando G.McDonald Hui Li. *Fractionation and characterization of industrial lignins.* Industrial Crops and Products, 62, 67–76, 2014.

Hyun-Su Bae, 2013. K. M. Kamruzzaman Selim Dong-Yoon Kang Eun-Jin Kim Inn-Kyu Kang Hyun-Su Bae, Adnan Haider. *Fabrication of highly porous PMMA electrospun fibers and their application in the removal of phenol and iodine.* Journal of Polymer Research, 20(158), 2013.

Ian Dallmeyer, 2010. Frank Ko John F. Kadla Ian Dallmeyer. *Electrospinning of Technical Lignins for the Production of Fibrous Networks.* Journal of Wood Chemistry and Technology, 30:4, 315–329, 2010.

Javad Sameni and Sain, 2014. Derval dos Santos Rosa Alcides Leao Javad Sameni, Sally Krigstin and Mohini Sain. *Thermal Characteristics of Lignin Residue from Industrial Processes*. Bioresources, 9(1), 725–737, 2014.

Javad Sameni, 2017. Mohini Sain Javad Sameni, Sally Krigstin. *solubility of lignin and acetylated lignin in organic solvents*. Bioresources, 12(1), 1548–1565, 2017.

Ji-Huan He and Yu, 2008. Yu-Qin Wan Ji-Huan He and Jian-Yong Yu. *Effect of Concentration on Electrospun Polyacrylonitrile (PAN) Nanofibers*. Fibres and Polymers, 9, 140–142, 2008.

Jian-Yi Zheng and Sun, 2014. Zhao-Jie Yu Gao-Feng Zheng Yang Zhao Han Wang Jian-Yi Zheng, Ming-Feng Zhuang and Dao-Heng Sun. *The Effect of Surfactants on the Diameter and Morphology of Electrospun Ultrafine Nanofiber*. Journal of Nanomaterials, 2014(689298), 2014.

Jiangling Li, 2013. Lei Zhou Vojtěch Kundrát Andrew M. Abbot Jiangling Li, Shi Su. *Carbon nanowalls grown by microwave plasma enhanced chemical vapor deposition during the carbonization of polyacrylonitrile fibers*. J. Appl. Phys., 113, 024313, 2013.

J.M. Deitzel, 2001. D. Harris N.C. Beck Tan J.M. Deitzel, J. Kleinmeyer. *The effect of processing variables on the morphology of electrospun nanofibers and textiles*. Polymer, 42, 261–272, 2001.

Joachim H. Wendorff and Greiner, 2012. Seema Agarwal Joachim H. Wendorff and Andreas Greiner. *Electrospinning : Materials, Processing, and Applications*. John Wiley & Sons, Incorporated, 2012.

Jonathan Stanger, 2009. Andrew Wallace Nigel Larsen Mark Staiger Roger Reeves Jonathan Stanger, Nick Tucker. *The Effect of Electrode Configuration and Substrate Material on the Mass Deposition Rate of Electrospinning*. Journal of Applied Polymer Science, 112, 1729–1737, 2009.

Joon Seok Lee, 2004. Han Do Ghim Sam Soo Kim Du Hwan Chun Hak Yong Kim Won Seok Lyoo Joon Seok Lee, Kyu Ha Choi. *Role of Molecular Weight of Atactic Poly(vinyl alcohol) (PVA) in the Structure and Properties of PVA Nanofabric Prepared by Electrospinning*. Journal of Applied Polymer Science, 93(4), 1638–1646, 2004.

Jun-Wei Liang and Lu, 2019. Shi-Cai Wang Jia-Lin Wu Jun-Wei Liang, Gajula Prasad and Sheng-Guo Lu. *Enhancement of the Oil Absorption Capacity of Poly(Lactic Acid) Nano Porous Fibrous Membranes Derived via a Facile Electrospinning Method*. Applied Science, 9, 1014, 2019.

K. Nasouri and Kaflou, 2012. A.M. Shoushtari K. Nasouri and A. Kaflou. *Investigation of polyacrylonitrile electrospun nanofibres morphology as a function of polymer concentration, viscosity and berry number*. Micro Nano Letters, 7(5), 423 – 426, 2012.

Kubo and Kadla, 2005. Satoshi Kubo and John F. Kadla. *Hydrogen Bonding in Lignin: A Fourier Transform Infrared Model Compound Study.* Biomacromolecules, 6, 2815–2821, 2005.

Larkin, 2011. Peter Larkin. *INFRARED AND RAMAN SPECTROSCOPY PRINCIPLES AND SPECTRAL INTERPRETATION.* Elsevier, 2011.

Larrondo and Manley, 1981. L. Larrondo and R. St. John Manley. *Electrostatic fiber spinning from polymer melts. I. Experimental observations on fiber formation and properties.* Journal of Polymer Science: Polymer Physics Edition, 19(6), 909–920, 1981.

Li and Xia, 2004. D. Li and Y. Xia. *Electrospinning of Nanofibers:Reinventing the Wheel?* Advanced Materials, 16, 1151–1170, 2004.

Li Meng-Meng and Zhi-Ming, 2011. Yin Hong-Xing Li Meng-Meng, Long Yun-Ze and Zhang Zhi-Ming. *Electrospun cerium nitrate/polymer composite fibres: synthesis, characterization and fibre-division model.* Chin. Phys. B Vol., 20, No. 4, 048101, 2011.

Li Yao, 2003. Anthony Guiseppi-Elie-Gary L. Bowlin David. G. Simpson Gary E. Wnek Li Yao, Thomas W. Haas. *Electrospinning and Stabilization of Fully Hydrolyzed Poly(Vinyl Alcohol) Fibers.* Chemistry of Materials, 15, 1860–1864, 2003.

Liu L, 2008. Dzenis YA. Liu L. *Analysis of the effects of the residual charge and gap size on electrospun nanofiber alignment in a gap method.* Nanotechnology, 19(35), 355307, 2008.

M. Dhanalakshmi, 2008. J. P. Jog M. Dhanalakshmi. *Preparation and characterization of electrospun fibers of Nylon 11.* eXPRESS Polymer Letters, 2, No.8, 540–545, 2008.

Manuel A.Alfaro De Prá, 2017. M.Maraschin Beatriz Veleirinho Manuel A.Alfaro De Prá, Rosa M.Ribeiro-do-Valle. *Effect of collector design on the morphological properties of polycaprolactone electrospun fibers.* Materials Letters, 193, 154–157, 2017.

Manuel Lallave and Loscertales, 2007. Ramiro Ruiz-Rosas-José Rodríguez-Mirasol Tomás Cordero Juan C. Otero Manuel Marquez Antonio Barrero Manuel Lallave, Jorge Bedia and Ignacio G. Loscertales. *Filled and Hollow Carbon Nanofibers by Coaxial Electrospinning of Alcell Lignin without Binder Polymers.* Advanced Materials, 19, 4292–4296, 2007.

Mariko Ago and Rojas, 2012. Joseph E. Jakes-Sunkyu Park Mariko Ago, Kunihiko Okajima and Orlando J. Rojas. *Lignin-Based Electrospun Nanofibers Reinforced with Cellulose Nanocrystals.* Bio Macromolecules, 13, 918–926, 2012.

Meng Zhang, 2014. Amod A. Ogale Meng Zhang. *Carbon fibers from dry-spinning of acetylated softwood kraft lignin.* CARBON, 69, 626 – 629, 2014.

M.M. Demir, 2002. E. Yilgor B. Erman M.M. Demir, I. Yilgor. *Electrospinning of polyurethane fibres.* Polymer, 43(11), 3303–3309, 2002.

Mo XM, 2004. Kotaki M Ramakrishna S Mo XM, Xu CY. *Electrospun P(LLA-CL) nanofiber: a biomimetic extracellular matrix for smooth muscle cell and endothelial cell proliferation.* Biomaterials, 25(10), 1883–90, 2004.

Nakagawa Yuya and Kim, **2010**. BYOUNG-SUHK Kim Nakagawa Yuya, WEI KAI and ICK-SOO Kim. *MORPHOLOGY CONTROLLED ELECTROSPUN POLY(VINYL PYRROLIDONE) FIBERS: EFFECTS OF ORGANIC SOLVENT AND RELATIVE HUMIDITY.* Journal of Materials Science and Engineering with Advanced Technology, 2(1), 97–112, 2010.

Nezarati R.M., **2013**. Cosgriff-Hernandez E. Nezarati R.M., Eifert M.B. *Effects of Humidity and Solution Viscosity on Electrospun Fiber Morphology.* Tissue Eng Part C Methods, 19(10), 810–9, 2013.

Panda, **2007**. Prasanta Kumar Panda. *Ceramic Nanofibers by Electrospinning Technique—A Review.* Transactions - Indian Ceramic Society, 66(2), 65–76, 2007.

Pirjo Heikkilä, **2008**. Ali Harlin Pirjo Heikkilä. *Parameter study of electrospinning of polyamide-6.* European Polymer Journal, 44(10), 3067–3079, 2008.

R. V. N. Krishnappa, **2003**. K. Desai Changmo Sung R. V. N. Krishnappa. *Morphological study of electrospun polycarbonates as a function of the solvent and processing voltage.* Journal of Materials Science, 38, 2357–2365, 2003.

Raziyeh Ghelich, **2015**. Amir Ali Youzbashi Raziyeh Ghelich, Mansoor Keyanpour Rad. *Study on Morphology and Size Distribution of Electrospun NiO-GDC Composite Nanofibers.* Journal of Engineered Fibers and Fabrics, 10, 12–19, 2015.

Reneker and Yarin, **2008**. Darrell H. Reneker and Alexander L. Yarin. *Electrospinning jets and polymer nanofibers.* Polymer, 49, 2387–2425, 2008.

Royal Kessick, **2004**. Gary Tepper Royal Kessick, John Fenn. *The use of AC potentials in electrospraying and electrospinning processes.* Polymer, 45(9), 2981–2984, 2004.

Seeram Ramakrishna and Fujihara, **2005**. Wee-Eong Teo Seeram Ramakrishna, Teik-Cheng Lim and Kazutoshi Fujihara. *An Introduction to Electrospinning and Nanofibers.* World Scientific Publishing Co Pte Ltd, 2005.

Shamim Zargham, **2012**. Amir Tavakoli-Abo Saied Rashidi-Rogheih Damerchely Shamim Zargham, Saeed Bazgir. *The Effect of Flow Rate on Morphology and Deposition Area of Electrospun Nylon 6 Nanofiber.* Journal of Engineered Fibers and Fabrics, 7(4), 42–49, 2012.

Sheng-Han Chen, **2014a**. Kueir-Rarn Lee Juin-Yih Lai Sheng-Han Chen, Yung Chang. *A three-dimensional dual-layer nano/microfibrous structure of electrospun chitosan/poly(D,L-lactide) membrane for the improvement of cytocompatibility.* Journal of Membrane Science, 450, 224–234, 2014.

Sheng-Han Chen, **2014b**. Kueir-Rarn Lee Juin-Yih Lai Sheng-Han Chen, Yung Chang. *A three-dimensional dual-layer nano/microfibrous structure of electrospun chitosan/poly(D,L-lactide) membrane for the improvement of cytocompatibility.* Journal of Membrane Science, 450, 224–234, 2014.

Shengli Zhao, **2004**. Linge Wang-Yong Huang Shengli Zhao, Xiaohui Wu. *Electrospinning of Ethyl–Cyanoethyl Cellulose/Tetrahydrofuran Solutions.* Journal of Applied Polymer Science, 91(1), 242–246, 2004.

Shimizu, **1992**. K. Sudo K. Shimizu. *A new carbon fiber from lignin.* Applied polymer science, 44, Issue1, 127–134, 1992.

Silke Megelski, **2002**. D. Bruce Chase John F. Rabolt Silke Megelski, Jean S. Stephens. *Micro- and Nanostructured Surface Morphology on Electrospun Polymer Fibers.* Macromolecules, 35(22), 8456–8466, 2002.

Sun, **2010**. Run-Cang Sun. *Cereal Straw as a Resource for Sustainable Biomaterials and Biofuels: Chemistry, Extractives, Lignins, Hemicelluloses and Cellulose.* Elsevier, 2010.

Sungyeoul Kim and Yoon, **2015**. Dahye Kim DaAe Ko Dojin Kim Hyojin Kim Sungyeoul Kim, Hyundong Lee and Soon-Gil Yoon. *Transparent Conductive Films of Copper Nanofiber Network Fabricated by Electrospinning.* Journal of Nanomaterials, 2015, 2015.

Sureeporn Koombhongse, **2001**. Darrell H. Reneker Sureeporn Koombhongse, Wenxia Liu. *Flat ribbons and other shapes by electrospinning.* Journal of Polymer Science Part B Polymer Physics, 39(21), 2598 – 2606, 2001.

Sureeporn Tripatanasuwan, **2007**. Darrell H. Reneker Sureeporn Tripatanasuwan, Zhenxin Zhong. *Effect of evaporation and solidification of the charged jet in electrospinning of poly(ethylene oxide) aqueous solution.* Polymer, 48(19), 5742–5746, 2007.

Taylor, **1969**. Sir Geoffrey Taylor. *Electrically driven jet.* Royal Society of London A., 313, 453—475, 1969.

Tayra Rodrigues Brazil and Rezende, **2018**. Marcos Massi Tayra Rodrigues Brazil, Rogeria Nunes Costa and Mirabel Cerqueira Rezende. *Structural, morphological, and thermal characterization of kraft lignin and its charcoals obtained at different heating rates.* Material Research Express, 5, 045502, 2018.

Teeradech Jarusuwannapoom, **2005**. Sujinda Jitjaicham LadawanWannatong Manit Nithitanakul Cattaleeya Pattamaprom Piyawit Koombhongse Ratthapol Rangkupan Pitt Supaphol Teeradech Jarusuwannapoom, Walaiporn Hongrojjanawiwat. *Effect of solvents on electro-spinnability of polystyrene solutions and morphological appearance of resulting electrospun polystyrene fibers.* European Polymer Journal, 41(3), 409–421, 2005.

Tohru Okuzono and Doi, **2006**. Kin'ya Ozawa Tohru Okuzono and Masao Doi. *Simple Model of Skin Formation Caused by Solvent Evaporation in Polymer Solutions.* PHYSICAL REVIEW LETTERS, 97, 136103, 2006.

Tugrul Ogulata, **2013**. Halil İ. İçoğlu Tugrul Ogulata. *Effect of Ambient Parameters on Morphology of Electrospun Polyetherimide (PEI) Fibers.* Tekstil ve Konfeksiyon, 23(4), 313–318, 2013.

Varvara Tserki, 2006. Costas Panayiotou Varvara Tserki, Ioannis Filippou. *Preparation and Characterization of Electrospun Poly(butylene succinate-co-butylene adipate) Nanofibrous Nonwoven Mats.* Part N: Journal of Nanoengineering and Nanosystems, 220, 71–79, 2006.

Vida Poursorkhabi and Misra, 2015. Amar K. Mohanty Vida Poursorkhabi and Manjusri Misra. *Electrospinning of Aqueous Lignin/Poly(ethylene oxide) Complexes.* Journal of Applied Polymer Science, 132(2), 2015.

Vipul Dav and Glasser, 1993. Herv Marandt Vipul Dav, Abaneshwar Prasadt and Wolfgang G. Glasser. *Molecular organization of lignin during carbonization.* POLYMER, 34, Number 15, 3144–3154, 1993.

Weiwei Zuo and Zhang, 2005. Wen Yang Weiwei Zuo, Meifang Zhu and Yu Zhang. *Experimental Study on Relationship Between Jet Instability and Formation of Beaded Fibers During Electrospinning.* Polymer Engineering and Science, 45(5), 704 – 709, 2005.

William O.S. Doherty, 2011. Christopher M. Fellows William O.S. Doherty, Payam Mousavioun. *Value-adding to cellulosic ethanol: Lignin polymers.* Industrial Crops and Products, 33, 259–276, 2011.

Xinhua Zong and Chua, 2002. Dufei Fang Shaofeng Ran Benjamin S. Hsiao Xinhua Zong, Kwangsok Kim and Benjamin Chua. *Structure and process relationship of electrospun bioabsorbable nanofiber membranes.* Polymer, 43, 4403–4412, 2002.

Yasuhiro Miyauchi and Shiratori, 2006. Bin Ding Yasuhiro Miyauchi and Seimei Shiratori. *Fabrication of a silver-ragwort-leaf-like super-hydrophobic micro/nanoporous fibrous mat surface by electrospinning.* Nanotechnology, 17, 5151, 2006.

Ylva Nordström, 2007. Elisabeth Sjöholm Rickard Drougge Ylva Nordström, Ida Norberg. *A new softening agent for melt spinning of softwood kraft lignin.* Journal of Applied Polymer Science, 129(3), 1274–1276, 2007.

Yoshihiro YAMASHITA, 2007. Akira TANAKA Hajime MIYAKE Yoshihiro YAMASHITA, Frank KO. *Characteristics of Elastomeric Nanofiber Membranes Produced by Electrospinning.* Journal of Textile Engineering., 53 Issue 4, 137–142, 2007.

ZENG Jing, 2012. KANG YanHong SU GuiTian ZENG Jing. *Formation of drug-loaded electrospun twin fibers.* Polymer Chemistry, 57, No.11, 1275–1279, 2012.